69-17,057

KIENLE, Jürgen, 1938-
GRAVITY SURVEY IN THE GENERAL AREA OF THE KATMAI NATIONAL MONUMENT, ALASKA.

University of Alaska, Ph.D., 1969
Physics, general

University Microfilms, Inc., Ann Arbor, Michigan

GRAVITY SURVEY IN THE GENERAL AREA OF THE KATMAI NATIONAL MONUMENT, ALASKA

A

DISSERTATION

Presented to the Faculty of the
University of Alaska in Partial Fulfillment
of the Requirements
for the Degree of
DOCTOR OF PHILOSOPHY

by

Jürgen Kienle, Dipl. Nat.

College, Alaska

May, 1969

GRAVITY SURVEY IN THE GENERAL AREA OF THE

KATMAI NATIONAL MONUMENT, ALASKA

APPROVED:

Chairman

Department Head

APPROVED: _____ DATE: 9/16/68

Dean of the College of Mathematics,
Physical Sciences and Engineering

Vice President for Research and Advanced Study

ABSTRACT

The principal data for gravity observations in the general area of the Katmai National Monument, Alaska, during the summers of 1965 to 1967 are presented.

Simple Bouguer, complete Bouguer and free-air anomaly maps are discussed in terms of regional crustal structure and near surface geology.

Near zero free-air and Bouguer anomalies in a section from Katmai to Kodiak Island indicate a crust typical of continental margins with an average depth to the Moho of 32 km. This is in substantial agreement with earlier seismic observations in Katmai.

Most local variations in Bouguer gravity values in Katmai can be explained by density contrasts occurring in the upper crust and in the near surface geology of that area. These clearly reflect Mesozoic and Cenozoic structural trends. A crustal section across the volcanic range was deduced from geologic, seismic and gravimetric data. A structural basin, created by a relative downdropped center block bound by the Bruin Bay fault to the northwest and the volcanic axis to the southeast, is occupied by Mesozoic sediments. The volcanic alignment seems to be fault controlled.

A gravity low situated in the immediate vicinity of Mt. Trident on the volcanic axis has been reinterpreted in terms of a very shallow mass anomaly. A correlation to earlier seismically detected deeper magma chambers in the same area may exist but is not yet clear.

A local gravity survey across the Valley of Ten Thousand Smokes in Katmai resulted in first estimates of the thickness and volume of the 1912 ash flow by geophysical means. An ash flow volume of 3.8 km^3 was derived.

ACKNOWLEDGEMENTS

I wish to thank my committee chairman, Professor E. Berg, Geophysical Institute, for the suggestion and direction of this project through stimulating discussion and constructive criticism. I would also like to express my gratitude to Professor R. B. Forbes, Head of the Geology Department and also associated with the Geophysical Institute for his guidance in the geologic aspects of the project. The help of Dr. D. Stone, Geophysical Institute through discussions and critical review of the thesis is gratefully acknowledged. I am also indebted to Professor K. B. Mather, Director, Geophysical Institute, for his continued interest and support of the Katmai projects.

The field assistance received from my wife Linde Kienle, Dr. D. K. Ray and Mr. N. Sperlich (all of the Geophysical Institute) under sometimes harsh environmental conditions is heartily acknowledged.

I also wish to thank Dr. G. P. Woollard and W. E. Strange, Hawaii Institute of Geophysics, for the loan of the Worden Geodesist gravimeter and for their computer program for determining Bouguer and free-air anomalies and Dr. P. Dehlinger, Oregon State University, for providing a readout of the Talwani computer program to determine gravity effects of two-dimensional mass anomalies.

This research has been supported by the National Science Foundation under grants GA-900, GP-4360 and GA-469 and by the Air Force Office of Scientific Research under grants 701-64 and 701-66.

Special thanks are extended to the Alaskan Air Command and the 5017th Operational Squadrons. Without the expert flying skill of its

helicopter pilots Majors W. Kuschel, N. Miller, T. Argo, S. Silver, W. Fox and Captains R. McGeechan, J. Keel, L. Belanger and H. Rhodes the gravity survey, which in the completely uninhabited and inaccessible Katmai National Monument was entirely dependent on helicopter support, would have been literally impossible.

Thanks are due to Dr. W. Hartman and Mr. and Mrs. R. Dewey, U. S. Fish and Wildlife Service, and Mr. D. Coe, National Park Service, for their kind hospitality during field operations.

I am particularly obliged to Mrs. N. McRoy and Mr. L. Gedney for editing the final version of this thesis.

TABLE OF CONTENTS

LIST OF ILLUSTRATIONS

LIST OF TABLES

CHAPTER I

INTRODUCTION

1.1 Foreword

Katmai National Monument, located on the Alaska Peninsula is characterized by recent and continuing volcanism. The Alaska Peninsula as part of the Aleutian Archipelago is bounded on the southeast by the continental shelf and the Aleutian Trench, and to the northwest by the continental shelf of the Bering Sea (Fig. 1). Interesting transitions between oceanic island arc and continental crust can be expected in this area. The gravity studies presented in this thesis, as complemented by seismic data, should contribute to a better understanding of the crustal composition and structure of the Alaska Peninsula and the tectonic setting of Pacific Rim volcanism.

1.2 Geophysical Methods - Gravity

Unfortunately, the geologist's hammer can only sample surface outcrops. To get additional information one needs devices that can acquire data from the subsurface. Geophysical methods such as magnetic, gravity and seismic surveys, to name the most important ones, provide the means. Other methods include telluric currents, various electric methods, heat flow and radioactivity measurements. Of the above methods, magnetic and gravity surveys are the cheapest and fastest. Due to the extreme mobility and compactness of the instruments very large areas can be covered in a very short time; a reading at a single station can be made in minutes. Magnetic and gravity methods are therefore particularly suitable for reconnaissance work. Gravity and magnetic contour maps

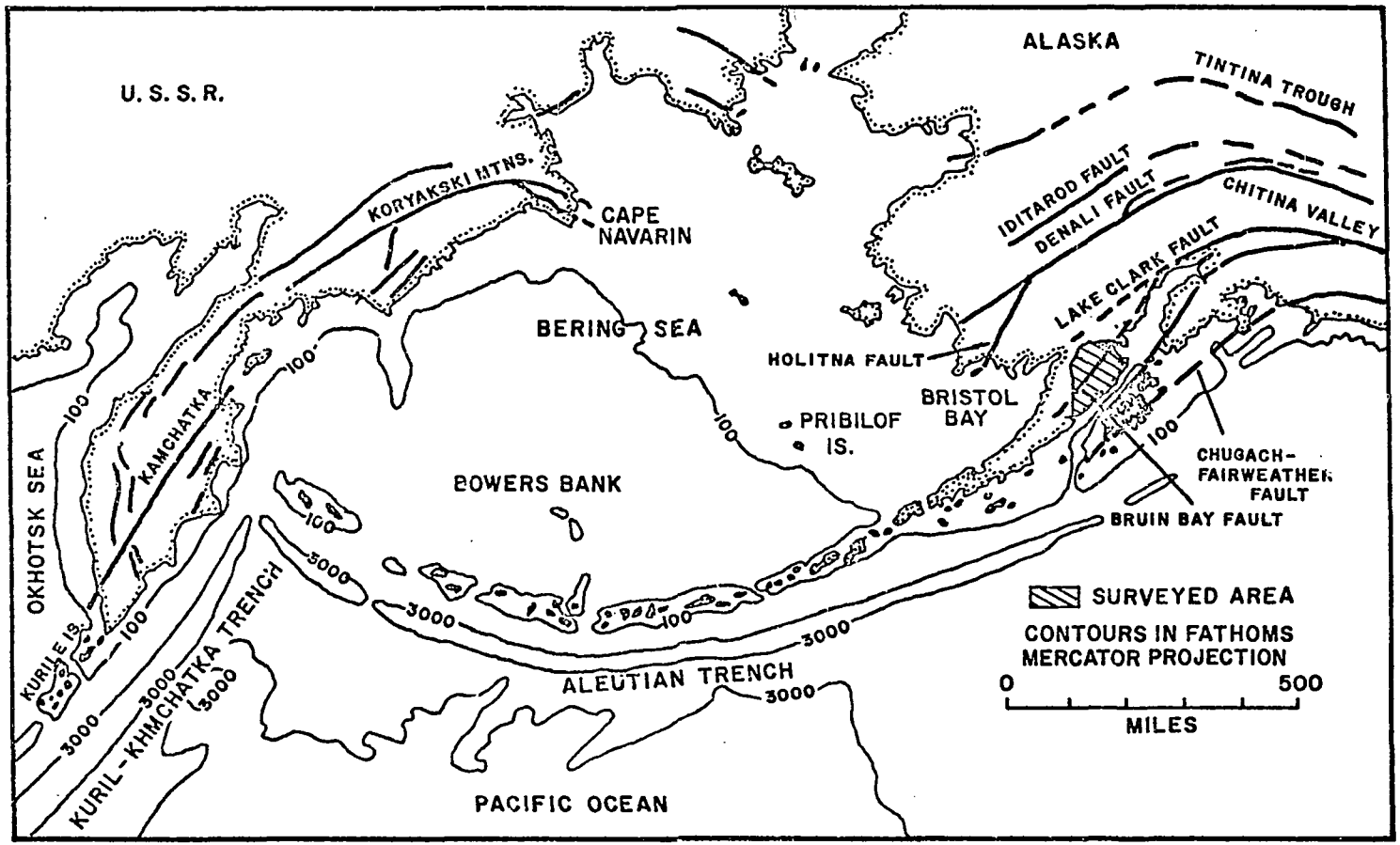

Figure 1. Bering Sea and adjacent continental areas, showing principal faults and surveyed area (modified after Burk, 1965 and Stoneley, 1967).

clearly display tectonic trends and local anomalies. Unfortunately, the solution to inverse potential problems, i.e., the geometry of the source which produces a certain potential field on the surface is never unique, however, certain constraints do exist. For instance, a shallow mass anomaly can never be wider than the gravity anomaly that it produces, and a deep anomaly has a certain depth limit derived from the sharpness of the gravity effect (Nettleton, 1940). In addition, gravity surveys can be very useful to interpolate structural interfaces between points where absolute depths were determined by drilling or seismic profiling.

Regional gravity anomalies are often indicative of the isostatic state of segments of the earth's crust.

1.3 Continental Margins and Island Arcs, the Aleutian Archipelago

Island arcs and continental margins are underlain by transition zones from oceanic to continental crust. These zones have been widely discussed, with many divergent opinions expressed by earth scientists. It is in these zones of unstable crustal conditions that new mountain ranges may be born and where most of the world's present tectonic activity is concentrated. All of the young folded mountain belts, island arcs, most of the world's active volcanoes and the majority of the world's shallow and deep earthquakes lie in two relatively narrow belts around the earth (Jacobs et al, 1959),(1) the Eurasian-Melanesian belt and (2) the circum-Pacific Rim.

Island arcs are characterized by certain types of gravity anomalies, earthquake hypocenter concentrations and heat flow and magnetic anomalies. Their relationship to volcanism, oceanic trench formation,

active faulting, geosynclinal subsidence and sedimentation, and mountain building is established.

The geometry and characteristic location of island arcs have intrigued many researchers and several megatectonic concepts have been developed to explain them.

From small deviations of the path of an orbiting satellite, Schwiderski (1967) derived density anomalies of the mantle on the earth surface, and at a surface in the upper mantle. The density anomalies represent deviations of less than 0.16°/00 (!) of the mean outer mantle density of 3.3 g/cc and are presented as isoanomaly maps at the two surfaces. All interpretations given by the author are derived strictly from the fluid mantle theory. A fluid mantle is supposedly heated from below, producing thermally driven convection cells. Each density low would thus correspond to a source, and each density high to a heat sink. The flow of material from sources to sinks on the mantle surface exerts vertical and horizontal forces acting on the plastic, overlying crust. Depending on the intensity of the flow, i.e. the magnitude and direction of forces, the thickness of the crust to be deformed, the prevailing temperature gradients and other factors, Schwiderski derived several simple translation principles for interpreting the density anomalies in terms of major tectonic features. He deduces very low density sources, situated beneath the Canadian Shield and the Gulf of Mexico, which thrust the entire North American continent in a southwesterly direction. A trough-like high density sink is located under the Rocky Mts. and the Sierra Madre. The slippage between the counterclockwise rotating Pacific and clockwise rotating North American blocks takes place along circum-Pacific

wrench faults. Examples might include the San Andreas fault system of California and the East Aleutian thrust zone in the Katmai-Kodiak region. The motion is accompanied by shallow earthquake activity. In the North Pacific the southerly drift of North America and Eurasia, acting as a coherent continental unit including the Bering Bridge area, causes the North Pacific oceanic crust to be underthrust under the Aleutian arc, the Alaska Peninsula and the Bering platform. The Aleutian Islands and the Trench may be the expression of this process. The deformation in this area is governed by large density changes, i.e. powerful flow and extreme temperature gradients (Schwiderski, translation principle IV, p. 24). In addition to overthrusting from the north, three low density sources in the North Pacific could also produce underthrusting of oceanic crust below the continent. Only a few hundred kilometers northeast of the Katmai area, deep within the continental block, the tectonic belts and lineaments define a sharp arcuate bend from northeast to southwest to merge with the east Pacific Rim. This could well be an expression of a differential motion between the southwest drifting North American continent and Alaska, produced by the above described processes as proposed by Schwiderski.

Carey (1956) proposed a major rotation about a point in the Gulf of Alaska, which is perhaps reflected in the curvature of the Alaska and Coast Ranges and adjacent faults. This movement may be associated with the openings of the Arctic and Atlantic Oceans that now separate the Eurasian and North American continents.

Jacobs et al (1959, p. 305, Fig. 14-7) explain the sharp curvature of tectonic trends in southern Alaska as a so-called "narrow belt junction"

of the Cordilleran and Aleutian arcs. According to the concept of a contracting earth the Alaska Range would be a typical secondary arc or buckling ridge, which spans the junction (Scheidegger, 1958, pp. 172-177).

If, indeed, the splitting of the North American-Eurasian-supercontinent formed the Arctic and Atlantic ocean as proposed by Carey (1956), major rotations and translations must have occurred in Alaska. One might expect different polar wandering curves, as derived from paleomagnetic work, for the Aleutians, southern Alaska and the Brooks Range, and these should perhaps lie between those of the continental masses of Eurasia and North America (D. Stone, Geophysical Institute Report, 1967). If this is true, then the relative motions of the sampling sites through geologic time can be detected by studying their paleopole positions. For this reason D. Stone collected basaltic rock samples in Katmai in 1965 and extended his sampling in 1967 and 1968 throughout the Aleutians and mainland Alaska in a large scale program to calculate the paleopole positions for rocks of various sites and various ages in Alaska.

That some large scale motions have taken place in the North Pacific is perhaps indicated by Elvers et al (1967), who have recently discovered a "great magnetic bight" at about 160° longitude just south of the Aleutian Trench. This correlates with magnetic lineations to the south, which can be traced across the major East Pacific fracture zones and roughly parallel the coastline of western North America. These are indicative of a complex ocean floor spreading mechanism. The magnetic lineations in the northeastern Pacific also indicate a very complex structure of the oceanic crust, especially of its transition to the Aleutian Trench and continental margin.

In contrast to the other island arcs in the Pacific, the Indian Ocean and the Caribbean Sea, the Aleutians archipelago has been neglected until present time due to its remoteness. Some geophysical and geological data are available, especially for the eastern Aleutians, but information is still sparse for the archipelago as a province. The Aleutian islands form the major archipelago in the North Pacific and they are contiguous with the North American continent through the Alaska Peninsula and the Katmai area (Fig. 1).

The Aleutian arc is a zone of tectonic stress accompanied by intense tectonic activity. The characteristic hypocenter distribution of island arcs on a worldwide basis shows increasing focal depth of the hypocenters towards the concave side of the structure with maximum focal depths of about 700 km. The seismic framework of the Aleutian arc, however, is exceptional in that no deep earthquakes in the 300 to 700 km depth range have been observed (Alaskan earthquakes from 1788-1961, Davis and Echols, 1962). The tectonic stress system in the Aleutians was studied by various authors. Balakina (1962) finds that in circum-Pacific earthquakes and particularly those of the Aleutian zone, "the compressive stress forms small angles with the horizontal and is oriented almost perpendicularly to the structural trend". Stauder (1966) presents focal mechanisms for a whole series of aftershocks following the March, 1964, Alaskan earthquake, with hypocenters south of Kodiak Island. The pressure axes in Stauder's fault plane solutions for 18 of these shocks, trend 12° to 61° west of north. This is in substantial agreement with Balakina's (1962) and Lensen's (1960) proposed stress system for the Aleutian arc, which is roughly perpendicular to the tectonic trend. As to the mechanism

of the Alaskan earthquake aftershocks, Stauder (1966) prefers displacement along a low angle thrust plane. Press and Jackson (1965) favor dip slip motion on a high angle fault. Burk (1965) noted that the zone of aftershocks of the 1964 Prince William Sound earthquake parallels the trend of the continental shelf and is sharply terminated southwest of Kodiak Island. This could indicate that the Aleutian arc may be broken into blocks by transverse fractures. One of these tear faults may extend from southwest of Kodiak Island to the Alaskan Peninsula.

Coats (1962) compared first motions of earthquakes in the Alaska Peninsula and the Aleutians to the orientation of linear tectonic elements. He believes that the oceanic crust is underthrust under the continental crust. In his structural model the hanging wall above the major thrust plane breaks into tear faults, which in turn become avenues for the eruption of lavas and pyroclastics.

Magnetic data for the Aleutian Archipelago and southern Alaska are very sparse. Zeitz and others (1959) conducted an aeromagnetic study in the Cook Inlet area, Keller et al. (1954) completed eight aeromagnetic traverses across the Aleutian trench, and 3 Aleutian volcanoes on Adak, Great Sitkin and Umnak Islands, Peter (1965) discovered large (up to 800γ) residual magnetic anomalies in the trench south of Kodiak Island and Andreasen and others (1963a,b) and Henderson and others (1963) have published aeromagnetic maps of the head of Bristol Bay.

Some, but not very detailed, gravity data is available for the Aleutian Archipelago and mainland events.

Worzel (1965) produced a Bouguer gravity anomaly map based on submarine pendulum gravity measurements covering the coastal waters of Alaska

from 120° to 180° longitude and from 45° to 75° latitude. The area includes the southern Beaufort Sea, the Bering Strait, the eastern Bering Sea, the eastern Aleutian Trench area and the Gulf of Alaska.

Woollard and Strange (1962) published free-air anomaly, Bouguer anomaly and mantle elevation maps of the Pacific Basin. All three maps cover the Gulf of Alaska, the Aleutian Trench and the Bering Sea.

Peter (1965) compiled bathymetric, magnetic total intensity and free-air anomaly contour maps of an area bounded by 155.5° to 158°W longitude and 53° to 55°N latitude, which includes the Aleutian Trench south of Kodiak Island. He also calculated a two-dimensional crustal structure across the Trench from the gravity, seismic and magnetic data.

Elvers et al (1967) also present a free air anomaly map covering an area from 155.5° to 158.5°W and 45° to 55°N. A -70 to -80 mgal low is located 20 km north of the Trench axis, followed by a +70 to +90 mgal high over the continental shelf.

First gravity studies on continental Alaska were accomplished by Thiel et al (1959) when they established 513 gravity stations throughout Alaska. Nine of them were primary pendulum base stations and the remainder were Worden gravity meter measurements, tied into the primary base stations. Woollard and others (1960) using the values from these stations prepared a Bouguer isoanomaly map of continental Alaska. They also gave a structural interpretation of selected areas.

The only more detailed gravity work in the vicinity of the Katmai National Monument was done by Barnes. Barnes (1967) presented a detailed Bouguer anomaly map of the Alaska and Kenai Peninsulas including coastal waters out to the Aleutian Trench, together with Bouguer anomaly maps of northwest, north central and southeast interior Alaska.

The gravity survey discussed in this thesis will partially fill the existing gap in gravity coverage between Barnes (1967) data to the southeast and Woollard's et al (1960) gravity measurements at the shores of Bristol Bay.

1.4 Regional Geology and Tectonic Setting of the Study Area

The study covers an area about 120 by 160 km, on the Alaska Peninsula, north of Kodiak Island. It is bounded by Naknek, Nonvianuk, Kukaklek and Iliamna Lakes in the north and by the Shelikof Strait to the south; and it comprises all areas included in the Katmai National Monument (Figs. 2 and 3). The area is mountainous; its main feature is an arcuate belt of glaciated active volcanoes, which is convex to the southeast. These volcanoes represent the northeastern extension of the Aleutian volcanic arc. Martin, Mageik, Trident, Katmai, Snowy, Denison, Stellar, Kukak, Kaguyak, Fourpeaked and Douglas volcanoes form the arc in the Katmai area. The active volcanoes Mt. Griggs (formerly Knife Peak) and Novarupta are offset to the northwest from this belt. The continental volcanoes which are northeast of Katmai are located on a straight line extending from Mt. Douglas through Augustine Island, Mt. Iliamna and Mt. Redoubt to Mt. Spurr. This alignment cuts across the Bruin Bay and Lake Clark faults, and other pre-Quartenary structural trends. This belt forms an angle of about 140° with the Katmai volcanic trend and coincides with a narrow zone of shallow and intermediate depth earthquakes, as plotted on recent monthly epicenter maps compiled by the seismographic station of the Geophysical Institute (Figs. 4 and 5) and as earlier observed by Tobin and Sykes (1966). This zone extends north-northeast from Katmai to the Cook Inlet along the volcanic axis, to the Susitna Valley and on to Mt. McKinley.

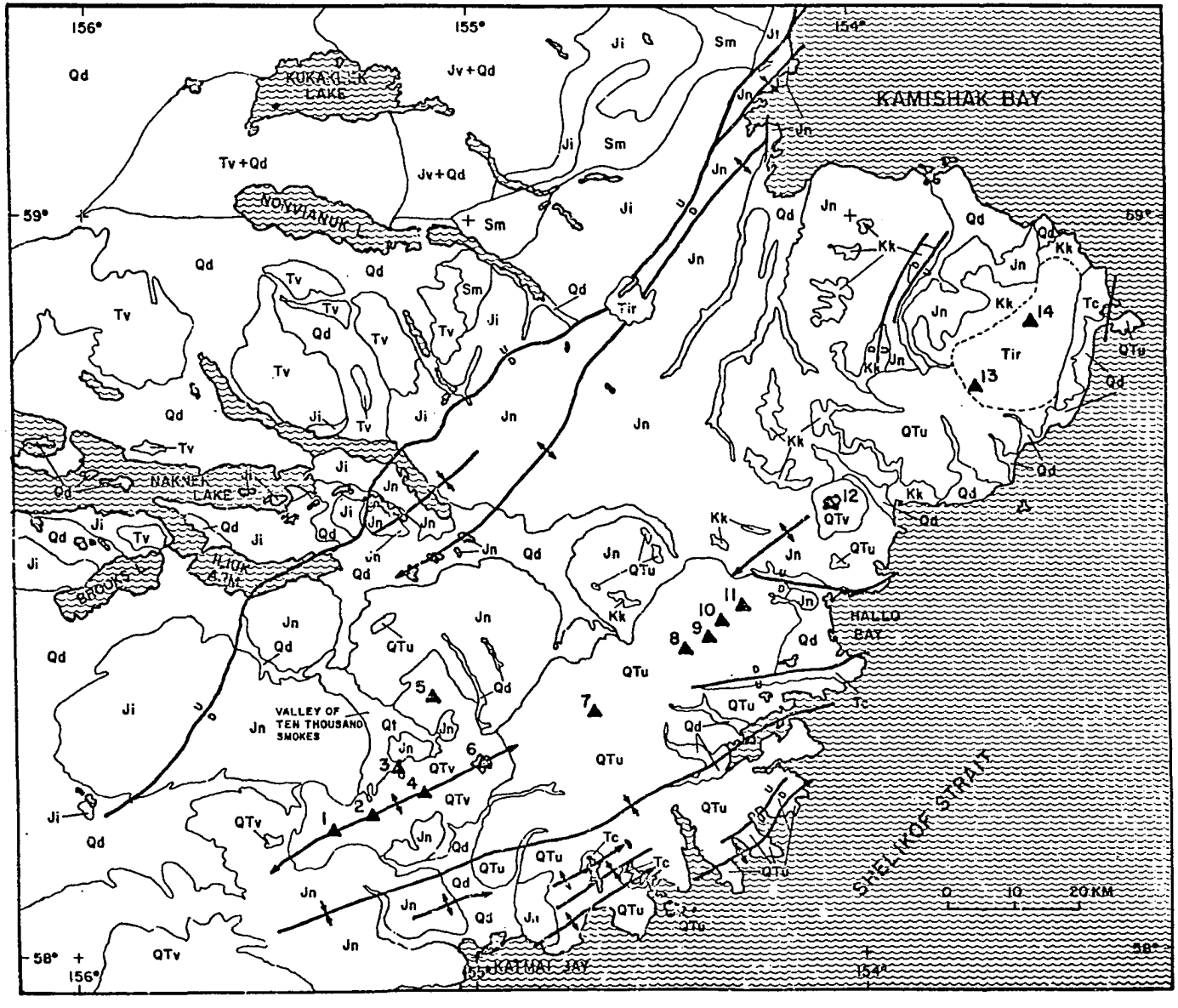

Figure 2. Geologic map of Katmai area, showing principal geologic units, structures and volcanic necks (after Keller and Reiser, 1959 and Burk, 1965). For legend see Fig. 3.

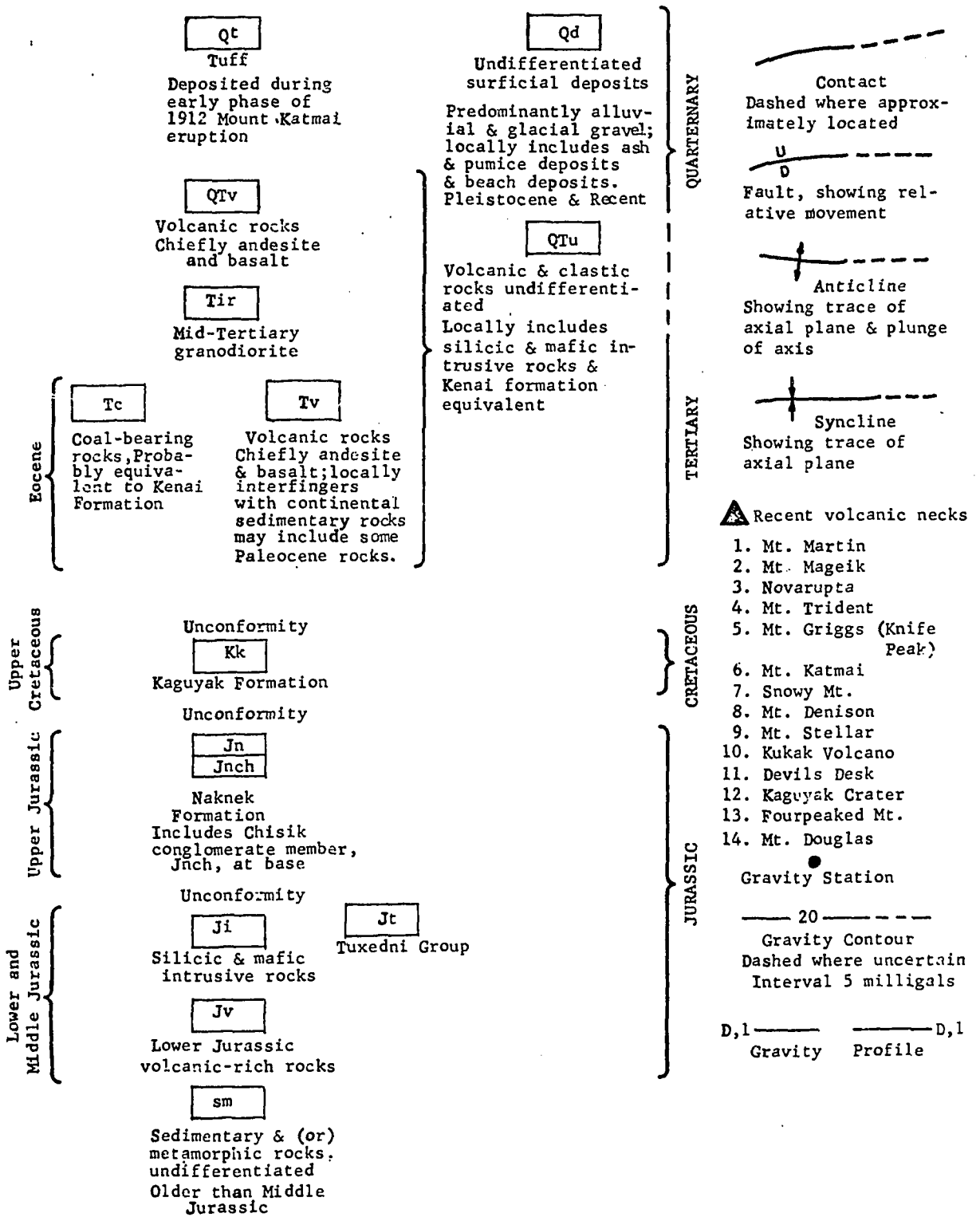

Figure 3. Legend to geologic map (Fig. 2), simple Bouguer (2.67) gravity map (Fig. 9) and complete Bouguer (2.67) gravity map (Fig. 10).

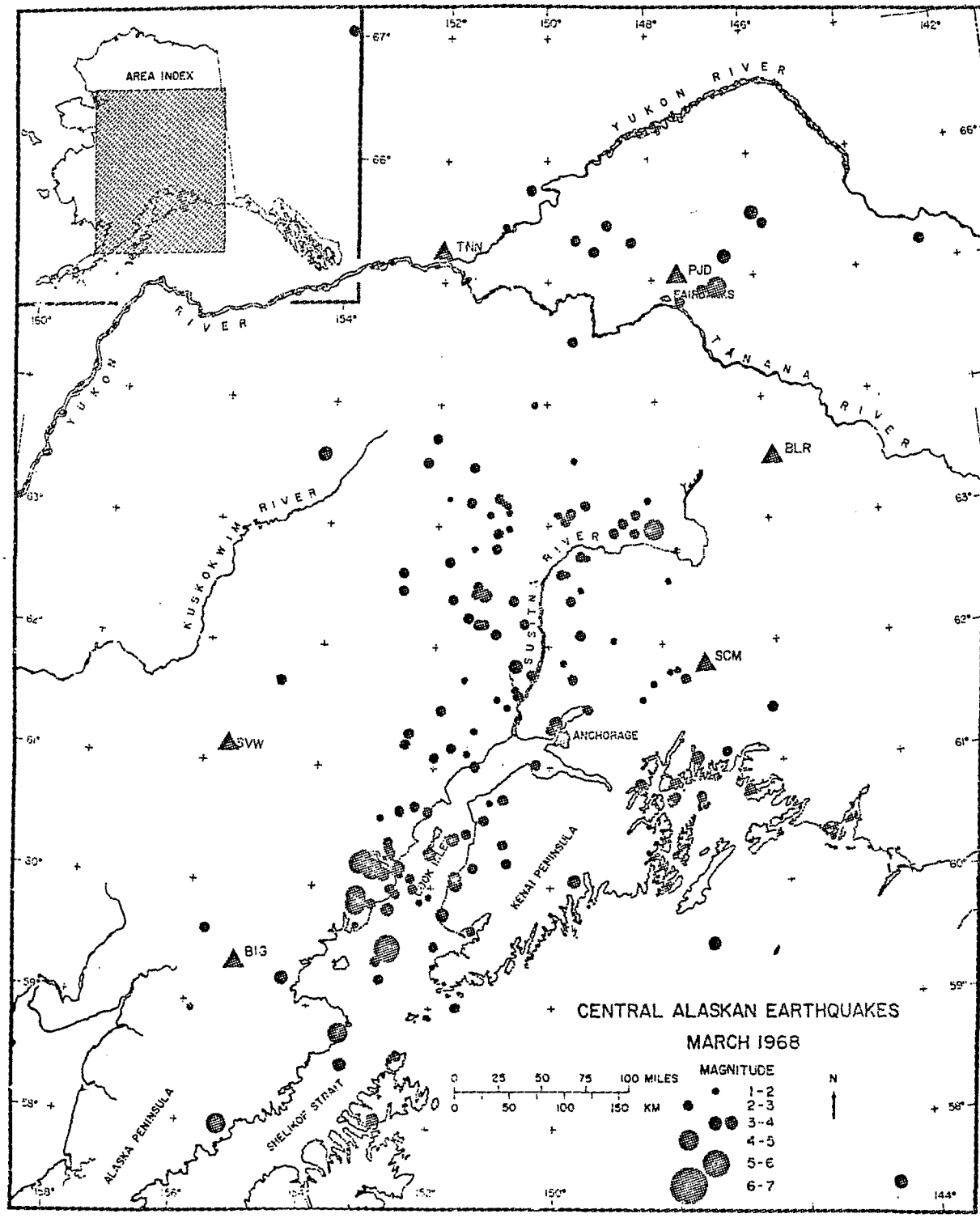

Figure 4. Shallow and intermediate depth earthquakes in central and southern Alaska of March 1968 (monthly epicenter maps of seismographic station of the Geophys. Inst., Univ. of Alaska).

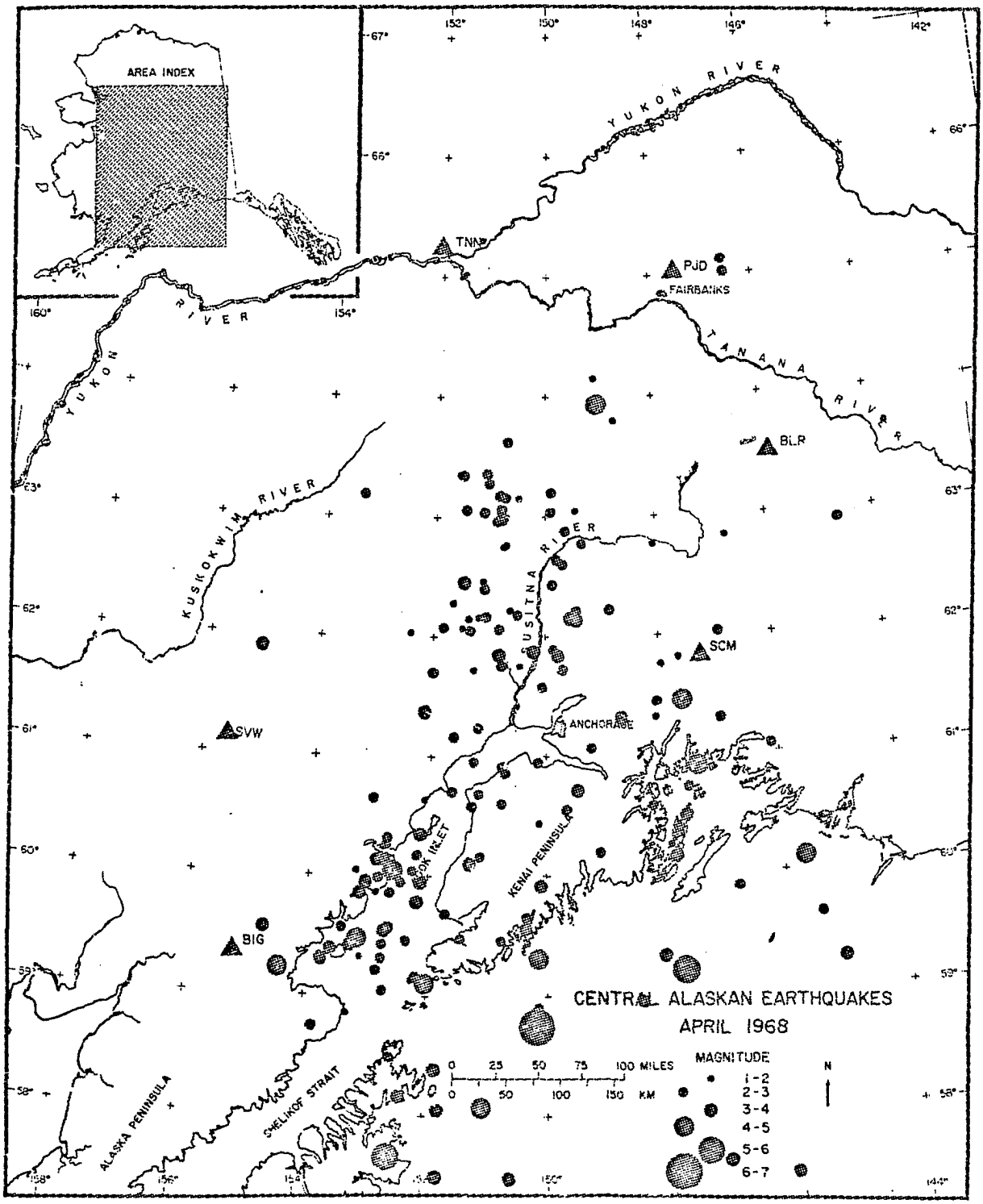

Figure 5. Shallow and intermediate depth earthquakes in central and southern Alaska of April 1968 (monthly epicenter maps of seismographic station of the Geophys. Inst., Univ. of Alaska).

In 1912 one of the world's most violent historic volcanic eruptions created the Mt. Katmai calders, Novarupta plug dome and the "ash flow" in the Valley of Ten Thousand Smokes (Fig. 6). This was the second largest eruption in historic time with a volume ejecta around 21 km^3 (Tsuya, 1963). The newly formed cone of Mt. Trident has shown very extensive activity in the last 15 years, and it has produced approximately 0.4 km^3 of blocky andesitic lava since 1953 (Ward and Matumoto, 1967).

Since Spurr's first traverse in 1898 (Spurr, 1900) many contributions have been made to the regional geology of the Katmai area. These contributions and more recent work are contained in the report by Keller and Reiser (1959), which includes a 1:250,000 scale geological reconnaissance map. The adjacent southwestern Alaska Peninsula has been mapped in considerable detail by Burk (1965), who also gives a thorough discussion of its structure and stratigraphy. A simplified geologic and tectonic map based on the work of the above authors is given in Figs. 2 and 3.

Jurassic (Naknek Formation), late Cretaceous (Kaguyak Formation) and Eocene nonmarine, coal-bearing sediments form the bulk of the exposed rocks. The Naknek Formation consists of a basal conglomerate, overlain by 6000 to 9000 feet of fossiliferous sandstone, siltstone and shale. The Kaguyak Formation is composed of 4500 feet of siltstone, sandstone and shale. The Eocene rocks (Kenai Formation equivalent) include several hundred feet of conglomerate,sandstone, siltstone, shale and coal, locally interfingered with volcanic rocks. These rocks are exposed in isolated areas along the shores of Shelikof Strait (Keller and Reiser, 1959).

To the northwest, the northeast trending Bruin Bay fault separates younger sedimentary rocks from a Lower and Middle Jurassic igneous complex

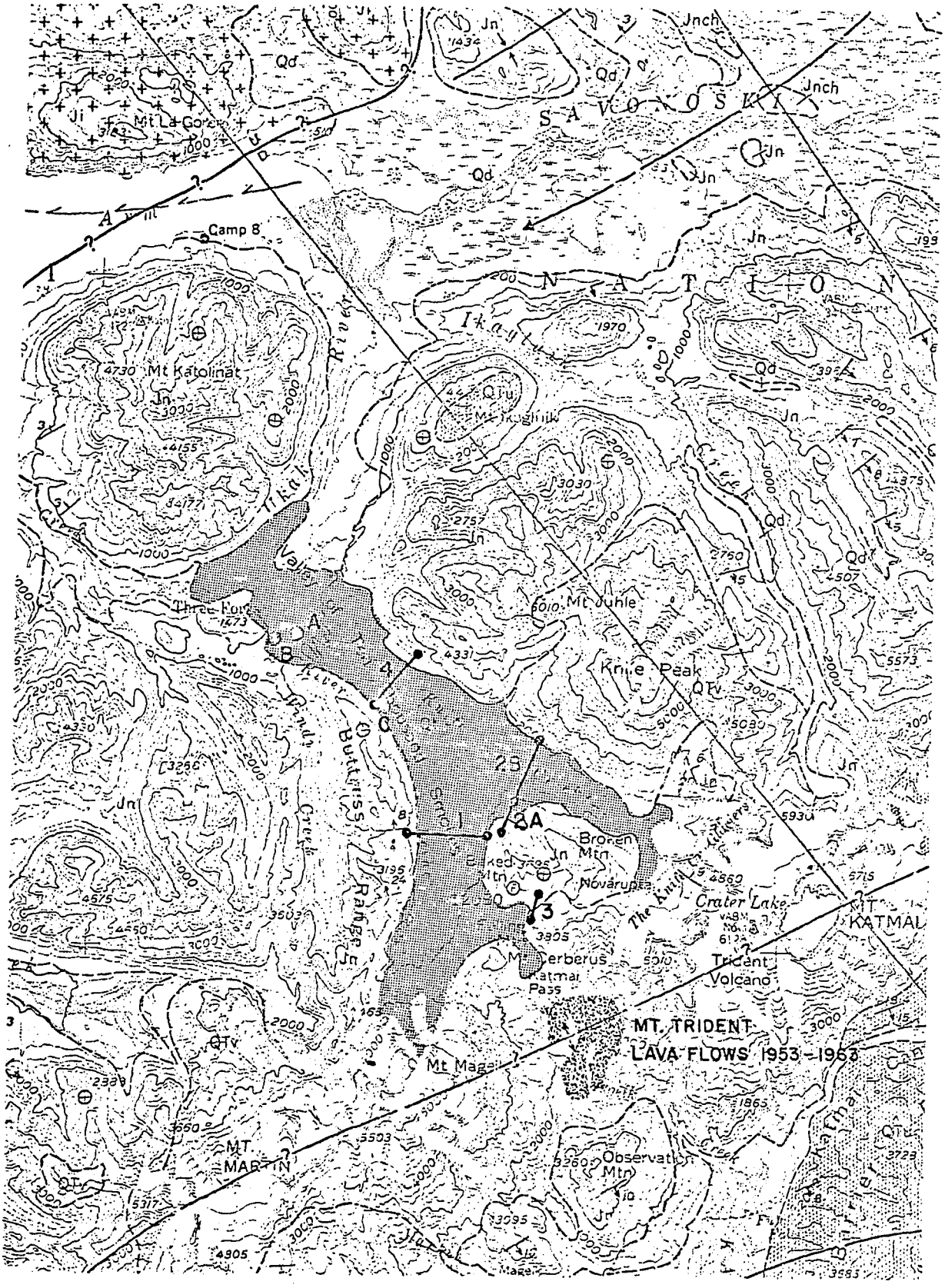

Figure 6. Topographic and geologic map showing the tuff and ash deposits in the Valley of Ten Thousand Smokes (stippled), the location of the Valley gravity profiles and density sampling sites and the recent lava flows of Mt. Trident from 1953-1963.

of batholithic dimensions. This mass varies greatly in composition but consists predominantly of hornblende and biotite grandodiorites and quartz diorite. Boulders of the hornblende granodiorite occur in the basal conglomerate of the Naknek Formation.

Sedimentary and metamorphic rocks of possible Paleozoic age and the closely associated Jurassic igneous complex form a narrow zone north and adjacent to the Bruin Bay fault, which extends from Becharof Lake northeast to Kamishak Bay. Farther to the northwest, this zone is bordered by a Lower Jurassic sequence containing dominant volcanics and folded Eocene volcanic units, chiefly andesites and basalts. This volcanic sequence is separated from the early Jurassic intrusives and possible paleozoic sedimentary and metamorphic rocks by an unconformity and they are probably of the same age as the coal-bearing rocks exposed along the shoreline of Shelikof Strait.

Tertiary, Quaternary and recent andesitic-dacitic and basaltic volcanic rocks overlie Jurassic and Cretaceous sediments. This sequence is relatively undeformed. Keller and Reiser (1959) show the volcanoes in the Katmai area as situated on the crest of a gentle anticline of deformed Naknek rocks and suggest deep-seated linear fault control of the volcanic vents. Fenner (1923), in earlier work, did not describe this anticline.

An undifferentiated sequence containing both folded Eocene and young massive volcanic units is exposed along the Shelikof Strait from Hallo Bay to Katmai Bay. Locally, it is also composed of units believed to be equivalent to the Kenai Formation. It also contains Tertiary intrusive rocks, and has a stratigraphic thickness of up to 6000 feet (Keller and Reiser, 1959).

Tertiary intrusive rocks cut the sedimentary units as dikes and sills. Mid-Tertiary granodiorites occur at Cape Douglas and also intrude the crest of the Kamishak Anticline, near Kulik Lake.

Figure 1, modified after Burk (1965) and Stoneley (1967), illustrates the most important faults which cut the continental blocks adjacent to the Bering Sea, and the location of the Kuril-Kamtchatka and Aleutian Archipelagoes. The surveyed area is dominated by the Bruin Bay fault, the Katmai volcanic trend and the straight volcanic axis that extends from Mt. Douglas to Mt. Spurr and crosscuts the major faults. Figure 7, after Payne (1955) and Ray (1967), shows the principal tectonic units of southwestern Alaska. The Katmai area is dominated by the Matanuska Geosyncline. It borders the Shelikof Trough to the southwest and the Talkeetna Geanticline to the northwest.

The region between Lake Iliamna and the Shelikof Strait is characterized by a broad structural arc with the crest coinciding with the Bruin Bay fault. Where observed, the fault dips steeply northwest with no geologic evidence of wrench faulting. Movement has been chiefly vertical. The fault separates the subsiding trough to the southeast from the rising source area to the northwest and has been active since Middle Jurassic times (Burk, 1965), it is presently seismically active (Figs, 4 and 5). To the southeast shallow water Jurassic and younger formations dip homoclinally towards the Shelikof Strait. Parallel to the volcanic trend, several low amplitude symmetrical folds and a few faults are superimposed on the regional southeasterly dip. Two faults which strike east-west at Hallo Bay, deviate from the general tectonic trend.

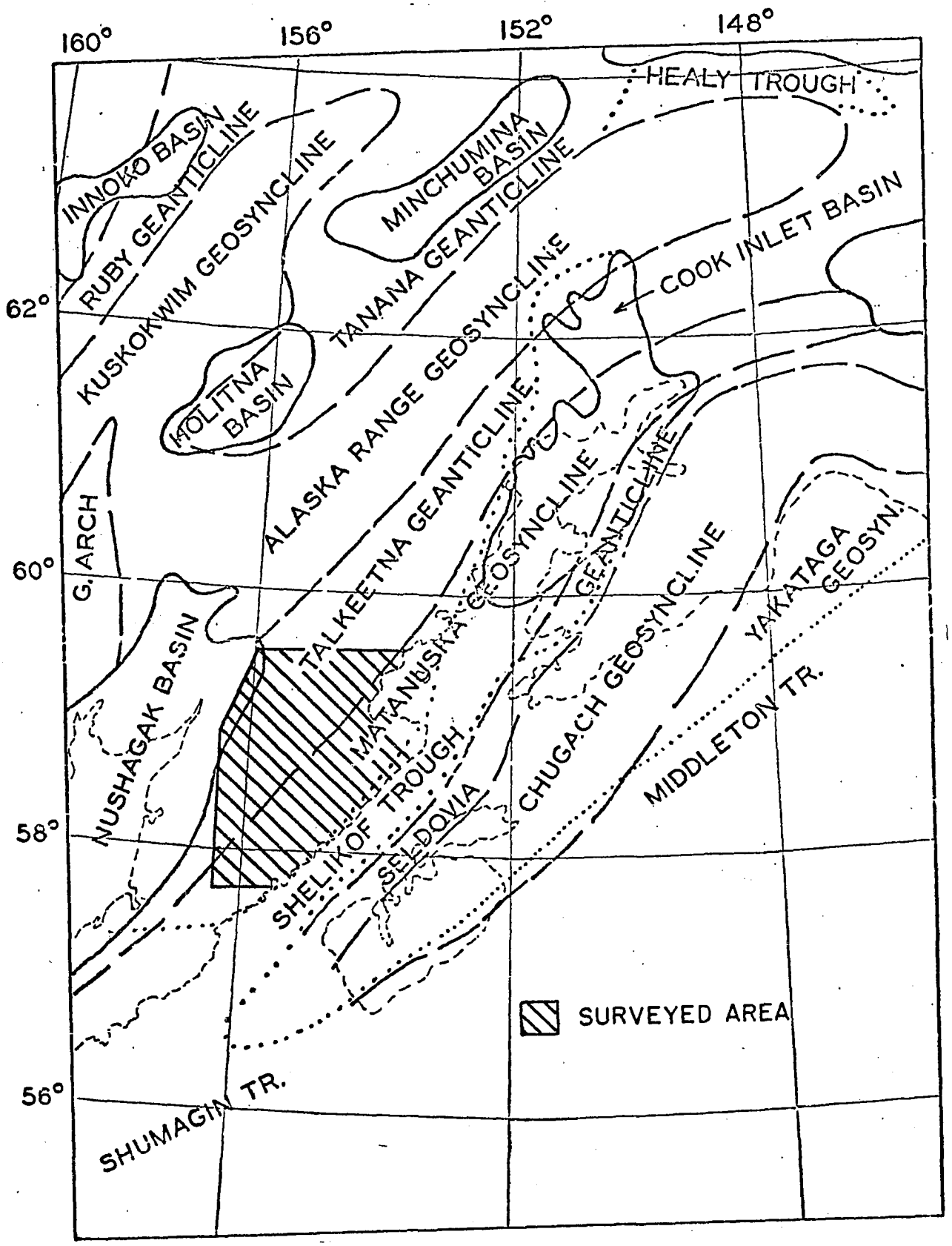

Figure 7. Principal tectonic units of southern Alaska (modified after Payne, 1955 and Ray, 1967).

The Alaska Peninsula was essentially a trough of subsidence and deposition until Pliocene time. A strong orogenic deformation took place between the Eocene and Quarternary time as dated by the angular unconformity between folded volcanics and intercalated Eocene sediments, and undeformed Quarternary volcanics. This orogeny created most of the present structures.

Volcanic activity was widespread in the Alaska Peninsula from Permian to early Jurassic time; and volcanism was renewed in the early Tertiary, which has persisted to the present.

1.5 Recent Geophysical and Petrological Investigations in the Katmai National Monument, Alaska.

Worldwide attention was drawn to southern Alaska by two spectacular manifestations of volcanic and tectonic activity, the June 1912 Mt. Katmai eruption and the March 1964 Prince William Sound earthquake, whose active tectonic failure zone borders the Katmai National Monument to the southeast

The first seismic and gravity investigations in the Katmai National Monument were sponsored by the Geophysical Institute of the University of Alaska in 1963. R. Decker operated a vertical seismometer at Brooks Camp and the north end of the Valley of Ten Thousand Smokes, and found that local epicenter concentrations were close to active volcanoes. His gravity profile extended from the north shore of Lake Naknek to Mt. Trident, and included 3 stations along Lake Dakavak on the Shelikof Strait (Decker, 1963, unpublished report). Decker's data have been used and acknowledged in this thesis.

In the summers of 1965, 1966 and 1967 researchers from Lamont Geological Observatory of Columbia University, under the leadership of

T. Matumoto conducted a microearthquake study of the Katmai area. Seismic stations were installed at Brooks Lake, Overlook Cabin on the northern end of the Valley of Ten Thousand Smokes, Katmai Canyon and at Hidden Lake, 10 km northeast of Mt. Griggs. The 1965 records showed both volcanic and tectonic shocks with the majority of hypocenters at depths shallower than 10 km. A seismicity map shows a fair correlation between regions of high seismicity and recent volcanic activity (Matumoto and Ward, 1967).

During these same summers the Geophysical Institute was operating seismic stations which spanned the Katmai National Monument and adjacent areas, located at Kodiak, Mt. Douglas, Big Mountain, Lake Iliamna, Brooks Lake, the Baked Mountain volcanological observatory and the Savonoski Valley. In 1965 almost 1500 seismic events were recorded in 2 months of operation at the Baked Mountain Station (Berg, Kubota and Kienle, 1967). An initial determination of hypocenters was attempted using S and P arrivals at Kodiak and at two stations in the Monument, but deviations of observed travel times from those of the Jeffrey-Bullen tables were rather large, resulting in poorly located foci. An attempt was then made to explain these inconsistencies by modification of the Jeffrey-Bullen crustal structure model. It was necessary to apply a composite model with significantly different structures on opposite blocks of the volcanic axis. Table 1 describes our composite seismic model.

Table 1

Composite seismic model across the volcanic range in the Katmai National Monument (Berg, Kubota and Kienle, 1967).

NW section (for determination from BMH, BRO and SVN) (KM-28)

Layer	Thickness	Depth to Bottom	V_p	V_s		(J-B)
1	15 km	15 km	5.50 km/sec	3.33 km/sec	0.21	0.21
2	23 km	38 km	6.50 km/sec	3.67 km/sec	0.27	0.25
Moho						
Upper Mantle			8.10 km/sec	4.35 km/sec	0.30	0.27

SE section (for determination from KOD) (KM-36)

Layer	Thickness	Depth to Bottom	V_p	V_s	
1	12 km	12 km	5.50 km/sec	3.37 km/sec	0.20
2	20 km	32 km	6.50 km/sec	3.91 km/sec	0.22
Moho					
Upper Mantle			8.10 km/sec	4.44 km/sec	0.29

The authors derived this model in the following way:

a) Determination of Poisson's ratio in the upper crustal layer and the upper mantle in the Baked Mountain-Brooks section.

b) Adjustment of the crustal structure on both sides of the volcanic axis to obtain best fits for calculated origin times at all stations.

c) Previous determinations of velocities and thicknesses in adjacent regions.

d) Preliminary estimates of crustal thickness, based on the gravity data.

Another significant finding concerned the high Poisson's ratio of 0.3, which was determined for the upper mantle in the Katmai area, as compared

to 0.27 as used in the Jeffrey-Bullen model. This indicates that some of the upper mantle material in this area could be in a molten or semi-molten state. Kubota and Berg (1967) using equations derived by Shimozuru (1963a,b) estimate that at least 8 volume % of the upper mantle in the study area is molten. The authors also observed an attenuation of the vertical component of the elastic shear waves across the volcanic range, which may indicate the presence of magma in the crust. This effect has also been noted by Matumoto and Ward (1967). Possible magma reservoirs were located by observing the attenuation of S waves along calculated wave paths across the volcanic range. Magma chambers may exist at all depths down to the upper mantle (Kubota and Berg 1967). A correlation between a shallow seismically detected magma reservoir in the vicinity of Mt. Trident and a very localized negative gravity low was suggested by the same authors.

Using the gravity data of five gravity traverses surveyed in 1965 (Berg and Kienle, 1966) a preliminary Bouguer anomaly map of the Katmai area (Fig. 8) was compiled. A very steep Bouguer anomaly is associated with the active volcanic centers, which was tentatively interpreted as a fault at a depth of 12 to 15 km, with the southeastern block upthrown by 3 km. This uplift of about 3 km correlates well with the difference in depth of the first layer of the composite seismic model discussed above.

In 1965 and 1966 geologists and geophysicists from the University of Alaska focussed their interest on the presently active Mt. Trident near Mt. Katmai. Ray et al (in press) studied the geochemistry and petrology of the recent Mt. Trident flows from 1953 to 1963. Ray found the successive Trident andesite flows to be "a differentiated sequence from a parental magma, which was slightly undersaturated in silica." During two periods before each of

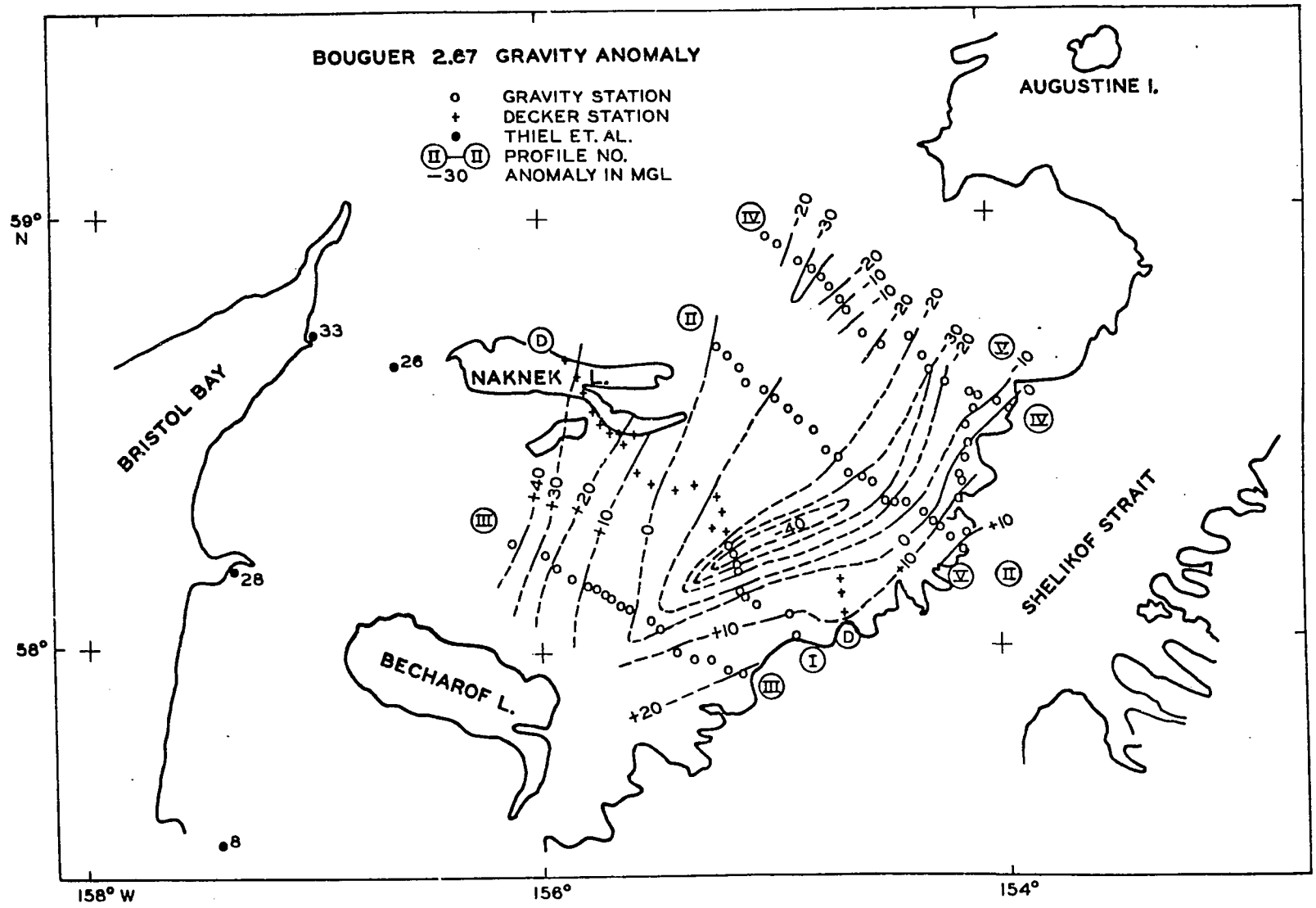

Figure 8. Preliminary simple Bouguer (2.67) gravity map of Katmai area (Berg, Kubota and Kienle, 1967, p. 1386, Fig. 17).

the 2 eruptive subcycles of 1953-1954 and 1957-1963 further differentiation seems to have occurred in the magma reservoir. The parent magma may have had both high alumina and alkali affinities, and could have been derived from the partial fusion of a basaltic layer at the base of the crust. Such an origin is consistent with Kubota and Berg's (1967) observed high Poisson's ratio and the location and distribution of magma reservoirs in the Katmai area.

CHAPTER II

DATA ACQUISITION

2.1 Instrumentation

Gravity Meter: For both field seasons of 1965 and 1966 the gravity meter used was the Worden Geodesist No. 607, Model 121. This instrument is thermostatically controlled with an average dial constant of 0.1145 mgal per division, but "has a screw effect which causes the calibration constant to vary from 0.1140 to 0.1150 mgal per meter unit for different ranges of the gravimeter. The exact nature of this screw effect has not been definitely established, but since the error to be expected from this source would generally be 0.2 mgal or less no attempt was made to take it into account in the reductions", (Strange et al, 1965a, p. 353). Its range is 5500 mgal. For operations in Katmai the thermostat temperature was set at about 85°F.

Altimeter: The altimeter was an American Paulin System precision surveying altimeter, model M-2. It has an elevation range from 0 to 10,000 feet. Divisions are at 2 foot intervals with a reading accuracy of $\pm$ 1 foot. The altimeter is temperature - compensated and the dial is calibrated for a temperature of 50°F. At this mean air temperature between 2 stations the altimeter reads the true difference in elevation for constant barometric pressure. For other temperatures elevation corrections have to be applied.

2.2 Gravity Survey

a) Mapping

Of the 278 Katmai gravity stations obtained in the summers of 1965 and 1966, 193 regional stations were surveyed by helicopter (H21). Without the enthusiastis support of the helicopter pilots, crews and staff of the 5017th Operation Squadron of the Alaskan Air Command, the survey would have been literally impossible. No settlement, road or trail exists in the area and the only way to travel is by helicopter. For station locations clear topographic features, usually lakes or river bends and forks were selected from the air and plotted on U.S.G.S. maps at a scale of one mile to the inch and should be accurate to within 0.1 minutes. Four traverses which include 85 stations across the Valley of Ten Thousand Smokes were carried out on foot.

b) Gravity Bases

The Katmai net was linked to the gravity net of the North American Continent by the two international gravity bases located at College, Geophysical Institute, Telephone Room and at MATS Terminal 2 Elmendorf AFB. These stations were used

a) to check the calibration constant of the gravimeter

b) to establish secondary bases at King Salmon and at Baked Mountain Hut.

In 1965 the Geophysical Institute of the University of Alaska established the Baked Mountain volcanological observatory at the head of the Valley of Ten Thousand Smokes near Mt. Katmai. The observatory has served as a valuable base camp for the seismic, gravity and petrological studies of the Katmai National Monument in the summers of 1965 and 1967.

All gravity base values have been determined without corrections for solid earth tides, which are of the order of ± 0.15 milligal (Wychoff, 1936). The new values of the base stations, as used here, are from Woollard and Rose's "International Gravity Measurements",

College, Geophysical Institute, Telephone Terminal 982 246.2 mgal

Elmendorf AFB, MATS Terminal 2 981 938.2 mgal

The average calibration constant of 0.1145 for the gravimeter was confirmed on two College - Elmendorf runs (308.0 mgal difference) and in agreement with the measurements of Berg and Kienle (1966) using the same gravimeter. Values deduced for the secondary base stations are shown below

King Salmon (NE corner of loading area at the N side of runway) 981 842.8 ± 0.1 mgal,

Baked Mountain Hut (SW corner) 981 615.0 ± 0.2 mgal

The errors are those obtained when the value is compared to Elmendorf AFB, MATS Terminal 2. The gravity links have been established as listed in Table 2. Linear drift extrapolations have been used to calculate gravity values at the secondary base stations. The maximum error for the average gravity differences between the base stations used in Table 2 is taken to be 3 times the mean error of the arithmetic mean which is given by

$$E = \sqrt{\frac{\Sigma \varepsilon_i^2}{n(n-1)}} \qquad i = 1, \ldots, n$$

where n is the number of observations and ε the deviation of the ith measurement from the arithmetic mean.

c) Drift rates

The elastic system of the Worden gravimeter is made of fused quartz. Aging of the quartz causes a steady drift of the zero position

Table 2.

Gravity links between primary gravity base stations in Alaska and secondary gravity base stations in Katmai.

Link	Date	Railroad	Air (normal)	Helicopter	Difference in mgal	Average
College-Elmendorf	1 July 1965	x			308.42	
	21 June 1966	x			307.90	
	4 Sept 1966		x		307.44	307.9 ± 0.7
Elmendorf - King Salmon	3 July 1965		x		95.33	
	25 June 1966		x		95.41	
	3 Sept 1966		x		95.44	95.4 ± 0.1
King Salmon - Baked Mt. Hut	10 July 1965			x	227.97	
	12 July 1965			x	227.96	
	22 July 1965			x	227.88	
	14 Aug 1965			x	227.92	
	18 July 1966			x	227.74	
	21 July 1966			x	228.05	
	1 Sept 1966			x	227.75	
King Salmon - Baked Mt. Hut - King Salmon	3 July 1965			x	227.69	227.9 ± 0.1
Baked Mt. Hut - Elmendorf	3 July 1965		x	x	323.02	
	24 Aug 1965		x	x	322.99	
	25 June 1966		x	x	322.79	322.9 ± 0.2

of this null instrument. After the initial warm-up period the average drift prior to departure for the field work was found to be about + 2.5 scale divisions or 0.29 mgal per day. Transportation of the gravimeter by railroad and fixed wing plane did not greatly affect this average drift rate. Helicopter flights and back packing, however, steepened, flattened or even reversed the drift. After such transportation the drift was usually disturbed for about another half day and then resumed its "normal value". This is the value obtained if one extrapolates the normal or steady drift prior to the rough transportation. No matter how disturbed the drift may be within a few hours, over long periods of time it is smoothly varying. In a few instances the heater batteries ran out of power and the drift suffered accordingly (the Geodesist is temperature compensated to also operate without the thermostatically controlled heating system).

As observed at Elmendorf in 1965 the overall drift for the field season from July 1 to August 24 was 137 scale divisions or 2.5 div/day (Berg and Kienle, 1966). In 1966, from June 21 to Sept. 3, it was 159 scale divisions or 2.1 div/day. This was in both cases in rough agreement with the rate observed prior to departure for the field in College. In 1965 the average drift rate was somewhat less than the College rate, in 1966 it was identical. As the quartz of the elastic system ages, there seems to be a slight but systematic decrease in the drift rate. This has been observed during the 2 individual field seasons of 1965 and 1966 as well as by comparison to the overall drift in 1965 of 2.5 div/day to the 2.1 div/day of 1966. The drift was monitored very carefully during both field seasons and all the data are drift corrected.

In most cases readings were taken prior to departure and upon return to the Baked Mountain Hut. In a few other cases the run started at the Hut (or King Salmon) and ended at King Salmon (or Hut) or started and ended at King Salmon. Since a run lasted only for several hours (in most cases 3-6 hours), the drift corrections determined by linear interpolation in time introduce much smaller errors than other sources (mainly inaccurate elevation control).

d) Elevation Control

Elevations were determined with the above described American Paulin System altimeter and in a few cases with a Taylor pocket altimeter with a reading accuracy of at best $\pm$ 5 feet. Altitudes have been corrected for temperature and barometric pressure changes. Wherever possible the altimetry was tied to known elevations such as ocean levels (using Tide Tables, Coast and Geodetic Survey, 1965 and 1966), lake levels and points with known elevation (checked and unchecked) from the U.S. Geological Survey maps (1 inch to the mile). The few bench marks in the area were unfortunately so inaccessible that they could not be used in the survey.

Barometric pressure changes were detected by

a) tying into points of known elevation

b) repeated measurements at the same location (as always done on departure and return to Baked Mountain Hut).

and then linearly interpolated over the time intervals between measurements at these check points. Barometric corrections were then applied to the individual stations. For measurements very remote from the locations at which the barometric pressure change was observed, regional

pressure gradients as indicated on the U.S. Weather Maps were also taken into account. In all cases the elevation obtained by altimetry was compared to altitudes taken from the 1 inch to the mile topographic maps. If the discrepancy was too big, the map elevation was used, and a higher error limit was assigned to the gravity station.

The elevation accuracy was classified as follows:

X ± 3 ft. (0.2 mgal) related to known elevations

a) from mean sea level with tidal corrections from tide tables,

b) from known lake levels,

c) from checked elevations on the 1:63360 maps (1 inch to the mile)

Y ± 20 ft. (1.2 mgal) altimetry,

Z ± 30 ft. (1.8 mgal) estimated elevations from 1:63360 map and river gradients,

Decker (Stations 289-316) used a different classification:

B ± 1 ft. (0.06 mgal) tied to lake level

Y ± 20 ft. (1.2 mgal) photogrammetric control

D ± 50 ft. (3.0 mgal) aneroid or topographic contours.

The error in mgal in parentheses is the combined elevation correction for ρ = 2.67 g/cc that corresponds to the elevation error. In steep terrain, where there was also an uncertainty of the station location, higher error limits have been assigned in feet; 100 ft. correspond to 6.0 mgal.

CHAPTER III

DATA REDUCTION

3.1 Simple Bouguer Reduction

The international gravity formula of 1930

$$g_o \text{ (mgal)} = 978{,}049\ (1 + 5.2884 \cdot 10^{-3} \sin^2 \theta - 5.9 \cdot 10^{-6} \sin^2 2\theta$$

is used in computing the normal gravity field g_o of the earth, assuming that the earth can be approximated by an ellipsoid of revolution. The first term is the absolute sea level gravity value at the equator based on the absolute gravity value at Potsdam, Germany, and could be in error by more than 5 mgal absolute. Assuming that the earth is an ellipsoid of revolution with an ellipticity of 1/297 and is of uniform density, the second term takes into account the effect of geometrical flattening, and the influence of the centrifugal force, i.e., the increase of g_o with increasing latitude θ. If the density of a rotating fluid is not uniform but increases towards the center, its external shape is no longer an ellipsoid of revolution. The surface will be depressed below the ellipsoid, the depression being zero at the poles and the equator and reaching a minimum of about 3 m for the earth at latitudes 45°. The third term in the above equation corrects for this (Garland, 1965).

If we observe gravity at some elevation h and we want to know what the gravity value would be at a selected reference level (usually sea level), three corrections have to be applied to the observed values: first, the terrain corrections, which eliminate the gravity reducing effects of the surrounding valleys and hills at the station; second, the free-air correction, which accounts for the increase in gravity

with decreasing elevation; and third, the Bouguer correction, which accounts for the attraction of the material between the station level and the reference level. If all three corrections are applied, we obtain the complete Bouguer anomaly. If the terrain correction is neglected, the result is the simple Bouguer anomaly.

In the following discussion the formulas will contain two units of length, the centimeter and the foot, due to the unfortunate fact that the U. S. Geological Survey topographic maps are still given in the traditional British units of miles and feet.

The free-air anomaly is defined as

$$g_f \text{ (mgal)} = g_{obs} - g_o + 0.09406 \cdot h$$

where g_{obs} is the gravity value in mgal, observed at the elevation h (ft) above the reference level.

A negative sign for the third term is required if the gravity observation is taken below the reference level.

The Bouguer correction reduces the free-air effect. Its sign is therefore always opposite to that of the free-air correction. For local surveys the actual crustal shell is commonly approximated by a horizontal infinite slab, the Bouguer plate. The simple Bouguer anomaly in mgal for a station above the reference level is defined as

$$g_B = g_f - 0.01276 \cdot \rho \cdot h,$$

where ρ is the density in g/cc of the Bouguer plate and h the elevation in feet above the reference level. Free-air and Bouguer anomalies for nine different densities ranging from 2.2 g/cc to 2.9 g/cc have been

calculated for the Katmai gravity stations using the IBM 360/40 computer at the U/A. These principal data are listed in Table 3.

A simple Bouguer anomaly contour map (5 mgal contours) of the Katmai National Monument for a density of 2.67 g/cc is presented in Fig. 9. Figure 2 shows the geology, recent volcanic necks and the main tectonic elements of the same area.

3.2 Terrain Corrections - Complete Bouguer Anomaly

The terrain or topographic correction, which was neglected in the simple Bouguer anomaly, compensates for the actual topography on the Bouguer plane through the gravity station. The topography decreases the gravity value that would be observed if the surface were level. Both valleys and hills, i.e., mass deficiencies below and mass excesses above the Bouguer plane, have the same gravity reducing effect at the station. All topographic corrections are therefore positive.

Hammer (1939) designed a terrain correction zone chart which, if combined with his tables, permits the calculation of terrain effects to 0.1 mgal or better. A number of circular zones around a gravity station are subdivided into a number of compartments. If detailed topographic maps are available, the average elevation in each compartment can be estimated. The difference between this and the station elevation gives the height of a prism, whose gravity effect at the station in the center of the template is tabulated.

Hand calculation of terrain corrections are extremely time-consuming, even with the aid of Hammer's templates and tables. Computerized calculations would require digitized topographic maps but unfortunately such

Table 3

Principal facts for gravity observations in the general area of Katmai National Monument, Alaska. Stations 1-80 observed in 1965, after Berg and Kienle (1966). Stations 81-288 observed in 1966. Stations 289-316 after Decker (1963).

No.	LATITUDE	LONGITUDE	ELEV (FT)	OBSERVED	THEOR	FA	B2.2	B2.35	B2.5	B2.67	B2.75	B2.85
01	58 11.80N	155 9.10W	1860.0 z	981642.60	981780.1	37.4	-14.8	-18.4	-21.9	-25.9	-27.9	-30.2
02	58 8.80N	155 8.90W	703.0 y	981725.80	981776.1	15.8	- 3.9	- 5.3	- 6.6	- 8.1	- 8.8	- 9.7
03	58 7.40N	155 7.30W	462.0 y	981744.50	981774.2	13.7	0.8	- 0.2	- 1.0	- 2.0	- 2.5	- 3.1
04	58 6.50N	155 4.60W	153.0 y	981765.60	981773.0	7.0	2.7	2.4	2.1	1.8	1.6	1.4
05	58 5.00N	154 56.20W	40.0 z	981779.90	981771.0	12.7	11.6	11.5	11.4	11.3	11.3	11.2
06	58 2.30N	154 53.90W	40.0 y	981776.80	981767.3	13.3	12.1	12.1	12.0	11.9	11.8	11.8
07	58 14.30N	155 10.50W	2700.0 z	981582.80	981785.5	53.2	-22.5	-27.7	-32.9	-38.7	-41.5	-45.0
08	58 12.90N	155 9.70W	2130.0 z	981611.70	981781.6	30.4	-29.4	-33.5	-38.5	-42.1	-44.3	-47.1
09	58 12.80N	155 9.30W	2100.0 z	981615.20	981781.5	31.2	-27.7	-31.7	-35.8	-40.3	-42.5	-45.1
10	58 12.50N	155 7.90W	2143.0 y	981621.00	981781.1	41.5	-18.7	-22.8	-26.9	-31.5	-33.7	-36.5
11	58 12.40N	155 6.70W	2584.0 y	981594.90	981781.0	57.0	-15.5	-20.5	-25.4	-31.0	-33.7	-37.0
12	58 12.60N	155 4.90W	2509.0 y	981607.70	981781.2	62.5	- 8.0	-12.8	-17.6	-23.0	-25.6	-28.8
13	58 11.30N	155 6.90W	1520.0 z	981677.20	981779.5	40.7	- 2.0	- 4.9	- 7.8	-11.1	-12.6	-14.6
14	58 11.10N	155 8.30W	1610.0 z	981663.80	981779.2	36.0	- 9.2	-12.2	-15.3	-18.8	-20.5	-22.5
15	58 13.90N	155 8.80W	3200.0±100	981557.00	981783.0	75.0	-14.8	-21.0	-27.1	-34.0	-37.3	-41.4
16	58 13.50N	154 9.30W	53.0 y	981786.60	98.782.4	9.1	7.7	7.6	7.5	7.3	7.3	7.2
17	58 15.10N	154 13.70W	54.0 y	981795.40	981784.6	15.9	14.4	14.3	14.2	14.0	14.0	13.9
18	58 16.50N	154 15.30W	12.0 x	981797.30	981786.5	11.9	11.6	11.6	11.6	11.5	11.5	11.5
19	58 17.50N	154 17.10W	142.0 y	981786.10	981787.8	11.6	7.6	7.6	7.1	6.8	6.6	6.4
20	58 18.80N	154 19.90W	75.0 y	981783.00	981789.6	0.5	- 1.6	- 1.8	- 1.9	- 2.1	- 2.2	- 2.3
21	58 20.10N	154 23.80W	330.0 z	981761.50	981791.3	1.2	- 3.1	- 8.7	- 9.3	-10.0	-10.4	-10.8
22	58 19.90N	154 27.10W	649.0 y	981726.90	981791.1	-3.1	-21.3	-22.6	-23.8	-25.2	-25.9	-26.7
23	58 20.50N	154 29.10W	1070.0 z	981696.90	98.791.9	5.7	-24.4	-26.4	-28.5	-30.8	-31.9	-33.2
24	58 23.30N	154 31.30W	3477.0 y	981555.00	981795.7	86.4	-11.2	-17.9	-24.5	-32.0	-35.6	-40.1
25	58 24.00N	154 34.90W	2256.0±50	981623.60	981796.6	39.2	-24.1	-28.5	-32.8	-37.6	-40.0	-42.9
26	58 24.30N	154 37.90W	1509.0±50	981682.90	981797.0	27.8	-14.5	-17.4	-20.3	-23.6	-25.1	-27.0
27	58 27.00N	154 41.10W	831.0±50	981730.20	981800.6	7.7	-15.6	-17.2	-18.8	-20.6	-21.4	-22.5
28	58 27.90N	154 44.20W	581.0 y	981750.60	981801.8	3.4	-12.9	-14.0	-15.1	-16.4	-17.0	-17.7
29	58 30.50N	154 47.20W	399.0 y	981765.10	981805.3	-2.7	-13.9	-14.7	-15.4	-16.3	-16.7	-17.2

Table 3 continued

No.	LATITUDE	LONGITUDE	ELEV (FT)	OBSERVED	THEOR	FA	B2.2	B2.35	B2.5	B2.67	B2.75	B2.85
30	58 32.30N	154 51.40W	262.0 y	981775.60	981807.8	-7.5	-14.9	-15.4	-15.9	-16.4	-16.4	-17.0
31	58.34.00N	154 53.80W	237.0 y	981783.10	981810.0	-4.6	-11.3	-11.7	-12.2	-12.7	-13.0	-13.3
32	58 35.50N	154 56.20W	150.0 z	981789.90	981812.0	-8.0	-12.2	-12.5	-12.8	-13.1	-13.3	-13.5
33	58 36.50N	155 0.20W	277.0 y	981787.70	981813.4	0.4	- 7.4	- 7.9	- 8.5	- 9.1	- 9.4	- 9.7
34	58 37.60N	155 5.10W	216.0 y	981794.20	981814.9	-0.3	- 6.4	- 6.8	- 7.2	- 7.7	- 7.9	- 8.2
35	58 39.50N	155 7.30W	109.0 x	981805.50	981817.4	-1.7	- 4.7	- 4.9	- 5.1	- 5.4	- 5.5	- 5.6
36	58 41.30N	155 9.90W	165.0 y	981807.20	981819.8	2.9	- 1.7	- 2.0	- 2.4	- 2.7	- 2.9	- 3.1
37	58 42.20N	155 12.40W	126.0 y	981812.90	981821.0	3.7	0.2	- 0.0	- 0.3	- 0.6	- 0.7	- 0.8
38	57 57.00N	155 7.60W	11.0 x	981780.30	981760.1	21.2	20.9	20.9	20.9	20.8	20.8	20.8
39	57 57.30N	155 11.70W	87.0 y	981771.60	981760.5	19.3	16.8	16.6	16.5	16.3	16.2	16.1
40	57 58.80N	155 16.70W	380.0 z	981749.80	981762.6	23.0	12.3	11.6	10.9	10.0	9.7	9.2
41	57 59.00N	155 21.10W	1307.0 y	981694.80	981762.8	54.9	18.2	15.7	13.2	10.4	9.0	7.4
42	58 0.30N	155 24.90W	350.0 z	981753.80	981764.6	22.1	12.3	11.6	11.0	10.2	9.9	9.4
43	58 3.60N	155 29.30W	916.0 y	981712.40	981769.1	29.5	3.8	2.0	0.3	- 1.7	- 2.6	- 3.8
44	58 4.70N	155 32.40W	2160.0 y	981639.30	981770.6	71.9	11.3	7.1	3.0	- 1.7	- 3.9	- 6.6
45	58 5.40N	155 36.00W	855.0 z	981721.20	981771.5	30.1	6.1	4.5	2.8	1.0	0.1	- 1.0
46	58 6.40N	155 37.80W	800.0 z	981725.50	981772.9	27.9	5.4	3.9	2.4	0.6	- 0.2	- 1.2
47	58 7.40N	155 41.00W	730.0 z	981731.00	981774.2	25.5	5.0	3.6	2.2	0.6	- 0.2	- 1.1
48	58 8.10N	155 42.80W	698.0 z	981736.60	981775.2	27.1	7.5	6.2	4.8	3.3	2.6	1.7
49	58 8.70N	155 44.50W	705.0 y	981738.10	981776.0	28.5	8.7	7.3	6.0	4.4	3.7	2.8
50	58 9.70N	155 48.10W	629.0 y	981748.10	981777.3	30.0	12.3	11.1	9.9	8.5	7.9	7.1
51	58 10.20N	155 52.50W	584.0 y	981758.00	981778.0	34.9	18.5	17.4	16.3	15.0	14.4	13.7
52	58 11.70N	155 55.90W	578.0 y	981763.40	981780.0	37.8	21.5	20.4	19.3	18.1	17.5	16.7
53	58 13.60N	155 59.40W	590.0 y	981773.60	981782.6	46.5	29.9	28.8	27.7	26.4	25.8	25.1
54	58 14.70N	156 7.60W	489.0 y	981799.00	981784.1	60.9	47.2	46.3	45.3	44.3	43.8	43.1
55	58 57.50N	154 58.20W	695.0 y	981786.50	981841.5	10.4	- 9.1	-10.4	-11.8	-13.3	-14.0	-14.9
56	58 56.50N	154 55.50W	618.0 x	981784.50	981840.1	2.5	-14.8	-16.0	-17.2	-18.5	-19.2	-20.0
57	58 53.90N	154 49.90W	670.0 x	981774.70	981836.7	1.1	-17.7	-19.0	-20.3	-21.8	-22.4	-23.3
58	58 52.90N	154 46.50W	650.0 z	981768.10	981835.3	-6.1	-24.4	-25.6	-26.8	-28.3	-28.9	-29.8

Table 3 continued

NO.	LATITUDE	LONGITUDE	ELEV (FT)	OBSERVED	THEOR	FA	B2.2	B2.35	B2.5	B2.67	B2.75	B2.85
59	58 51.70N	154 44.00W	710.0 z	981764.30	981833.7	-2.6	-22.5	-23.9	-25.3	-26.8	-27.5	-28.4
60	58 50.40N	154 42.60W	820.0±50	981755.60	981832.0	0.7	-22.3	-23.8	-25.4	-27.2	-28.0	-29.1
61	58 48.60N	154 39.00W	1880.0±50	981702.80	981829.6	50.1	- 2.7	- 6.3	- 9.9	-14.0	-15.9	-18.3
62	58 46.70N	154 38.30W	2650.0±50	981661.80	981827.0	84.0	9.6	4.6	- 0.5	- 6.2	- 9.0	-12.4
63	58 44.20N	154 34.40W	1710.0 z	981708.00	981823.7	45.1	- 2.9	- 6.1	- 9.4	-13.1	-14.9	-17.1
64	58 42.00N	154 27.20W	940.0 z	981742.60	981820.8	10.3	-16.1	-17.9	-19.7	-21.8	-22.7	-23.9
65	58 43.90N	154 21.50W	560.0 z	981774.20	981823.3	3.6	-12.1	-13.2	-14.3	-15.5	-16.1	-16.8
66	58 40.40N	154 18.40W	680.0 z	981750.90	981818.6	-3.8	-22.8	-24.1	-25.4	-26.9	-27.6	-28.5
67	58 38.80N	154 16.80W	875.0 y	981733.60	981816.5	-0.6	-25.1	-26.8	-28.5	-30.4	-31.3	-32.4
68	58 36.90N	154 11.90W	707.0 y	981751.30	981813.9	3.9	-16.0	-17.3	-18.7	-20.2	-20.9	-21.8
69	58 35.30N	154 6.10W	547.0 y	981760.60	981811.8	0.3	-15.1	-16.1	-17.2	-18.4	-18.9	-19.6
70	58 34.00N	153 59.90W	208.0 y	981788.90	981810.0	-1.6	- 7.4	- 7.8	- 8.2	- 8.6	- 8.9	- 9.1
71	58 33.20N	153 54.70W	28.0 y	981809.80	981809.0	3.5	2.7	2.6	2.6	2.5	2.5	2.5
72	58 34.20N	154 2.70W	340.0 z	981770.20	981810.3	-8.1	-17.7	-18.3	-19.0	-19.7	-20.1	-20.5
73	58 33.20N	154 4.30W	1111.0 y	981732.70	981809.0	28.2	- 2.9	- 5.1	- 7.2	- 9.6	-10.7	-12.2
74	58 30.50N	154 7.10W	69.0 y	981793.20	981805.3	-5.6	- 7.6	- 7.7	- 7.8	- 8.0	- 8.1	- 8.2
75	58 28.00N	154 6.10W	40.0 z	981799.80	981802.0	1.6	0.5	0.4	0.3	0.2	0.2	0.1
76	58 26.20N	154 8.10W	55.0 y	981799.10	981799.6	4.7	3.2	3.1	3.0	2.8	2.8	2.7
77	58 24.00N	154 9.50W	140.0 z	981788.10	981796.6	4.7	0.7	0.5	0.2	- 0.1	- 0.2	- 0.4
78	58 23.00N	154 9.40W	111.0 y	981786.30	981795.3	1.5	- 1.6	- 1.8	- 2.1	- 2.3	- 2.4	- 2.6
79	58 20.20N	154 9.80W	9.0 x	981802.70	981791.5	12.1	11.8	11.8	11.8	11.8	11.7	11.7
80	58 15.70N	154 10.10W	12.0 x	981796.50	981785.4	12.2	11.9	11.9	11.8	11.8	11.8	11.8

Table 3 continued

STATION		LATITUDE	LONGITUDE	ELEV(FT)	Q	OBSERVED	NORMAL	F.AIR	B 2.20	2.30	2.50	2.60	2.67	2.75	2.80	2.85	2.90
K02-23	81	58 42.30N	155 15.00W	186.0	Y	981813.3	981821.2	9.6	4.4	4.2	3.7	3.5	3.3	3.1	3.0	2.9	2.7
K02-24	82	58 43.10N	155 17.70W	250.0	Z	981816.3	981822.2	17.6	10.6	10.2	9.6	9.3	9.1	8.8	8.6	8.5	8.3
K02-25	83	58 43.20N	155 18.10W	245.0	Y	981819.3	981822.4	20.0	13.1	12.8	12.2	11.8	11.6	11.4	11.2	11.1	10.9
K02-26	84	58 43.60N	155 21.10W	297.0	Y	981823.4	981822.9	28.4	20.1	19.7	19.0	18.6	18.3	18.0	17.8	17.6	17.4
K02-27	85	58 43.20N	155 29.50W	108.0	X	981829.7	981822.4	17.5	14.5	14.3	14.0	13.9	13.8	13.7	13.6	13.6	13.5
KNM-01	86	58 1.40N	155 5.60W	51.0	Y	981774.8	981766.1	13.5	12.1	12.0	11.9	11.8	11.8	11.7	11.7	11.7	11.6
KNM-02	87	58 1.90N	155 14.20W	181.0	Y	981760.1	981766.8	10.4	5.3	5.0	4.6	4.3	4.2	4.0	3.9	3.8	3.7
KNM-03	88	58 4.20N	155 13.20W	396.0	Y	981743.5	981769.9	10.9	-0.3	-0.8	-1.8	-2.3	-2.6	-3.0	-3.3	-3.5	-3.8
KNM-04	89	58 6.80N	155 17.80W	1278.0	Y	981688.8	981773.4	35.6	-0.3	-1.9	-5.2	-6.8	-8.0	-9.3	-10.1	-10.9	-11.7
KNM-05	90	58 7.60N	155 14.30W	1309.0	Y	981685.7	981774.5	34.3	-2.4	-4.1	-7.4	-9.1	-10.3	-11.6	-12.5	-13.3	-14.1
KNM-06	91	58 14.10N	155 22.10W	1820.0	Y	981666.2	981783.3	54.1	3.0	0.7	-4.0	-6.3	-7.9	-9.8	-10.9	-12.1	-13.3
KNM-07	92	58 13.30N	155 29.90W	1014.0	Y	981716.9	981782.2	30.1	1.6	0.3	-2.3	-3.6	-4.5	-5.5	-6.2	-6.8	-7.4
KNM-08	93	58 10.90N	155 27.90W	1555.0	Y	981673.6	981778.9	40.9	-2.8	-4.7	-8.7	-10.7	-12.1	-13.7	-14.7	-15.7	-16.7
KNM-09	94	58 9.30N	155 33.80W	1445.0	Y	981683.8	981776.8	42.9	2.3	0.5	-3.2	-5.0	-6.3	-7.8	-8.7	-9.6	-10.6
KNM-10	95	58 14.00N	155 39.10W	813.0	Y	981734.1	981783.1	27.4	4.6	3.6	1.5	0.5	-0.3	-1.1	-1.6	-2.1	-2.7
KNM-11	96	58 16.80N	155 33.70W	1677.0	Y	981687.9	981786.9	58.7	11.6	9.5	5.2	3.1	1.6	-0.1	-1.2	-2.3	-3.4
KNM-12	97	58 12.60N	155 23.60W	2247.0	Y	981639.3	981781.2	69.4	6.3	3.4	-2.3	-5.2	-7.2	-9.5	-10.9	-12.3	-13.8
KNM-13	98	58 14.90N	155 15.90W	1979.0	Y	981648.7	981784.3	50.5	-5.1	-7.6	-12.7	-15.2	-17.0	-19.0	-20.2	-21.5	-22.8
KNM-14	99	58 16.00N	155 10.40W	2350.0	Y	981622.6	981785.8	57.8	-8.2	-11.2	-17.2	-20.2	-22.3	-24.7	-26.2	-27.7	-29.2

Table 3 continued

STATION	LATITUDE	LONGITUDE	ELEV(FT)	Q	OBSERVED	NORMAL	F.AIR	B 2.20	2.30	2.50	2.60	2.67	2.75	2.80	2.85	2.90
KNS-01 100	58 9.10N	155 1.00W	210.0	Z	981763.1	981776.5	6.3	0.4	0.2	-0.4	-0.6	-0.8	-1.0	-1.2	-1.3	-1.4
KNS-02 101	58 11.10N	154 58.50W	398.0	Y	981753.6	981779.2	11.8	0.6	0.1	-0.9	-1.4	-1.7	-2.1	-2.4	-2.7	-2.9
KNS-03 102	58 13.20N	154 54.50W	875.0	Y	981720.3	981782.0	20.6	-4.0	-5.1	-7.4	-8.5	-9.3	-10.2	-10.7	-11.3	-11.8
KNS-04 103	58 13.50N	154 49.90W	1136.0	Y	981708.2	981782.4	32.6	0.7	-0.8	-3.7	-5.1	-6.1	-7.3	-8.0	-8.7	-9.5
KNS-05 104	58 13.10N	154 42.70W	1566.0	Y	981681.6	981781.9	47.0	3.0	1.0	-3.0	-5.0	-6.4	-8.0	-9.0	-10.0	-11.0
KNS-06 105	58 10.00N	154 41.70W	461.0	Y	981751.5	981777.7	17.1	4.2	3.6	2.4	1.8	1.4	1.0	0.7	0.4	0.1
KNS-07 106	58 10.10N	154 34.40W	416.0	Y	981752.5	981777.9	13.8	2.1	1.6	0.5	-0.0	-0.4	-0.8	-1.1	-1.4	-1.6
KNS-08 107	58 9.80N	154 33.50W	275.0	Y	981761.0	981777.5	9.4	1.7	1.3	0.6	0.3	0.0	-0.2	-0.4	-0.6	-0.8
KNS-09 108	58 7.30N	154 36.00W	14.0	X	981777.8	981774.1	5.0	4.7	4.6	4.6	4.6	4.6	4.6	4.5	4.5	4.5
KNS-10 109	58 13.00N	154 35.10W	872.0	Y	981727.8	981781.8	28.0	3.6	2.4	0.2	-0.9	-1.7	-2.6	-3.1	-3.7	-4.2
KNS-11 110	58 11.70N	154 29.80W	11.0	X	981780.3	981780.0	1.3	1.0	1.0	1.0	1.0	0.9	0.9	0.9	0.9	0.9
KNS-12 111	58 11.60N	154 26.20W	13.0	Y	981782.8	981779.9	4.1	3.8	3.8	3.7	3.7	3.7	3.7	3.7	3.7	3.7
KNS-13 112	58 17.30N	154 29.80W	387.0	Y	981750.6	981787.6	-0.6	-11.4	-11.9	-12.9	-13.4	-13.8	-14.2	-14.4	-14.7	-14.9
KNS-14 113	58 14.90N	154 21.80W	36.0	Y	981787.3	981784.3	6.3	5.3	5.3	5.2	5.2	5.1	5.1	5.1	5.0	5.0
KNS-15 114	58 11.30N	154 15.80W	10.0	X	981787.4	981779.5	8.9	8.6	8.6	8.5	8.5	8.5	8.5	8.5	8.5	8.5
KNS-16 115	58 8.20N	154 17.20W	9.0	X	981779.1	981775.3	4.7	4.4	4.4	4.4	4.4	4.3	4.3	4.3	4.3	4.3
KNS-17 116	58 9.50N	154 20.10W	14.0	Y	981779.0	981777.0	3.3	2.9	2.9	2.8	2.8	2.8	2.8	2.8	2.8	2.8
KNS-18 117	58 5.20N	154 19.00W	6.0	X	981767.4	981771.2	-3.3	-3.4	-3.4	-3.5	-3.5	-3.5	-3.5	-3.5	-3.5	-3.5
KNS-19 118	58 7.70N.	154 24.30W	6.0	X	981776.8	981774.6	2.8	2.6	2.6	2.6	2.6	2.5	2.5	2.5	2.5	2.5
KNS-20 119	58 5.00N	154 27.90W	4.0	X	981774.1	981771.0	3.5	3.4	3.4	3.4	3.4	3.4	3.4	3.4	3.4	3.4
KNS-21 120	58 1.40N	154 34.10W	101.0	Y	981760.5	981766.1	3.9	1.1	0.9	0.7	0.6	0.5	0.4	0.3	0.2	0.2
KNS-22 121	58 4.00N	154 40.50W	5.0	X	981777.1	981769.6	8.0	7.8	7.8	7.8	7.8	7.8	7.8	7.8	7.8	7.8
KNS-23 122	58 0.90N	154 43.80W	3.0	X	981776.9	981765.4	11.8	11.7	11.7	11.7	11.7	11.7	11.7	11.7	11.7	11.7

Table 3 continued

STATION	LATITUDE	LONGITUDE	ELEV(FT)	Q	OBSERVED	NORMAL	F.AIR	B 2.20	2.30	2.50	2.60	2.67	2.75	2.80	2.85	2.90
K06-01 123	58 41.10N	155 23.00W	144.0	Y	981824.7	981819.6	18.7	14.6	14.5	14.1	13.9	13.8	13.6	13.5	13.5	13.4
K06-02 124	58 39.70N	155 21.80W	231.0	Y	981812.4	981817.7	15.4	10.0	9.7	9.1	8.8	8.6	8.3	8.2	8.0	7.9
K06-03 125	58 38.40N	155 19.80W	44.0	Y	981818.4	981815.9	6.6	5.4	5.3	5.2	5.1	5.1	5.1	5.0	5.0	5.0
K06-04 126	58 37.50N	155 18.10W	39.0	Y	981811.5	981814.7	0.4	-0.7	-0.7	-0.8	-0.9	-0.9	-0.9	-1.0	-1.0	-1.0
K06-05 127	58 36.10N	155 17.00W	46.0	Y	981804.0	981812.9	-4.5	-5.8	-5.9	-6.0	-6.1	-6.1	-6.1	-6.2	-6.2	-6.2
K06-06 128	58 33.90N	155 14.20W	55.0	Y	981796.9	981809.9	-7.8	-9.4	-9.4	-9.6	-9.7	-9.7	-9.8	-9.8	-9.8	-9.9
K06-07 129	58 31.70N	155 9.60W	61.0	Y	981790.8	981807.0	-10.4	-12.1	-12.2	-12.4	-12.4	-12.5	-12.6	-12.6	-12.6	-12.7
K06-08 130	58 28.10N	155 6.50W	735.0	Y	981741.5	981802.1	8.5	-12.1	-13.1	-14.9	-15.9	-16.5	-17.3	-17.8	-18.2	-18.7
K06-09 131	58 24.80N	155 1.60W	840.0	Z	981724.6	981797.7	5.9	-17.7	-18.7	-20.9	-22.0	-22.7	-23.6	-24.1	-24.6	-25.2
K06-10 132	58 22.60N	154 59.30W	1105.0	Y	981707.0	981794.7	16.2	-14.8	-16.2	-19.1	-20.5	-21.5	-22.6	-23.3	-24.0	-24.7
K06-11 133	58 19.70N	154 59.20W	1623.0	Y	981673.2	981790.8	35.0	-10.5	-12.6	-16.8	-18.8	-20.3	-21.9	-23.0	-24.0	-25.0
KHL 134	58 25.90N	154 57.90W	1719.0	Y	981680.0	981799.2	42.5	-5.8	-7.9	-12.3	-14.5	-16.1	-17.8	-18.9	-20.0	-21.1
K07-01 135	58 28.60N	154 4.50W	14.0	X	981798.1	981802.8	-3.4	-3.8	-3.8	-3.8	-3.8	-3.8	-3.9	-3.9	-3.9	-3.9
K07-02 136	58 31.00N	154 13.30W	321.0	Y	981766.8	981806.0	-9.0	-18.0	-18.4	-19.3	-19.7	-20.0	-20.3	-20.5	-20.7	-20.9
K07-03 137	58 30.80N	154 17.80W	634.0	Y	981747.1	981805.7	1.0	-16.8	-17.6	-19.2	-20.1	-20.6	-21.3	-21.7	-22.1	-22.5
K07-04 138	58 30.10N	154 21.30W	2300.0E100		981637.7	981804.8	49.2	-15.4	-18.3	-24.2	-27.1	-29.2	-31.5	-33.0	-34.5	-35.9
K07-05 139	58 31.70N	154 26.40W	885.0	Y	981730.8	981807.0	7.1	-17.8	-18.9	-21.2	-22.3	-23.1	-24.0	-24.5	-25.1	-25.7
K07-06 140	58 32.70N	154 28.40W	723.0	Y	981741.8	981808.3	1.5	-18.8	-19.7	-21.6	-22.5	-23.1	-23.9	-24.3	-24.8	-25.3
K07-07 141	58 34.70N	154 29.90W	554.0	Y	981754.9	981811.0	-4.0	-19.5	-20.2	-21.7	-22.4	-22.9	-23.4	-23.8	-24.1	-24.5
K07-08 142	58 36.40N	154 36.20W	412.0	Y	981765.7	981813.3	-8.3	-20.4	-20.9	-22.0	-22.5	-22.8	-23.3	-23.5	-23.8	-24.1
K07-09 143	58 37.70N	154 40.90W	553.0	Y	981760.9	981815.0	-2.1	-17.6	-18.3	-19.7	-20.4	-20.9	-21.5	-21.9	-22.2	-22.6
K07-10 144	58 37.70N	154 46.70W	379.0	Y	981775.7	981815.0	-3.7	-14.3	-14.8	-15.7	-16.2	-16.6	-17.0	-17.2	-17.4	-17.7

Table 3 continued

STATION	LATITUDE	LONGITUDE	ELEV(FT)	Q	OBSERVED	NORMAL	F.AIR B	2.20	2.30	2.50	2.60	2.67	2.75	2.80	2.85	2.90
K07-11 145	58 40.20N	154 49.60W	740.0	Y	981761.6	981818.3	12.9	-7.9	-8.9	-10.8	-11.7	-12.4	-13.1	-13.6	-14.1	-14.5
K07-12 146	58 42.50N	154 55.30W	1640.0	Z	981722.2	981821.4	55.0	9.0	6.9	2.7	0.6	-0.9	-2.6	-3.6	-4.6	-5.7
K07-13 147	58 44.50N	154 57.50W	1880.0	Z	981711.8	981824.1	64.5	11.7	9.3	4.5	2.1	0.4	-1.5	-2.7	-3.9	-5.1
K07-14 148	58 45.20N	154 59.50W	1847.0	Y	981713.1	981825.0	61.8	9.9	7.5	2.8	0.5	-1.2	-3.1	-4.2	-5.4	-6.6
K07-15 149	58 46.30N	155 1.80W	1648.0	Y	981728.2	981826.5	56.7	10.4	8.3	4.1	2.0	0.5	-1.2	-2.2	-3.3	-4.3
K07-16 150	58 47.90N	155 5.10W	1648.0	Y	981732.9	981828.6	59.3	13.0	10.9	6.7	4.6	3.1	1.4	0.3	-0.7	-1.8
K07-17 151	58 50.40N	155 7.00W	1603.0	Y	981737.8	981832.0	56.6	11.6	9.5	5.4	3.4	1.9	0.3	-0.7	-1.7	-2.8
K07-18 152	58 52.70N	155 9.50W	1624.0	Y	981737.3	981835.1	55.0	9.4	7.3	3.2	1.1	-0.4	-2.0	-3.1	-4.1	-5.1
K08-01 153	58 36.90N	153 39.60W	46.0	Z	981822.6	981813.9	13.0	11.7	11.6	11.5	11.5	11.4	11.4	11.4	11.3	11.3
K08-02 154	58 39.90N	153 44.00W	160.0	Z	981819.9	981817.9	17.0	12.5	12.3	11.9	11.7	11.5	11.4	11.3	11.2	11.1
K08-03 155	58 41.90N	153 44.80W	400.0	Z	981800.6	981820.6	17.6	6.4	5.9	4.8	4.3	4.0	3.6	3.3	3.0	2.8
K08-04 156	58 44.40N	153 46.90W	1665.0	Z	981723.5	981824.0	56.1	9.4	7.2	3.0	0.9	-0.6	-2.3	-3.4	-4.4	-5.5
K08-05 157	58 44.10N	153 53.20W	1098.0	Z	981753.4	981823.6	33.1	2.3	0.9	-1.9	-3.3	-4.3	-5.4	-6.1	-6.8	-7.5
K08-06 158	58 47.80N	153 58.50W	700.0	Z	981769.9	981828.5	7.2	-12.4	-13.3	-15.1	-16.0	-16.6	-17.4	-17.8	-18.2	-18.7
K08-07 159	58 46.70N	154 3.80W	485.0	Y	981779.2	981827.0	-2.2	-15.8	-16.5	-17.7	-18.3	-18.8	-19.3	-19.6	-19.9	-20.2
K08-08 160	58 49.90N	154 8.70W	245.0	Y	981800.2	981831.3	-8.1	-15.0	-15.3	-15.9	-16.2	-16.4	-16.7	-16.8	-17.0	-17.1
K08-09 161	58 51.90N	154 12.90W	148.0	Y	981813.7	981834.0	-6.4	-10.5	-10.7	-11.1	-11.3	-11.4	-11.6	-11.7	-11.8	-11.8
K08-10 162	58 54.50N	154 18.70W	210.0	Y	981815.3	981837.5	-2.4	-8.3	-8.6	-9.1	-9.4	-9.6	-9.8	-9.9	-10.0	-10.2
K08-11 163	58 55.30N	154 26.70W	1415.0	Y	981745.4	981838.5	40.0	0.2	-1.6	-5.2	-7.0	-8.3	-9.7	-10.6	-11.5	-12.4
K08-12 164	58 57.30N	154 31.00W	790.0	Z	981790.6	981841.2	23.7	1.5	0.5	-1.5	-2.5	-3.2	-4.0	-4.5	-5.0	-5.5
K08-13 165	58 58.40N	154 35.20W	1700.0	Z	981741.2	981842.7	58.4	10.7	8.5	4.2	2.0	0.5	-1.2	-2.3	-3.4	-4.5
K08-14 166	58 59.50N	154 36.30W	620.0	Z	981810.9	981844.1	25.1	7.7	6.9	5.3	4.5	4.0	3.3	2.9	2.5	2.1
KLI 167	59 22.20N	155 22.70W	43.0	Z	981893.6	981874.2	23.4	22.2	22.1	22.0	22.0	21.9	21.9	21.9	21.8	21.8

Table 3 continued

STATION	LATITUDE	LONGITUDE	ELEV(FT)	Q	OBSERVED	NORMAL	F.AIR B	2.20	2.30	2.50	2.60	2.67	2.75	2.80	2.85	2.90
K09-01 168	58 41.50N	153 32.30W	16.0	X	981830.3	981820.1	11.7	11.3	11.2	11.2	11.2	11.2	11.2	11.1	11.1	11.1
K09-02 169	58 44.50N	153 24.30W	24.0	Y	981832.2	981824.1	10.4	9.7	9.6	9.6	9.6	9.5	9.5	9.5	9.5	9.5
K09-03 170	58 51.10N	153 19.70W	15.0	X	981843.9	981832.9	12.4	12.0	11.9	11.9	11.9	11.9	11.9	11.9	11.8	11.8
K09-04 171	58 55.90N	153 22.40W	14.0	X	981855.5	981839.3	17.5	17.1	17.1	17.0	17.0	17.0	17.0	17.0	17.0	17.0
K09-05 172	58 58.50N	153 25.70W	13.0	X	981856.4	981842.8	14.8	14.5	14.5	14.4	14.4	14.4	14.4	14.4	14.4	14.4
K09-06 173	58 59.80N	153 28.70W	47.0	X	981852.0	981844.5	11.9	10.6	10.5	10.4	10.3	10.3	10.3	10.2	10.2	10.2
K09-07 174	59 0.50N	153 37.20W	44.0	Y	981844.4	981845.5	3.1	1.9	1.8	1.7	1.6	1.6	1.5	1.5	1.5	1.5
K09-08 175	59 3.10N	153 44.50W	41.0	Y	981846.2	981848.9	1.1	-0.0	-0.1	-0.2	-0.2	-0.3	-0.3	-0.3	-0.3	-0.4
K09-09 176	59 3.30N	153 51.50W	41.0	Y	981846.3	981849.2	1.0	-0.2	-0.2	-0.3	-0.4	-0.4	-0.5	-0.5	-0.5	-0.5
K09-10 177	59 3.70N	153 55.30W	39.0	Y	981847.0	981849.7	1.0	-0.1	-0.2	-0.3	-0.3	-0.4	-0.4	-0.4	-0.5	-0.5
K09-11 178	59 4.60N	154 0.80W	30.0	Y	981849.4	981850.9	1.3	0.5	0.4	0.4	0.3	0.3	0.3	0.2	0.2	0.2
K09-12 179	59 2.70N	154 6.50W	40.0	Y	981843.5	981848.4	-1.1	-2.2	-2.3	-2.4	-2.4	-2.5	-2.5	-2.5	-2.6	-2.6
K09-13 180	59 4.10N	154 10.80W	38.0	Y	981848.9	981850.2	2.2	1.2	1.1	1.0	1.0	0.9	0.9	0.9	0.9	0.8
K09-14 181	59 7.00N	154 14.50W	35.0	Y	981854.7	981854.1	3.9	2.9	2.9	2.8	2.7	2.7	2.7	2.6	2.6	2.6
K09-15 182	59 9.50N	154 20.30W	134.0	Y	981858.5	981857.4	13.7	9.9	9.8	9.4	9.2	9.1	9.0	8.9	8.8	8.7
K09-16 183	59 10.10N	154 25.70W	338.0	Z	981869.0	981858.2	42.6	33.1	32.7	31.8	31.4	31.1	30.7	30.5	30.3	30.1
K09-17 184	59 11.70N	154 30.00W	459.0	Y	981862.2	981860.3	45.0	32.1	31.6	30.4	29.8	29.4	28.9	28.6	28.3	28.0
K09-18 185	59 14.20N	154 30.90W	530.0	Y	981867.4	981863.6	53.6	38.7	38.0	36.7	36.0	35.5	35.0	34.7	34.3	34.0
K09-19 186	59 17.30N	154 31.80W	510.0	Y	981874.1	981867.8	54.3	40.0	39.3	38.0	37.4	36.9	36.4	36.1	35.8	35.4
K09-20 187	59 20.10N	154 34.40W	204.0	Y	981879.3	981871.5	27.0	21.3	21.0	20.5	20.3	20.1	19.9	19.7	19.6	19.5
K09-21 188	59 21.10N	154 39.10W	180.0	Y	981879.2	981872.8	23.3	18.3	18.1	17.6	17.4	17.2	17.0	16.9	16.8	16.7
K09-22 189	59 23.00N	154 46.90W	181.0	Y	981898.0	981875.3	39.7	34.6	34.4	34.0	33.7	33.6	33.4	33.3	33.1	33.0
K09-23 190	59 26.20N	154 51.00W	54.0	Z	981892.2	981879.5	17.8	16.2	16.2	16.0	16.0	15.9	15.9	15.8	15.8	15.8

Table 3 continued

STATION	LATITUDE	LONGITUDE	ELEV(FT)	Q	OBSERVED	NORMAL	F.AIR	B 1.40	1.60	1.80	1.90	2.00	2.20	2.40	2.67	2.85
K A-01 201	58 22.00N	155 21.10W	875.0	Y	981735.4	981793.9	23.8	8.2	5.9	3.7	2.6	1.4	-0.8	-3.0	-6.0	-8.0
K A-02 202	58 22.00N	155 21.10W	793.0	Y	981740.7	981793.9	21.4	7.2	5.2	3.2	2.1	1.1	-0.9	-2.9	-5.7	-7.5
K A-03 203	58 22.10N	155 21.00W	875.0	Y	981734.9	981794.0	23.2	7.5	5.3	3.0	1.9	0.8	-1.4	-3.7	-6.7	-8.7
KV1-01 204	58 17.60N	155 12.50W	2063.0	Y	981646.6	981788.0	52.7	15.8	10.5	5.3	2.6	-0.0	-5.3	-10.6	-17.7	-22.4
KV1-02 205	58 17.60N	155 12.50W	2034.0	Y	981647.8	981788.0	51.1	14.8	9.6	4.4	1.8	-0.8	-6.0	-11.2	-18.2	-22.9
KV1-03 206	58 17.60N	155 12.70W	2003.0	Y	981649.5	981788.0	49.9	14.1	9.0	3.9	1.3	-1.2	-6.3	-11.5	-18.4	-23.0
KV1-04 207	58 17.60N	155 12.70W	1967.0	Y	981651.9	981788.0	48.9	13.8	8.8	3.7	1.2	-1.3	-6.3	-11.3	-18.1	-22.8
KV1-05 208	58 17.60N	155 12.80W	1909.0	Y	981655.5	981788.0	47.1	13.0	8.1	3.2	0.8	-1.7	-6.5	-11.4	-18.0	-22.4
KV1-06 209	58 17.60N	155 12.90W	1871.0	Y	981657.6	981788.0	45.6	12.2	7.4	2.6	0.2	-2.2	-7.0	-11.7	-18.2	-22.5
KV1-07 210	58 17.60N	155 13.00W	1850.0	Z	981658.6	981788.0	44.6	11.6	6.8	2.1	-0.2	-2.6	-7.3	-12.1	-18.4	-22.7
KV1-08 211	58 17.60N	155 13.00W	1841.0	Y	981659.1	981788.0	44.3	11.4	6.7	2.0	-0.4	-2.7	-7.4	-12.1	-18.5	-22.7
KV1-09 212	58 17.60N	155 13.10W	1816.0	Y	981660.1	981788.0	42.9	10.5	5.8	1.2	-1.1	-3.4	-8.1	-12.7	-19.0	-23.2
KV1-10 213	58 17.60N	155 13.20W	1806.0	Y	981660.6	981788.0	42.5	10.2	5.6	1.0	-1.3	-3.6	-8.2	-12.9	-19.1	-23.2
KV1-11 214	58 17.60N	155 13.30W	1801.0	Y	981660.9	981788.0	42.3	10.1	5.5	0.9	-1.4	-3.7	-8.3	-12.9	-19.1	-23.2
KV1-12 215	58 17.60N	155 13.50W	1786.0	Y	981661.9	981788.0	41.9	10.0	5.4	0.9	-1.4	-3.7	-8.3	-12.8	-19.0	-23.1
KV1-13 216	58 17.60N	155 13.80W	1767.0	Y	981662.0	981788.0	40.2	8.6	4.1	-0.4	-2.6	-4.9	-9.4	-13.9	-20.0	-24.1
KV1-14 217	58 17.60N	155 14.00W	1764.0	Y	981662.7	981788.0	40.6	9.1	4.6	0.1	-2.2	-4.4	-8.9	-13.4	-19.5	-23.5
KV1-15 218	58 17.60N	155 14.30W	1763.0	Y	981662.4	981788.0	40.2	8.7	4.2	-0.3	-2.5	-4.8	-9.3	-13.8	-19.9	-23.9
KV1-16 219	58 17.60N	155 14.50W	1761.0	Y	981663.0	981788.0	40.7	9.2	4.7	0.2	-2.1	-4.3	-8.8	-13.3	-19.4	-23.4
KV1-17 220	58 17.60N	155 14.70W	1764.0	Y	981663.3	981788.0	41.2	9.7	5.2	0.7	-1.6	-3.8	-8.3	-12.8	-18.9	-22.9
KV1-18 221	58 17.60N	155 14.90W	1770.0	Z	981662.5	981788.0	41.0	9.4	4.8	0.3	-1.9	-4.2	-8.7	-13.2	-19.3	-23.4
KV1-19 222	58 17.60N	155 15.10W	1788.0	Z	981662.3	981788.0	42.5	10.5	6.0	1.4	-0.9	-3.2	-7.7	-12.3	-18.5	-22.6
KV1-20 223	58 17.60N	155 15.40W	1810.0	Z	981662.0	981788.0	44.5	11.9	7.3	2.7	0.4	-2.0	-6.6	-11.2	-17.4	-21.6
KV1-21 224	58 17.60N	155 15.70W	1860.0	Z	981659.7	981788.0	46.7	13.4	8.7	3.9	1.5	-0.8	-5.6	-10.3	-16.7	-21.0
KV1-22 225	58 17.60N	155 15.90W	1975.0	Y	981652.3	981788.0	50.1	14.8	9.7	4.7	2.2	-0.3	-5.4	-10.4	-17.2	-21.8
KV1-23 226	58 17.60N	155 16.00W	2010.0	Z	981650.6	981788.0	51.7	15.8	10.6	5.5	2.9	0.4	-4.8	- 9.9	-16.8	-21.5

Table 3 continued

STATION	LATITUDE	LONGITUDE	ELEV(FT)	Q	OBSERVED	NORMAL	F.AIR	B 1.40	1.60	1.80	1.90	2.00	2.20	2.40	2.67	2.85
KV2-01 227	58 17.70N	155 11.90W	2548.0	Y	981615.4	981789.1	66.9	21.4	14.9	8.4	5.1	1.9	-4.6	-11.1	-19.9	-25.8
KV2-02 228	58 17.70N	155 11.90W	2498.0	Y	981618.6	981788.1	65.4	20.8	14.4	8.0	4.8	1.7	-4.7	-11.1	-19.7	-25.5
KV2-03 229	58 17.70N	155 11.80W	2452.0	Y	981622.2	981783.1	64.7	20.9	14.6	8.4	5.2	2.1	-4.2	-10.4	-18.9	-24.5
KV2-04 230	58 17.80N	155 11.80W	2185.0	Y	981638.5	981788.2	55.8	16.7	11.1	5.6	2.8	-0.0	-5.6	-11.2	-18.7	-23.7
KV2-05 231	58 17.90N	155 11.70W	2165.0	Y	981640.5	981788.4	55.8	17.1	11.5	6.0	3.2	0.5	-5.1	-10.6	-18.1	-23.0
KV2-06 232	58 17.90N	155 11.70W	2154.0	Y	981640.9	981788.4	55.1	16.6	11.1	5.6	2.9	0.1	-5.4	-10.9	-18.3	-23.3
KV2-07 233	58 18.00N	155 11.60W	2141.0	Y	981641.7	981788.5	54.6	16.3	10.8	5.4	2.6	-0.1	-5.6	-11.0	-18.4	-23.3
KV2-08 234	58 18.10N	155 11.60W	2123.0	Y	981642.8	981788.7	53.8	15.9	10.5	5.0	2.3	-0.4	-5.8	-11.2	-18.5	-23.4
KV2-09 235	58 18.10N	155 11.50W	2117.0	Y	981643.3	981788.7	53.8	15.9	10.5	5.1	2.4	-0.3	-5.7	-11.1	-18.4	-23.3
KV2-10 236	58 18.20N	155 11.50W	2114.0	Y	981644.0	981788.8	54.1	16.3	10.9	5.5	2.8	0.1	-5.3	-10.7	-18.0	-22.9
KV2-11 237	58 18.20N	155 11.50W	2132.0	Y	981642.9	981788.8	54.6	16.5	11.1	5.6	2.9	0.2	-5.2	-10.7	-18.0	-22.9
KV2-12 238	58 18.30N	155 11.40W	2190.0	Y	981639.2	981788.9	56.3	17.1	11.5	5.9	3.1	0.3	-5.2	-10.8	-18.4	-23.4
KV2-13 239	58 18.40N	155 11.30W	2232.0	Y	981636.5	981789.1	57.4	17.5	11.8	6.1	3.2	0.4	-5.3	-11.0	-18.7	-23.8
KV2-14 240	58 18.40N	155 11.30W	2014.0	Y	981650.0	981789.1	50.4	14.4	9.2	4.1	1.5	-1.1	-6.2	-11.3	-18.3	-22.9
KV2-15 241	58 18.40N	155 11.20W	1962.0	Y	981653.1	981789.1	48.6	13.5	8.5	3.5	1.0	-1.5	-6.5	-11.5	-18.3	-22.8
KV2-16 242	58 18.50N	155 11.20W	1923.0	Y	981654.7	981789.2	46.4	12.0	7.1	2.2	-0.3	-2.7	-7.6	-12.5	-19.2	-23.6
KV2-17 243	58 18.60N	155 11.10W	1902.0	Y	981655.5	981789.3	45.1	11.1	6.2	1.4	-1.1	-3.5	-8.4	-13.2	-19.8	-24.1
KV2-18 244	58 18.70N	155 11.10W	1889.0	Y	981656.5	981789.5	44.7	10.9	6.1	1.3	-1.1	-3.5	-8.3	-13.2	-19.7	-24.0
KV2-19 245	58 18.70N	155 11.00W	1857.0	Y	981657.7	981789.5	42.9	9.7	5.0	0.2	-2.1	-4.5	-9.3	-14.0	-20.4	-24.7
KV2-20 246	58 18.80N	155 11.00W	1850.0	Y	981657.0	981789.6	41.4	8.3	3.6	-1.1	-3.5	-5.8	-10.6	-15.3	-21.7	-25.9
KV2-21 247	58 18.90N	155 10.90W	1847.0	Y	981657.5	981789.7	41.5	8.5	3.8	-1.0	-3.3	-5.7	-10.4	-15.1	-21.5	-25.7
KV2-22 248	58 19.00N	155 10.80W	1860.0	Y	981657.2	981789.9	42.3	9.0	4.3	-0.5	-2.8	-5.2	-10.0	-14.7	-21.1	-25.4
KV2-23 249	58 19.20N	155 10.70W	1860.0	Y	981658.5	981790.1	43.3	10.1	5.3	0.6	-1.8	-4.2	-8.9	-13.7	-20.1	-24.4

Table 3 continued

STATION	LATITUDE	LONGITUDE	ELEV(FT)	Q	OBSERVED	NORMAL	F.AIR	B 1.40	1.60	1.80	1.90	2.00	2.20	2.40	2.67	2.85
KV2-24 250	58 19.30N	155 10.60W	1855.0	Y	981659.4	981790.3	43.6	10.5	5.7	1.0	-1.4	-3.8	-8.5	-13.2	-19.6	-23.9
KV2-25 251	58 19.40N	155 10.50W	1869.0	Y	981659.2	981790.4	44.6	11.2	6.4	1.6	-0.7	-3.1	-7.9	-12.7	-19.1	-23.4
KV2-26 252	58 19.60N	155 10.40W	1865.0	Y	981659.2	981790.7	43.9	10.6	5.8	1.0	-1.3	-3.7	-8.5	-13.3	-19.7	-24.0
KV2-27 253	58 19.60N	155 10.40W	1874.0	Y	981659.2	981790.7	44.8	11.3	6.5	1.7	-0.7	-3.1	-7.8	-12.6	-19.1	-23.4
KV2-28 254	58 19.70N	155 10.30W	1887.0	Y	981658.1	981790.8	44.8	11.0	6.2	1.4	-1.0	-3.4	-8.2	-13.0	-19.5	-23.9
KV3-01 255	58 16.40N	155 11.00W	2400.0	Y	981622.3	981786.4	61.7	18.8	12.7	6.5	3.5	0.4	-5.7	-11.9	-20.1	-25.7
KV3-02 256	58 16.40N	155 11.00W	2380.0	Y	981623.3	981786.4	60.8	18.3	12.2	6.1	3.1	0.0	-6.1	-12.1	-20.3	-25.8
KV3-03 257	58 16.30N	155 10.90W	2360.0	Y	981623.5	981786.2	59.3	17.1	11.0	5.0	2.0	-1.0	-7.0	-13.1	-21.2	-26.6
KV3-04 258	58 16.20N	155 10.90W	2348.0	Y	981624.1	981786.1	58.9	16.9	10.9	4.9	1.9	-1.1	-7.1	-13.1	-21.2	-26.6
KV3-05 259	58 16.20N	155 10.90W	2341.0	Y	981624.0	981786.1	58.1	16.3	10.3	4.3	1.3	-1.7	-7.7	-13.6	-21.7	-27.1
KV3-06 260	58 16.10N	155 10.80W	2345.0	Y	981623.3	981786.0	57.9	16.0	10.0	4.0	1.0	-2.0	-8.0	-13.9	-22.0	-27.4
KV3-07 261	58 16.10N	155 10.60W	2332.0	Y	981622.9	981786.0	56.3	14.6	8.6	2.7	-0.3	-3.3	-9.2	-15.2	-23.2	-28.6
KV3-08 262	58 16.00N	155 10.80W	2332.0	Y	981622.3	981785.8	55.8	14.1	8.2	2.2	-0.7	-3.7	-9.7	-15.6	-23.7	-29.0
KV3-09 263	58 15.90N	155 10.70W	2334.0	Y	981621.3	981785.7	55.1	13.4	7.5	1.5	-1.5	-4.5	-10.4	-16.4	-24.4	-29.8
KV3-10 264	58 15.90N	155 10.70W	2338.0	Y	981620.7	981785.7	54.9	13.1	7.2	1.2	-1.8	-4.8	-10.8	-16.7	-24.8	-30.2
KV3-11 265	58 15.80N	155 10.70W	2348.0	Y	981619.5	981785.6	54.8	12.8	6.8	0.8	-2.2	-5.2	-11.2	-17.2	-25.2	-30.6
KV3-12 266	58 15.80N	155 10.60W	2352.0	Y	981617.7	981785.6	53.4	11.3	5.3	-0.7	-3.7	-6.7	-12.7	-18.7	-26.8	-32.2
KV3-13 267	58 15.70N	155 10.60W	2400.0	Y	981613.8	981785.4	54.1	11.2	5.1	-1.0	-4.1	-7.2	-13.3	-19.4	-27.7	-33.2
KV4-01 268	58 20.40N	155 17.70W	1274.0	Y	981700.4	981791.8	28.5	5.7	2.5	-0.8	-2.4	-4.1	-7.3	-10.6	-15.0	-17.9
KV4-02 269	58 20.50N	155 17.60W	1269.0	Y	981700.2	981791.9	27.7	5.0	1.7	-1.5	-3.1	-4.7	-8.0	-11.2	-15.6	-18.5
KV4-03 270	58 20.60N	155 17.50W	1273.0	Y	981699.0	981792.0	26.7	4.0	0.7	-2.5	-4.2	-5.8	-9.0	-12.3	-16.7	-19.6

Table 3 continued

STATION	LATITUDE	LONGITUDE	ELEV(FT)	Q	OBSERVED	NORMAL	F.AIR	B 1.40	1.60	1.80	1.90	2.00	2.20	2.40	2.67	2.85
KV4-04 271	58 20.60N	155 17.40W	1275.0	Y	981699.0	981792.0	26.9	4.1	0.9	-2.4	-4.0	-5.7	-8.9	-12.2	-16.6	-19.5
KV4-05 272	58 20.70N	155 17.20W	1292.0	Y	981698.2	981792.2	27.6	4.5	1.2	-2.1	-3.8	-5.4	-8.7	-12.0	-16.5	-19.4
KV4-06 273	58 20.80N	155 17.10W	1285.0	Y	981698.5	981792.3	27.1	4.1	0.8	-2.5	-4.1	-5.7	-9.0	-12.3	-16.7	-19.7
KV4-07 274	58 20.80N	155 17.00W	1290.0	Y	981698.1	981792.3	27.1	4.1	0.8	-2.5	-4.1	-5.8	-9.1	-12.4	-16.8	-19.8
KV4-08 275	58 20.90N	155 16.90W	1293.0	Y	981698.1	981792.4	27.3	4.2	0.9	-2.4	-4.1	-5.7	-9.0	-12.3	-16.8	-19.8
KV4-09 276	58 20.90N	155 16.80W	1295.0	Y	981698.3	981792.4	27.7	4.5	1.2	-2.1	-3.7	-5.4	-8.7	-12.0	-16.5	-19.4
KV4-10 277	58 21.00N	155 16.70W	1309.0	Y	981698.1	981792.6	28.7	5.3	1.9	-1.4	-3.1	-4.8	-8.1	-11.4	-16.0	-19.0
KV4-11 278	58 21.10N	155 16.60W	1310.0	Y	981697.8	981792.7	28.3	4.9	1.6	-1.8	-3.5	-5.1	-8.5	-11.8	-16.3	-19.3
KV4-12 279	58 21.20N	155 16.40W	1316.0	Y	981697.7	981792.8	28.7	5.1	1.8	-1.6	-3.3	-5.0	-8.3	-11.7	-16.2	-19.2
KV4-13 280	58 21.20N	155 16.30W	1316.0	Y	981697.2	981792.8	28.2	4.6	1.3	-2.1	-3.8	-5.5	-8.8	-12.2	-16.7	-19.7
KV4-14 281	58 21.30N	155 16.20W	1331.0	Y	981696.6	981793.0	28.8	5.0	1.6	-1.8	-3.5	-5.2	-8.6	-12.0	-16.5	-19.6
KV4-15 282	58 21.40N	155 16.10W	1363.0	Y	981694.8	981793.1	29.9	5.5	2.1	-1.4	-3.2	-4.9	-8.4	-11.9	-16.6	-19.7
KV4-16 283	58 21.50N	155 15.90W	1387.0	Y	981693.0	981793.2	30.2	5.4	1.9	-1.7	-3.4	-5.2	-8.7	-12.3	-17.1	-20.2
KV4-17 284	58 21.50N	155 15.80W	1411.0	Y	981692.1	981793.2	31.6	6.4	2.8	-0.8	-2.6	-4.4	-8.1	-11.7	-16.5	-19.8
KV4-18 285	58 21.60N	155 15.70W	1450.0	Y	981689.5	981793.4	32.5	6.6	2.9	-0.8	-2.7	-4.5	-8.2	-11.9	-16.9	-20.2
								B 2.20	2.30	2.50	2.60	2.67	2.75	2.80	2.85	2.90
KFW 286	58 32.90N	155 47.50W	69.0	X	981833.1	981808.6	31.0	29.1	29.0	28.8	28.7	28.7	28.6	28.6	28.5	28.5
KNCA 287	58 33.50N	155 46.60W	34.0	X	981836.7	981809.4	30.5	29.6	29.5	29.4	29.4	29.4	29.3	29.3	29.3	29.3
KOL 288	58 22.20N	155 22.80W	1275.0	Y	981709.1	981794.2	34.8	-1.0	-2.6	-5.8	-7.5	-8.6	-9.9	-10.7	-11.5	-12.4
KD-BRB 289	58 33.40N	155 46.50W	46.0	B	981836.3	981809.2	31.4	30.1	30.0	29.9	29.9	29.8	29.8	29.8	29.7	29.7
KD-R1 290	58 31.80N	155 43.90W	182.0	D	981824.7	981807.1	34.7	29.6	29.4	28.9	28.7	28.5	28.3	28.2	28.1	28.0
KD-R2 291	58 30.60N	155 41.70W	281.0	D	981816.1	981805.5	37.1	29.2	28.8	28.1	27.7	27.5	27.2	27.0	26.8	26.7
KD- 4 292	58 22.20N	155 24.50W	1473.0	Y	981698.4	981794.2	42.8	1.4	-0.5	-4.2	-6.1	-7.4	-8.9	-9.9	-10.8	-11.8

Table 3 continued

STATION		LATITUDE	LONGITUDE	ELEV(FT)	Q	OBSERVED	NORMAL	F.AIR	B 2.20	2.30	2.50	2.60	2.67	2.75	2.80	2.85	2.90
KD- 5	293	58 23.20N	155 29.00W	594.0	Y	981756.5	981795.5	16.8	0.2	-0.6	-2.1	-2.9	-3.4	-4.0	-4.4	-4.8	-5.1
KD- 6	294	58 23.30N	155 31.10W	843.0	Y	981743.7	981795.7	27.3	3.7	2.6	0.4	-0.7	-1.4	-2.3	-2.8	-3.3	-3.9
KD- 7	295	58 25.00N	155 34.90W	965.0	Y	981745.9	981797.9	38.7	11.6	10.4	7.9	6.7	5.8	4.8	4.2	3.6	3.0
KD- 3	296	58 28.40N	155 38.80W	685.0	Y	981775.7	981802.5	37.6	18.4	17.5	15.7	14.9	14.3	13.6	13.1	12.7	12.2
KD- 8	297	58 40.70N	155 53.30W	36.0	B	981847.2	981819.0	31.6	30.6	30.5	30.4	30.4	30.3	30.3	30.3	30.3	30.2
KD- 9	298	58 38.20N	155 50.70W	35.0	B	981839.9	981815.7	27.5	26.5	26.5	26.4	26.4	26.3	26.3	26.3	26.2	26.2
KD-10	299	58 35.80N	155 48.70W	37.0	B	981828.5	981814.5	19.5	18.5	18.4	18.3	18.3	18.3	18.2	18.2	18.2	18.2
KD-11	300	58 31.40N	155 43.20W	35.0	B	981830.9	981806.5	27.6	26.7	26.6	26.5	26.5	26.5	26.4	26.4	26.4	26.3
KD-12	301	58 22.60N	155 20.10W	904.0	Y	981728.9	981794.7	19.2	-6.2	-7.3	-9.6	-10.8	-11.6	-12.5	-13.1	-13.7	-14.3
KD-13	302	58 21.10N	155 14.70W	1504.0	Y	981686.4	981797.7	35.2	-7.1	-9.0	-12.8	-14.8	-16.1	-17.6	-18.6	-19.6	-20.5
KD-14	303	58 19.20N	155 14.40W	1650.0	D	981674.1	981790.1	39.2	-7.2	-9.3	-13.5	-15.6	-17.1	-18.8	-19.8	-20.9	-21.9
KD-15	304	58 17.10N	155 14.90W	1811.0	Y	981658.7	981787.3	41.7	-9.1	-11.4	-16.1	-18.4	-20.0	-21.9	-23.0	-24.2	-25.3
KD-16	305	58 16.00N	155 11.80W	2176.0	Y	981633.9	981785.8	52.8	-8.4	-11.2	-16.7	-19.5	-21.4	-23.7	-25.0	-26.4	-27.8
KD-17	306	58 14.30N	155 10.60W	2650.0	D	981586.8	981783.5	52.5	-21.9	-25.3	-32.1	-35.4	-37.8	-40.5	-42.2	-43.9	-45.6
KD-18	307	58 13.40N	155 10.40W	2765.0	Y	981579.1	981782.3	56.9	-20.8	-24.3	-31.4	-34.9	-37.4	-40.2	-42.0	-43.8	-45.5
KD-19	308	58 11.10N	155 8.60W	1630.0	D	981655.9	981779.2	30.0	-15.8	-17.9	-22.0	-24.1	-25.6	-27.2	-28.3	-29.3	-30.3
KD-20	309	58 30.30N	155 39.10W	35.0	B	981825.9	981809.1	24.1	23.1	23.1	23.0	23.0	22.9	22.9	22.9	22.8	22.8
KD-21	310	58 29.80N	155 37.40W	36.0	B	981818.8	981804.4	17.8	16.8	16.7	16.6	16.6	16.6	16.5	16.5	16.5	16.5
KD-22	311	58 30.00N	155 35.10W	35.0	B	981814.3	981804.7	12.9	11.9	11.9	11.8	11.8	11.7	11.7	11.7	11.7	11.6
KD-23	312	58 29.30N	155 34.20W	35.0	B	981811.4	981803.7	11.0	10.0	9.9	9.8	9.8	9.8	9.7	9.7	9.7	9.7
KD-24	313	58 29.60N	155 32.70W	35.0	B	981812.6	981804.1	11.8	10.8	10.7	10.6	10.6	10.6	10.5	10.5	10.5	10.5
KD-25	314	58 7.70N	155 41.60W	200.0	D	981762.4	981774.6	6.6	1.0	0.7	0.2	-0.0	-0.2	-0.4	-0.6	-0.7	-0.8
KD-26	315	58 9.50N	155 41.70W	400.0	D	981754.9	981777.0	15.5	4.2	3.7	2.7	2.2	1.8	1.4	1.2	0.9	0.7
KD-27	316	58 5.00N	155 40.80W	200.0	D	981766.9	981771.0	14.7	9.1	8.9	8.4	8.1	7.9	7.7	7.6	7.5	7.3

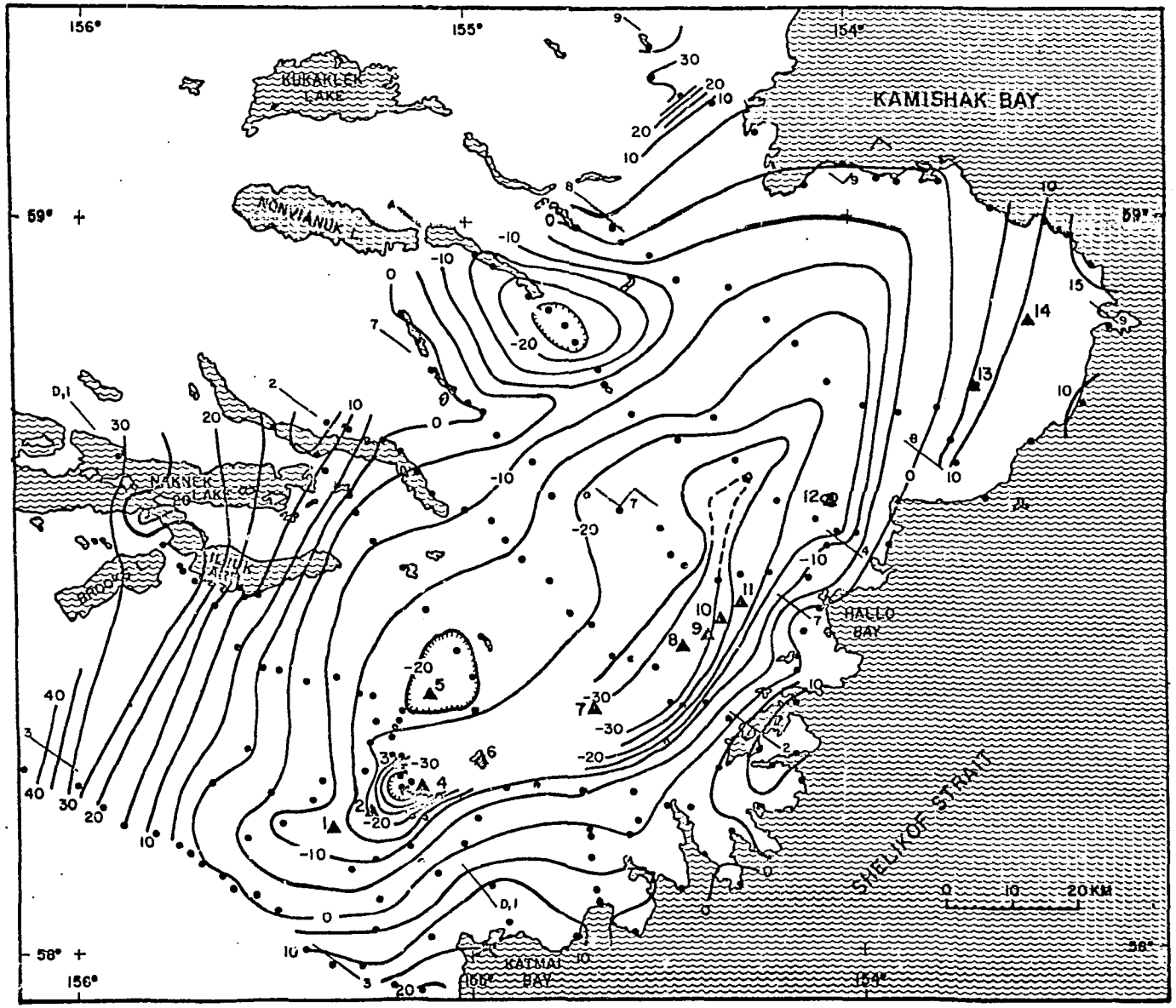

Figure 9. Simple Bouguer (2.67) gravity map of the Katmai area, showing gravity station locations gravity profiles and Quarternary and recent volcanic necks. Contour interval 5 mgal.

maps were not available for Katmai. Producing them is even more laborious than calculating the correction for a few selected stations, which then allows estimation of the terrain effect for others.

As a rule of thumb, terrain corrections are negligible except where the heights or depths of the topographic features exceed 1/20 of their distance from the gravity station (Grant and West, 1965). The Katmai National Monument is very mountainous and in most cases terrain corrections are not negligible, even though the location of most gravity stations was chosen such that the near topography was reasonably level. The regional gravity pattern, however, is not changed very much by topographic effects.

From the 221 regional gravity stations in Katmai, including Decker's data of 1963 and the 1965 gravity survey by Berg and Kienle (1966), the terrain corrections were calculated through Hammer's zone M (out to 21.94 km) for 61 stations and out to zone J (out to 4.47 km) for 17 stations. Most of these stations were located in relatively steep terrain. In Table 4, the corrections for the inner zones B-I and inner plus outer zones B-M are listed for two different densities; 2.0 g/cc as used in Hammer's tables and 2.67 g/cc, the average density assumed for the topography in Katmai. The topographic corrections are probably correct to within 10%. In addition, the complete Bouguer anomaly (simple Bouguer anomaly plus terrain correction through Hammer's zone M (2.67 g/cc) is given for all terrain corrected gravity stations to 0.1 mgal where all zones were calculated and to the even mgal, where only the inner zones B-I were calculated and the effect of the outer zones was estimated.

Table 4.

Terrain corrections and complete Bouguer (2.67) gravity anomalies for selected gravity stations in Katmai National Monument, Alaska.

Station No.	Elev.(ft)	Q	Terrain corrections in mgal for Hammer's zones B-I 2.0 g/cc	Terrain corrections in mgal for Hammer's zones B-I 2.67 g/cc	Terrain corrections in mgal for Hammer's zones B-M 2.0 g/cc	Terrain corrections in mgal for Hammer's zones B-M 2.67 g/cc	Complete Bouguer anomaly for 2.67 g/cc
K01-10 01	1860	z	1.7	2.3	3.4	4.6	-21.3
K01-11 02	703	y	3.3	4.4	5.4	7.2	-0.9
K01-12 03	462	y	0.7	0.9	2.4	3.1	1.1
K01-13 04	153	y	0.6	0.8	2.1	2.8	4.6
K01-14 05	40	z	0.5	0.7	1.6	2.1	13.4
K01-K.P.07	2700	z	1.5	2.0	3.0	4.0	-34.7
K01-T8 08	2130	z	2.9	3.8	3.9	5.2	-36.9
K01-T9 09	2100	z	2.9	3.8	3.9	5.2	-35.1
K01-T9a 10	2143	y	2.1	2.8	3.3	4.4	-27.1
K01-T9b 11	2584	y	4.1	5.5	5.3	7.1	-23.9
K01-T9c 12	2509	y	3.7	4.9	4.9	6.5	-16.5
K01-T9e 13	1520	z	1.2	1.6	3.0	4.0	-7.1
K01-T9f 14	1610	z	1.0	1.4	2.4	3.2	-15.6
K01-T9g 15	3200	±100	4.2	5.6	5.3	7.0	-27.0
K02-01 16	53	y	1.0	1.4	1.2	1.6	8.9
K02-06 21	330	z	2.8	3.8	6.1	8.2	-1.8
K02-08 23	1070	z	15.5	20.7(!)	18.0	24.1	-6.7
K02-09 24	3477	y	3.0	4.1	4.6	6.1	-25.9
K02-11 26	1509	±50	1.2	1.6	3.3	4.5	-19.1

Table 4 (Cont'd)

Station No.	Elev.(ft)	Q	Terrain corrections in mgal for Hammer's zones B-I 2.0 g/cc	Terrain corrections in mgal for Hammer's zones B-I 2.67 g/cc	Terrain corrections in mgal for Hammer's zones B-M 2.0 g/cc	Terrain corrections in mgal for Hammer's zones B-M 2.67 g/cc	Complete Bouguer anomaly for 2.67 g/cc
K02-16 31	237	y	0.1	0.1	1.0	1.3	-11.4
K02-22 37	126	y	0.8	1.1	2.5	3.3	2.7
K03-06 43	916	y	2.1	2.7			3
K03-07 44	2160	y	1.6	2.2	2.3	3.1	1.4
K03-08 45	855	z	1.0	1.3			4
K04-01 55	695	y	4.3	5.7			-6
K04-04 58	650	z	5.0	6.7			-20
K04-05 59	710	z	6.0	8.0			-17
K04-06 60	820	±50	10.4	13.9			-12
K04-07 61	1880	±50	6.6	8.8			-4
K04-08 62	2650	±50	1.0	1.3			-4
K04-10 64	940	z	4.0	5.3	5.2	7.0	-14.8
K04-13 67	875	y	6.8	9.0	7.7	10.3	-20.1
K04-14 68	707	y	2.7	3.6			-15
K05-01 72	340	z	1.8	2.4			-16
KNM-03 88	396	y	2.5	3.3	3.8	5.0	2.4
KNM-04 89	1278	y	1.9	2.6	3.4	4.5	-3.5
KNM-05 90	1309	y	2.4	3.2	3.4	4.5	-5.8
KNM-06 91	1820	y	1.4	1.9	2.7	3.6	-4.3
KNM-07 92	1014	y	0.8	1.0	2.8	3.8	-0.7

Table 4 (Cont'd)

Station No.	Elev.(ft)	Q	Terrain corrections in mgal for Hammer's zones B-I 2.0 g/cc	Terrain corrections in mgal for Hammer's zones B-I 2.67 g/cc	Terrain corrections in mgal for Hammer's zones B-M 2.0 g/cc	Terrain corrections in mgal for Hammer's zones B-M 2.67 g/cc	Complete Bouguer anomaly for 2.67 g/cc
KNM-08 93	1555	y	6.1	8.1	6.3	8.4	-3.7
KNM-09 94	1445	y	2.5	3.4	3.2	4.3	-2.0
KNM-11 96	1677	y	1.3	1.8	1.9	2.5	4.1
KNM-12 97	2247	y	1.2	1.6	2.3	3.1	-4.1
KNM-13 98	1979	y	1.6	2.1	2.6	3.5	-13.5
KNM-14 99	2350	y	1.1	1.4	1.9	2.6	-19.7
KNS-01 100	210	z	1.1	1.4	3.5	4.6	3.8
KNS-02 101	398	y	4.5	6.0	7.6	10.2	8.5
KNS-03 102	875	y	5.5	7.3	8.7	11.6	2.3
KNS-04 103	1136	y	3.8	5.1	6.0	8.0	1.9
KNS-05 104	1566	y	1.8	2.5	2.9	3.8	-2.6
KNS-06 105	461	y	2.5	3.3	3.1	4.1	5.5
K06-08 130	735	y	1.0	1.4	2.4	3.2	-13.3
K06-09 131	840	z	6.5	8.6	9.7	12.9	-9.8
K06-10 132	1105	y	9.0	12.0	12.5	16.7	-4.8
K06-11 133	1623	y	8.0	10.6	10.9	14.6	-5.7
KHL 134	1719	y	4.0	5.3	5.3	7.0	-9.1
K07-03 137	634	y	4.7	6.3			-10
K07-12 146	1640	z	1.7	2.2			2
K07-14 148	1847	y	1.2	1.7			1

Table 4 (Cont'd)

Station No.	Elev.(ft)	Q	Terrain corrections in mgal for Hammer's zones B-I 2.0 g/cc	Terrain corrections in mgal for Hammer's zones B-I 2.67 g/cc	Terrain corrections in mgal for Hammer's zones B-M 2.0 g/cc	Terrain corrections in mgal for Hammer's zones B-M 2.67 g/cc	Complete Bouguer anomaly for 2.67 g/cc
K08-03 155	400	z	6.8	9.0			17
K08-04 156	1665	z	7.0	9.4			12
K08-06 158	700	z	5.5	7.3			-7
KD-04 292	1473	y	2.3	3.0	2.7	3.6	-3.8
KD-05 293	594	y	0.8	1.1	2.0	2.6	-0.8
KD-06 294	843	y	0.7	1.0	1.6	2.1	0.7
KD-07 295	965	y	0.6	0.9	1.3	1.7	7.5
KD-03 296	685	y	1.5	1.9	1.9	2.5	16.8
KD-10 299	37	B	3.3	4.4			23
KD-12 301	904	y	0.2	0.3	1.3	1.7	-9.9
KD-13 302	1504	y	4.1	5.5	5.3	7.1	-9.0
KD-14 303	1650	D	0.3	0.4	1.3	1.8	-15.3
KD-15 304	1811	y	0.6	0.8	1.5	1.9	-18.1
KD-16 305	2176	y	0.7	0.9	1.5	2.1	-19.3
KD-17 306	2650	D	1.6	2.1	2.4	3.2	-34.6
KD-18 307	2765	y	2.3	3.0	3.1	4.2	-33.2
KD-19 308	1630	D	1.0	1.4	2.4	3.2	-22.4
KD-25 314	200	D	2.1	2.8	3.3	4.3	4.1
KD-26 315	400	D	3.7	4.9	4.9	6.6	8.4
KD-27 316	200	D	2.5	3.3	3.1	4.1	12.0

In most cases, the corrections resulting from the inner zones B-I were much greater than those from the outer zones J-M. The latter exceeded 2.5 mgal (2.67 g/cc) in 19.2% of all cases. The maximum correction from the outer zones was 4.7 mgal (2.67 g/cc). The topographic corrections from the inner zones B-I exceed 2.5 mgal (2.67 g/cc) for as many as 52.6% of all gravity stations and 5 mgal and 10 mgal for 29.5% and 5.1% of the stations. The maximum terrain effect for zones B-I was an exceptional 20.7 mgal for a station located in a deep valley and very close to the volcanic range.

A complete Bouguer anomaly map of the volcanic range from Kejulik Pass to Snowy Mountain and from the Shelikof Strait to Naknek Lake in the SE-NW direction is presented in Fig. 10 together with the local geology and main structural features. In steep terrain, i.e. in the volcanic range, corrections were calculated through Hammer's zone M (points in Fig. 10). More liberal corrections, where only the inner zones B-I were calculated and where the contribution of the outer zones J-M were estimated, are plotted with open circles. Open squares mark stations where the entire terrain correction was estimated using calculated values from stations with a similar topographic setting.

3.3 Errors

Errors in the observed gravity values can be introduced through nonlinearity of the gravimeter drift and earth and ocean tides, assuming that the gravity base values and the calibration constant of the gravimeter are correct. The drift rate of the gravimeter was monitored very carefully at the base station throughout the surveys in 1965 and 1966.

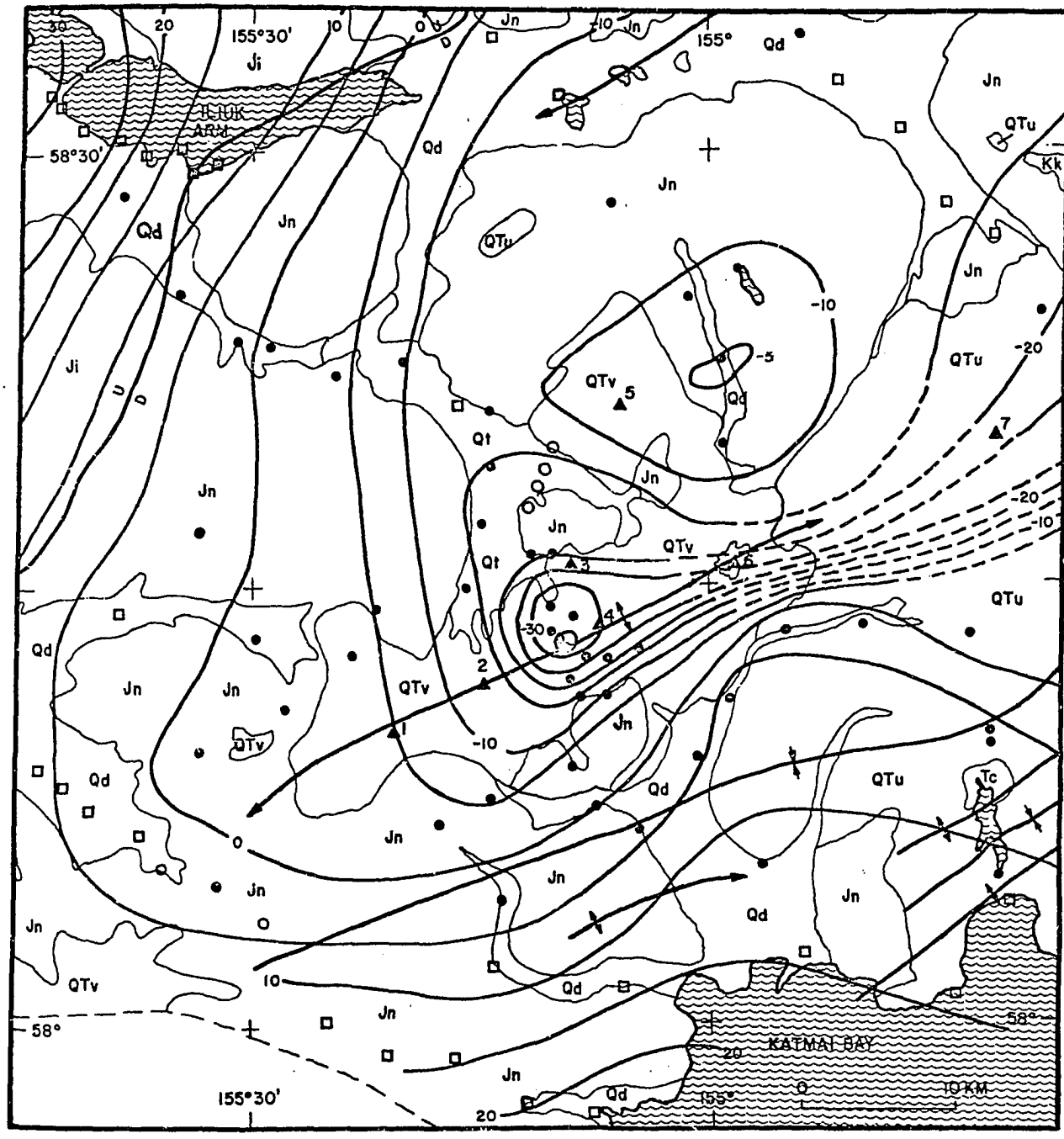

Figure 10. Complete Bouguer (2.67) gravity map of the Mt. Trident-Knife Peak area. Points: terrain correction calculated through Hammer's zone M, open circles: terrain corrections calculated through zone J, zones J through M estimated, open squares: all zones estimated.

All gravity observations are drift corrected. Errors introduced through linear drift interpolation between base readings probably do not exceed ± 0.05 mgal.

Earth tides could affect the observed gravity values by ± 0.15 mgal (Wychoff, 1936) and were not corrected for. The influence of ocean tides was also neglected. Most coastal gravity stations were located at the prevailing tide level in order to assure a good elevation control. Assuming that a gravity observation is made at the mean tide level, the difference in gravity at high and low tide at such a station can be approximated by considering the attraction of a semi-infinite horizontal sheet of water, if the land and sea are assumed to be separated by a straight coast line. The maximum difference between high and low tide in the Shelikof Strait is about 20 to 25 feet. Assuming this thickness for the semi-infinite water sheet of density 1.03 g/cc, the ocean tides could introduce a maximal error of ± 0.07 to ± 0.08 mgal at a gravity station located at mean tide level.

Observed gravity values are probably correct to ± 0.2 mgal (0.15 + 0.05) for stations remote from the coast and to ± 0.3 mgal for coastal stations.

Much larger errors in the Bouguer anomalies were introduced through inaccurate station elevations determined by altimetry. Bench marks in Katmai are sparse, often inaccessible and at locations that produce large gravimetric terrain effects.

Excluding the 85 gravity stations in the Valley of Ten Thousand Smokes, where only good relative altitudes are required, only 16% of the remaining 221 gravity stations in the Monument are accurate to ± 3 feet

or better. In terms of combined elevation correction this corresponds to 0.2 mgal (2.67 g/cc). The bulk of the stations, 58%, are accurate to ± 20 feet (1.2 mgal); 19% are accurate to ± 30 feet (1.8 mgal), 6% to ± 50 feet (3.0 mgal) and 1% to ± 100 feet (6.0 mgal).

Almost all elevations of the Valley of Ten Thousand Smokes gravity stations are accurate to only ± 20 feet absolute. Relative elevations (relative to the base station BMH), however, are much better and are discussed in Chapter V.

Summarizing, we find that the simple 2.67 g/cc Bouguer anomaly at 93% of all gravity stations is correct to within ± 2 mgal. This includes errors due to poor elevation control, nonlinear drift, earth tides and ocean tides.

Topographic corrections are probably correct to within 10%. The largest correction of 24.1 mgal for station 2-8 can be in error by 2.4 mgal. Most topographic corrections, however, amounted to less than 10 mgal and are in error by only ± 1 mgal or less.

CHAPTER IV

INTERPRETATION

4.1 Bouguer Gravity Maps

A Bouguer gravity map for a reduction density of 2.67 g/cc of the Katmai National Monument on the Alaska Peninsula is given in Fig. 9. It gives an improved picture of the gravity patterns in Katmai outlined in our 1967 Bouguer gravity map (Berg, Kubota and Kienle, 1967 and Fig. 8). The entire surveyed area of about 19,200 km^2 is dominated by a 20 to 25 mgal gravity low of large areal extent, which also has been independently outlined by Barnes (1967) in a generalized simple Bouguer gravity map of southern Alaska.

The anomaly is elongate in a northeast-wouthwest direction over 160 km from Kamishak Bay to the Kejulik Mountains and is approximately 60 km wide. The major axis parallels the two major tectonic elements of the area, the Bruin Bay fault and the volcanic arc and is arcuate and convex to the southeast. The northeastern part of the gravity low is very broad and of moderate amplitude (-25 mgal). Here, and on the northwestern flank of the low, gradients of about 1.0 to 1.5 mgal/km are present. The anomalies rise to high positive values in the southwest corner of the map in the Naknek Lake-Lake Brooks area (see Fig. 9). This seems to connect to the Bristol Bay high noted by Woollard et al (1960, p. 1036). Steep gravity gradients of 2-4 mgal/km are found just southeast of the volcanic chain from Mt. Mageik to Devils Desk (volcano Nos. 2 and 11, Fig. 9).

The great gravity low on the northern part of the Alaska Peninsula is confined within the boundaries of the Jurassic Naknek Formation and Cretaceous Kaguyak Formation of sedimentary conglomerate, sandstone and shale units, which dominate the area and form most of the topographic relief.

It is interesting to note that, even though the sedimentary basin of the Naknek Formation continues to the southwestern end of the Alaska Peninsula, where Naknek outcrops are still found in the cores of stripped anticlines about 400 km southwest of Becharof Lake, the major Katmai gravity low has a closure in the Kejulik Mountains northeast of Becharof Lake (Figs. 8 and 9) also shown in Barnes Bouguer 2.67 gravity map of southern Alaska (1967).

Two local anomalies are superimposed on this general gravity pattern, the Kulik Lake low and the Mt. Trident low. The Kulik Lake low, a roughly circular anomaly of some 30 to 35 km diameter, has an amplitude of 28 mgal (not terrain corrected). Gradients are on the order of 1.5 to 2 mgal/km. The center of this low is situated directly on the Bruin Bay fault 6 km southeast of the southeastern tip of Kulik Lake. Ten kilometers northeast of this point "the structurally high part of the Kamishak anticline, as well as the Bruin Bay thrust, is intruded by a quartz diorite stock of post-Cretaceous age. A wide contact metamorphic aureole is present within the Jurassic sediments" (Hazzard et al 1950, p. 2377). The bruin Bay fault in this area cuts the northwestern flank of the anticline at a distance of only 2 to 5 km from its crest. The roughly circular outcrop pattern of this quartz diorite stock is about 7 km in diameter and lies well within the gravity low in its northeastern

sector. The gravity data suggested this quartz diorite mass is of much larger extent, widening at depth and that the outcrop represents only a very small portion of the mass.

The other local anomaly, also negative, is again circular and much smaller being only about 10 km in diameter. It is centered at the foot of the active Mt. Trident flank cone in the Mageik Creek Valley,which separates Mts. Mageik and Trident and lies about 2 km south-southeast of Katmai Pass. Since terrain effects are severe in this area, a terrain corrected detail of the general gravity map (Fig. 9) is given in Fig. 10. The Mt. Trident low has very steep gradients of about 6 mgal/km indicating a shallow depth mass deficiency. The amplitude of the anomaly is about 13 mgal. Geologically, the anomaly lies in Quarternary and recent volcanic rocks, chiefly low density vesicular andesites and basaltic andesites which cap the sedimentary units in that area.

In the simple Katmai Bouguer anomaly map (Fig. 9) a minor gravity low associated with Knife Peak is found 20 km north of the Mt. Trident low. Applying terrain corrections that are on the order of 12 to 17 mgal (!) in the steep Ikagluik Valley northeast of Knife Peak converts the Knife Peak low into a minor gravity high of about 8 mgal amplitude. It is about 16 km in diameter with small gradients of 1 mgal/km but its outlines are not well defined due to the scarcity of the gravity stations. Knife Peak itself lies in the southwestern sector of the anomaly.

4.2 Density Determinations

The densities of 18 hand specimen, which were collected by Dipak K. Ray, Geophysical Institute U/A, now returned to the Geological Survey of India, from some of the gravity station locations were determined in the laboratory. The results are listed in Table 5, where

A = weight in grams of dry sample in air (oven drying was not necessary, because the samples were in storage for 2½ years in Fairbanks' extremely dry climate).

B = weight in grams of saturated surface dry (ssd) sample in air.

C = weight in grams of saturated sample in water.

$\frac{A}{B-C}$ = bulk dry density (g/cc).

$\frac{B}{B-C}$ = bulk ssd density (g/cc).

$\frac{A}{A-C}$ = apparent density (g/cc).

$\frac{B-A}{A} \cdot 100$ = absorption (%)

Densities of the undeformed recent and Quarternary volcanic rocks (QTv) (Keller and Reiser, 1959):

Two samples, a very porous (2.3%) recent Mt. Trident andesite and an older basaltic andesite from a basal flow of Knife Peak, were collected from this unit, which forms Knife Peak, Mt. Katmai, Mt. Trident, Mt. Mageik, and Mt. Martin and caps the Naknek Formation in that area. The mean density is 2.46 g/cc.

Strange et al (1965) reviewed various bulk density determinations for the Hawaiian volcanics obtained by direct seismic and gravimetric methods and found a bulk dry density of only 2.3 g/cc for the not

Table 5.

Densities of 18 hand specimen collected from selected gravity station locations in Katmai National Monument, Alaska

Collection Site (Locality or gravity station No.)	Sample No.	Rock Type	A	B	C	$\frac{A}{B-C}$ (bulk-dry)	$\frac{B}{B-C}$ (bulk-ssd)	$\frac{A}{A-C}$ (apparent)	$\frac{B-A}{A} .100$ (absorption)
Trident Volcano	KT-28	Porous andesite	1287	1316	777	2.39	2.44	2.52	2.3
Knife Peak	KKP2-1	Basaltic andesite	1092	1096	652	2.46	2.47	2.48	0.4
2-3	KG-35	Altered andesite	1738	1750	1092	2.64	2.66	2.69	0.7
2-9	KG-63	Unaltered andesite	931.5	943	593	2.66	2.69	2.75	1.2
2-23	KG-71	Naknek sandstone	1009	1026	631	2.55	2.60	2.67	1.7
3-6	KG-37	Fault gouge rock	347	356	210	2.38	2.44	2.53	0.3
3-6	KG-38	Naknek marly shale		716	441		2.60		
3-7	KG-39	Naknek shale	470	496	296	2.35	2.48	2.70	5.5
3-15	KG-83	Hornblende granite	1918	1922	1210	2.69	2.70	2.71	0.2
4-2	KG-66	Hornblende granite	2494	2512	1574	2.66	2.68	2.71	0.7
4-7	KG-68	Naknek tuff	2030	2040	1294	2.72	2.73	2.76	0.5
4-8	KG-69	Chisik conglomerate	4652.5	4666	2972	2.75	2.75	2.77	0.3
4-14	KG-72	Naknek sandstone	826	839	534	2.71	2.75	2.83	1.6
5-7	KG-77a	Dense altered andesite	1399.5	1404	921	2.90	2.91	2.92	0.3
5-7	KG-78a	Dense altered andesite	832	832	538	2.83	2.83	2.83	0
5-8	KG-79	Dense altered andesite	1310	1314	853	2.84	2.85	2.87	0.3
5-8	KG-80	Porphyritic altered andesite	602	609	381	2.64	2.67	2.72	1.2
5-8	KG-81	Dense altered andesite	734	740	473	2.75	2.77	2.81	0.8

water-saturated vesicular basaltic flows above sea level. This is, incidentally, also the average bulk density of the basaltic Jasper Seamount in the eastern Pacific (Harrison and Brisbin, 1959, as cited by Menard, 1964, p. 60, Fig. 4.3). Below the water table, which for the Hawaiian Islands generally is at sea level, indicating also a good permeability of the basalt, the porous water-saturated rocks down to a depth of 1.5 km have a density of 2.6 g/cc. These rocks above 1.5 km depth represent the material that was erupted above or near sea level.

In the light of these findings the low ssd bulk density of 2.46 g/cc for the undeformed andesites (QTv) of the Quarternary and recent volcanic cones in Katmai seems to be in general agreement with the Hawaiian results.

Densities of the undifferentiated igneous rocks (QTu) (Keller and Reiser, 1959):

This map unit includes the older folded volcanic rocks (partly of Eocene age) and the younger undeformed volcanic rocks. Locally it is also comprised of silicic and mafic Tertiary intrusive rocks and an equivalent sedimentary sequence of the Kenai Formation. At Tiny Island, which is located at the entrance of Kukak Bay (gravity station 5-7), two very dense altered andesites were sampled with an average density of 2.87 g/cc. Eight kilometers to the south two very similar dense altered andesites with an average density of 2.81 g/cc and one porphyritic altered andesite (2.67 g/cc) were collected on the northern shore of Kafia Bay. An altered andesite (2.66 g/cc) was found in the south corner of Kukak Bay (gravity station 2-3). All these rocks are very similar to the layered volcanic rocks of Keller and Reiser's section 5 in the vicinity of Kukak Bay (1959, pp. 284-286).

An unaltered andesite from an outcrop, which lies stratigraphically higher in the section of Serpent Tongue Glacier (gravity station 2-9), had a density of 2.69 g/cc.

The mean density of the volcanic rocks of this undifferentiated volcanic unit (QTu) is 2.78 g/cc.

Densities of the Hornblende and Biotite granites (Ji):

The granitic basement complex northwest of the Bruin Bay fault was sampled at Kulik Lake (gravity station 4-2) and 100 km southwest in the mountains west of Contact Creek (gravity station 3-15). The average density was 2.69 g/cc, a value which corresponds well to the 2.67 g/cc generally assumed for granites.

Densities of the Naknek Formation (Jn):

The sedimentary rocks of the Naknek Formation showed a significant variation in densities ranging from 2.44 to 2.75 g/cc. The Chisik basal conglomerate, collected from the crest of the Kamishak anticline (gravity station 4-8), had a desnity of 2.75 g/cc. A Naknek sandstone and a Naknek tuff collected at structural highs along the same gravity profile (4) at gravity stations 4-7 and 4-14 had a similar mean density of 2.74 g/cc. This is a good mean density for the basal Chisik conglomerate member of the Naknek Formation.

Other samples including a sandstone collected at Grosvenor Lake (gravity station 2-23), a shale and a marly shale from the Kejulik Mountains (gravity stations 3-7 and 3-6) had a mean density of 2.56 g/cc, which may be representative of the Naknek units that overlie the basal

conglomerate member. The average density of all the collected varieties of Naknek sediments was 2.62 g/cc.

4.3 Regional Crustal Structure

To obtain a first approximation of the crustal structure in Katmai, the depth to the Moho was estimated in profile A-A' (Fig. 11), using Woollard's empirical relation of 1962 between the Moho elevation in km below sea level and Bouguer gravity anomalies.

Gravity profile A-A' (Fig. 12) extends from the Nushagak flats across the Katmai Mountains, the Shelikof Strait and Kodiak Island to the Aleutian Trench, covering a distance of about 650 km. The simple Bouguer 2.67 gravity anomalies were taken from Woollard's gravity iso-anomalies in the Nushagak flats (from Woollard's Bouguer anomaly map of Alaska, 1960), from Barnes' generalized preliminary Bouguer 2.67 gravity map of southern Alaska (1967) covering the area southeast of Katmai, and from our new Katmai Bouguer 2.67 gravity map.

In order to free the data from shallow depth geological effects and because isostatic equilibrium is generally not established for crustal sections that are less than 160 km wide (Tsuboi, 1950, as cited by Woollard et al 1960, p. 1023), mean Bouguer values over 150 km wide profile sections were used to derive crustal thicknesses from Woollard's empirical 1962 curve. This is following a procedure applied by him and others to derive crustal sections in Alaska (op. cit.).

The resulting smoothed crustal section is shown in Fig. 11. In this section Moho dips about 6° to the northwest underneath the continental crust and away from the Aleutian Trench.

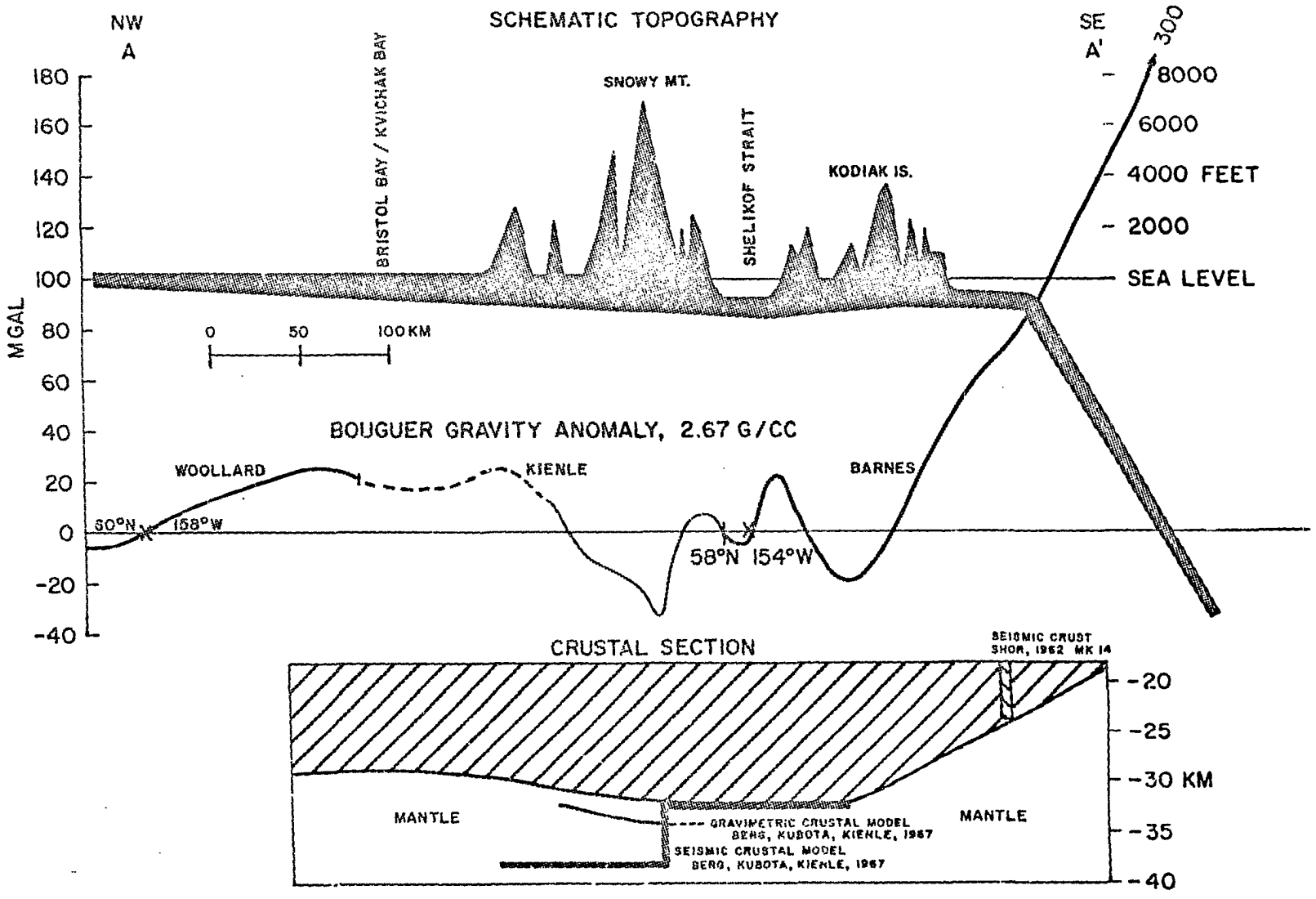

Figure 11. Relation of Bouguer gravity anomalies to topography and gravity derived crustal section in profile A-A' from Nushagak flats to Aleutian Trench. For location see Fig. 12.

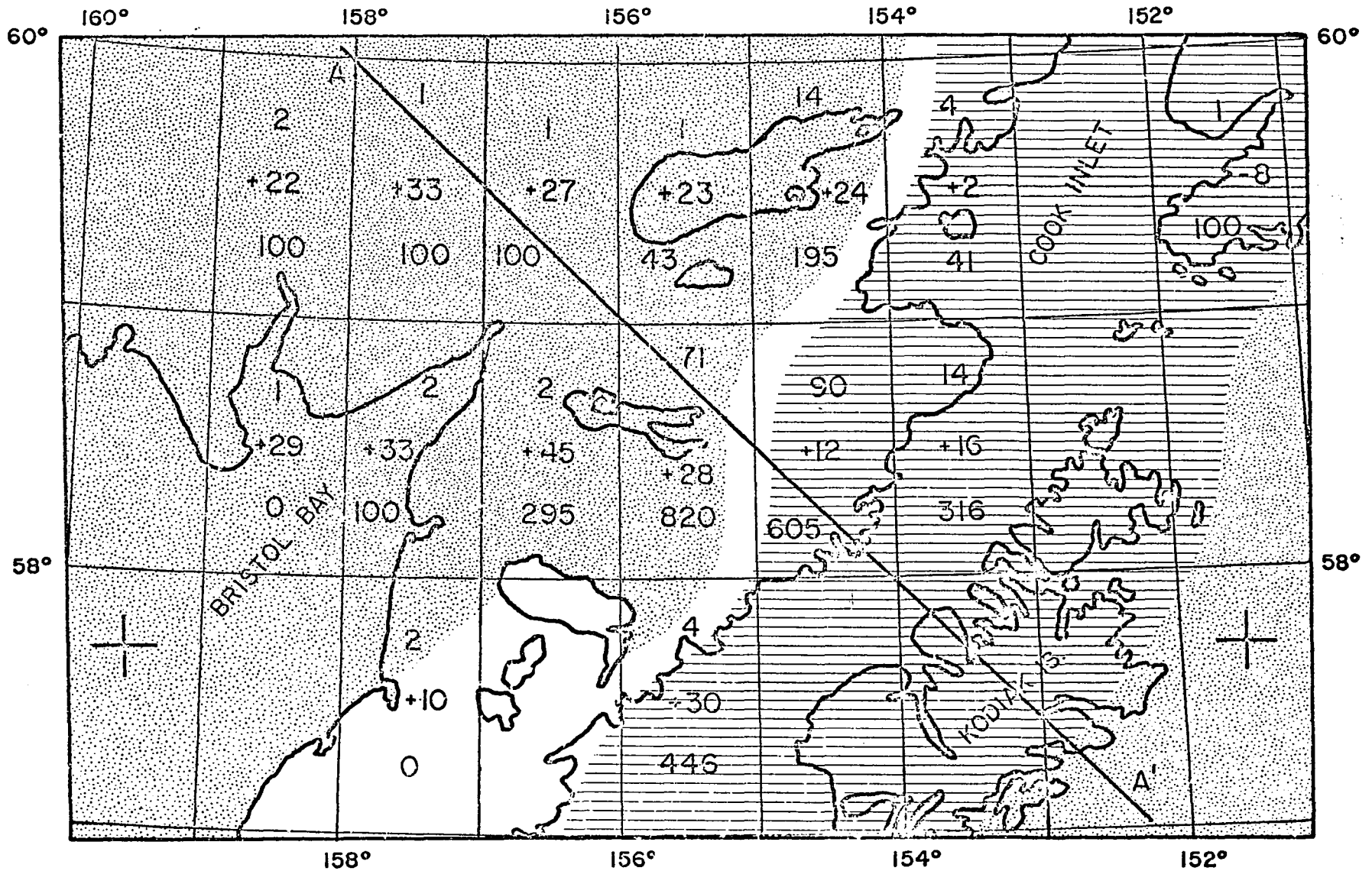

Figure 12. Free-air anomalies in 1° by 1° rectangles. Figures give from top to bottom: number of gravity stations per rectangle, mean free-air anomaly in mgal, mean altitude of gravity stations in feet (after Thiel et al, 1959). Cross hatched zone denotes areas, where free-air anomalies have no dominant sign between ± 20 mgal. Stippled zone denotes areas of positive free-air anomalies greater than + 20 mgal (after Woollard and Strange, 1962).

Shor (1962) found a depth to the Moho of 23 to 24 km from seismic refraction data at the continental shelf station MK-14 southeast of Kodiak Island, which is in excellent agreement with the depth derived from Barnes' gravity observations. At station MK-14 Shor detected low seismic velocity sediments overlying a lithified 4 km/sec layer, which is underlain by 6 km of 5.5 km/sec intermediate crustal material. He could not detect the oceanic layer and if it is present, it is masked by material of continental crust velocity (Shor, 1962, pp. 38, 42, 52).

A maximum and constant depth of 32 km to the Moho is found in the Shelikof Strait region between the volcanic axis of the Alaska Peninsula and the northwestern shore of Kodiak Island. The gravimetric depth to the Moho here is in substantial agreement with the average crustal thickness of 32 km derived for this section (Model KM-36, see Section 1.5) from earthquake data by Berg, Kubota and Kienle (1967).

Northwest of the volcanic axis the Moho rises slightly to about 31 km depth below the Bruin Bay fault, which does not agree with the average depth of 38 km for the seismic model between the Bruin Bay fault and the volcanic axis, but is in agreement with the earlier gravity interpretation by Berg, Kubota and Kienle (1967).

Further to the northwest the Moho seems to rise to an even more shallow depth of only 29 km, in the Nushagak lowlands assuming a crust of normal composition. Unfortunately, the northwestern one-third of gravity profile A-A' is at best only a first approximation of the true gravity pattern, because no gravity stations are available in the area

northwest of Naknek - and Nonvianuk Lake. Woollard's map, which was used to construct the profile is based on only a few stations at the shores of Bristol Bay.

Assuming that the general regional Bouguer gravity trend in the Bristol Bay and Nushagak lowlands is correct, a Moho rising to such a shallow depth in continental setting is not a very probable explanation for the observed positive Bouguer gravity.

Other possibilities are the presence of intracrustal mass anomalies. Woollard et al (1960, p. 1036) suggest a geologic situation similar to that observed in Price William Sound, where a mafic intracrustal pluton with no surface expression was detected seismically and is causing a local positive anomaly closure of considerable width (150 km). Judging from the width itself, the Prince William Sound anomaly could be interpreted as evidence of a thinner-than-normal crust; seismically, however, a thickner-than-normal crust of higher-than=normal velocity and strong horizontal velocity changes was detected (op. cit.). Free-air anomalies are positive and comparable to the Bristol Bay and Nushagek lowland anomalies.

Bouguer anomalies of + 30 mgal are observed around Brooks - and Naknek Lakes. If extrapolated to Woollard's Bristol Bay measurements these data define a very large positive closed Bouguer anomaly spanning some 300 km in width in the southeast-northwest direction which is twice as long in the southwest-northeast axis. The anomaly is of considerably larger areal extent than the Prince William Sound anomaly and of about the same aplitude (+ 40 mgal).

A detailed gravity net over the Nushagak-Kvichak River lowlands and the southeastern shores of Kvichak Bay, where no data are available would be very desirable to fill the existing gap in gravity coverage between Woollard's Bristol Bay and our Katmai gravity measurements.

Summarizing, the part of the crustal section postulated by model A-A' (Fig. 11) that lies southeast of the volcanic range is well confirmed by seismic measurements. The method of approximating crustal structures using Woollard's empirical relation (op. cit.) may not be adequate in the northwestern part of Section A-A', where anomalous crustal mass distributions could exist, and positive free-air anomalies have been observed. This of course should be tested seismically. Our seismic crustal model KM-28 (Berg, Kubota and Kienle, 1967, see Section 1.5) northwest of the volcanoes with an average depth of 38 km to the Moho may be a first indication that the anomalous mass causing the positive anomalies in the Bristol Bay area is not associated with an abnormally shallow Moho.

The Katmai Mountains are most likely compensated regionally and not locally because no mountain root is indicated seismically or gravimetrically. This would be expected following Tsubois' (1950) observation that crustal segments that are less than 160 km wide are compensated regionally. The Katmai Mountains are about 70 km wide--and also following Woollard's (1959, p. 1535) rule of thumb that "if the width of the topographic feature does not exceed three times the regional thickness as defined by Woollard's empirical relation, it is probably compensated on a regional basis over a wide area rather than locally." In Katmai

the regional crustal thickness is about 32 km, three times this thickness is 96 km, and the width of the Katmai Mountains is 70 km.

4.4 Free-air Anomalies

The basic data used by geodesists to determine undulations of the earth's geoid are mean values of the free-air anomalies in 1° by 1° rectangles over the surface of the earth. A mean free-air anomaly map in such rectangles for Alaska was started by Thiel and others (1959, p. 74, Fig. 6) using all available gravity data up to that date. With our new gravity measurements this map was updated for a few 1° by 1° rectangles in the Katmai area. Figure 12 shows the results. Following Woollard's et al classification of free-air anomalies in the Pacific (1962, p. 67, Fig. 3), the separation of the anomalies into areas of no dominant sign (between -20 and + 20 mgal) and areas with significant departures from zero mgal, either positive (greater than + 20 mgal) or negative (smaller than -20 mgal) results in a rather consistent pattern.

In their map, the Bristol Bay region is characterized by positive free-air anomalies. Figure 12 shows this positive zone extending into the Alaskan mainland north of Bristol Bay and into the western Alaska Peninsula, where the mean free-air anomalies range from +20 to +40 mgal. Both of these areas have a very low topography. The Bruin Bay fault approximately separates this positive zone from the zone of no dominant sign comprising the Katmai volcanoes, Shelikof Strait and Kodiak Island. The Katmai mountains are characterized by slightly positive +10 to +20 mgal free-air anomalies. According to the free-air anomaly map of the Pacific basin (op. cit.) the area south of the Aleutian Trench, Kodiak

Island and Kenai Peninsula is again marked by an extensive field of positive free-air anomalies.

On the basis of a homogeneous crust supported hydrostically by the underlying homogeneous mantle one would expect that zero free-air anomalies indicate isostatic equilibrium, that positive anomalies signify too thin a crust and that negative free-air anomalies are typical of too thick a crust. Woollard et al (1962, p. 61) pointed out however, that such departures to positive or negative free-air anomalies could also indicate areas of greater or less than normal crustal densities or corresponding changes in the upper mantle densities with established isostasy, regional rather than local compensation of the topography, or indeed, departure from isostasy due to stresses preventing isostatic compensation.

Empirical relations between crustal thickness and surface elevation or Bouguer gravity were established by various authors based on known seismic depths to the Moho and corresponding Bouguer anomalies or elevations. The scatter of worldwide data is considerable and various best fit curves were given by Demenitskaya, Woollard, and others, as summarized by Woollard et al. (1962). Since it is well established that generally isostasy is an operating principle in the earth's crust, such curves tend to describe isostatic equilibrium conditions of the earth's crust, characterized by zero free-air anomalies.

According to Woollard et al (1962), departures of the free air anomalies from zero both on land and in the ocean indicate abnormal crustal densities and thicknesses. Contrary to what one would expect under the assumption of a homogeneous crust supported hydrostatically by a homogeneous upper

mantle, a great number of refraction seismic observations showed that positive free-air anomalies are associated with a denser and thicker than normal crust; negative free-air anomalies with subnormal crustal density and a thinner than normal crust.

An excellent example showing this relationship is the Prince William Sound area in southern Alaska (op. cit., p. 64) where positive isostatic anomalies are associated with a crust that is about 18 km thicker (as deduced from seismic measurements) than the thickness of 32 km derived from surface elevations under hydrostatic conditions.

In Section 4.3, Woollard's et al (1962, p. 69, Fig. 5) new hyperbolic tangent relationship was used to estimate the crustal thickness for a regional profile from the Bristol Bay to the continental shelf southeast of Kodiak Island. As mentioned earlier, the Bruin Bay fault approximately separates the positive free-air anomaly zone of the Bristol Bay to the northwest from a relatively narrow zone of near zero free-air anomalies to the southwest. Seismic information in Katmai is unfortunately very sparse and limited to a composite seismic crustal model derived by Berg, Kubota and Kienle (1967). One crustal section on the continental shelf southeast of Kodiak Island was given by Shor (1962). Comparison of the seismic and gravimetric results in Katmai indeed confirms the observations by Woollard et al (1962). Excellent agreement between the seismic and gravity derived crustal structures is found in the zone of near zero free-air anomalies from the volcanic range to Kodiak Island (Fig. 11). A large discrepancy between our seismic model northwest of the volcanic range and the gravity derived crustal structure is found northwest of the range toward the zone of positive free-air anomalies (Fig. 11),

where the seismic depth to the Moho is about 6 km greater than that derived from gravity data.

Woollard et al (1962, pp. 67, 68) observed that in every case where the free-air anomalies were regionally positive, as in the gulf of Alaska and the Bering Sea, the depth to the Moho derived from gravity data was 2 km less than the seismic depth. The gravimetric depth to the Moho in the northwestern section of profile A-A' (Fig. 11) was found to be 29 to 30 km. Since this is an area of marked positive anomalies a greater depth to the base of the crust could be expected. Adapting a 2 km discrepancy between the seismic and gravimetric crust places the depth to the Moho at 31 to 32 km for that section. This compares to 32 km for the southeastern section, which means that no great changes in the depth to the Moho across the volcanic range can be expected gravimetrically.

Our composite seismic crustal model in Katmai derived from earthquake data describes an average structure and is divided by the volcanic axis into two sections (Berg, Kubota and Kienle, 1967). The sections, northwest and southeast of the volcanic range, both consist of a two layered crust with horizontal interfaces and identical layer velocities but different layer thicknesses. The northwestern section (KM-28), which describes a crustal model between the Bruin Bay fault and the volcanic axis is characterized by average depths of 15 km to the first interface (between seismic layers 1 and 2) and 38 km to the Moho. With respect to this section, the southwestern model is vertically displaced along the volcanic dividing line with average depths of 12 km to the first interface and 32 km to the Moho.

The layer velocities are v_p = 5.5 km/sec for the first seismic layer, v_p = 6.5 km/sec for the second seismic layer and v_p = 8.1 km/sec for the upper mantle. This corresponds to a density contrast of 0.25 g/cc between the first and second seismic layer and a density contrast of 0.5 between the second seismic layer and the upper mantle (Woollard, 1959, p. 1530, Fig. 7; Nafe and Drake, 1963).

The theoretical total gravity effect that would be observed in a profile across the two seismic crustal sections can easily be evaluated. The step in the first interface of 3 km would cause a gravity effect of

$$2\pi \cdot G \cdot \Delta\rho \cdot h = 2\pi \cdot 6.67 \cdot 10^{-8} \cdot 0.25 \cdot 3.10^5 \text{ gal} = 31 \text{ mgal.}$$

The 6 km step in the Moho would cause a gravity effect of

$$2\pi \cdot G \cdot \Delta\rho \cdot h = 2\pi \cdot 6.67 \cdot 10^{-8} \cdot 0.5 \cdot 6.10^5 \text{ gal} = 126 \text{ mgal.}$$

Since the two seismic sections describe <u>average</u> structures the crustal structure in Katmai could still be continuous across the volcanic range, but nevertheless a total gravity change of some 150 to 160 mgal should be observed in the crustal section between the Bruin Bay fault and Kodiak Island, if the above described seismic model is a reasonable approximation of the crustal parameters in the Katmai-Kodiak Island area. The observed Bouguer anomalies in this crustal segment, however, average out to zero mgal with superimposed local undulations in Bouguer gravity of about $\pm$ 20 mgal.

The discrepancy between a gravimetrically derived crustal structure using Woollard's (1959) empirical relation between Bouguer anomalies and depth to the Moho and the composite seismic model has already been observed by Berg, Kubota and Kienle (1967) and is shown in Fig. 11.

Significant changes in the seismic crustal model could be expected if the layering were not horizontal as assumed in the model. The depths to the interfaces in the two sections KM-28 and KM-36 (op. cit., p. 1385) would then change accordingly (Berg, personal communication).

Considering the limited accuracy of the seismic model described above and since the gravity effects that should be associated with such a structure are not observed, it is felt that a constant average depth to the Moho of about 32 km between the Bruin Bay fault and Kodiak Island as shown in Fig. 11 and 13 is a reasonable approximation of the true crust-mantle-interface in that area.

Regionally large, positive Bouguer and free-air anomalies northwest of the Bruin Bay fault may be associated with a denser and thicker than normal crust. Woollard et al (1960) have already suggested that the Bristol Bay high may be due to a large intracrustal pluton of mafic rocks in a setting similar to that of the Prince William Sound area, where such a pluton was detected by means of seismic refraction. No new crustal interpretation can be given for that area, since our Katmai seismic and gravimetric data is limited to the region southwest of the Bruin Bay fault.

4.5 Crustal Section Across the Volcanic Range

The composite seismic model discussed above (Berg, Kubota, and Kienle, 1967) describes the average crustal structures between the volcanic range and Kodiak Island and the average northwestern structure between the range and the Bruin Bay fault.

The average crustal density for the two layered northwest section would be 2.82 g/cc for a crust 38 km thick and composed of 15 km of

5.5 km/sec or 2.67 g/cc material and a 23 km layer of 6.5 km/sec or 2.91 g/cc, using the seismic P-wave velocity-density relation derived by Nafe and Drake (1963).

The average density for the two layered southwest section would also be 2.82 g/cc for a crust of 32 km thickness, where layer 1 consists of 12 km of 5.5 km/sec material and layer 2 of 20 km of 6.5 km/sec rock.

Since the average crustal densities of the 2 sections of the composite seismic model agree so well, this slightly low average crustal density of 2.82 g/cc was assigned to the crust in Katmai. Commonly densities between 2.84 g/cc and 2.87 g/cc are used for the average crust.

In the southeast section the average seismic depth to the Moho is 32 km, a depth typical of continental coast areas. Even though the Bouguer gravity undulates from $\pm$ 20 to $\pm$ 30 mgal (Fig. 11) the mean Bouguer anomaly across the section averages out to 0 mgal. Therefore, and for reasons already discussed under Sections 4.3 and 4.4, the normal average crust of the continental coast in the Katmai-Shelikof Strait-Kodiak Island region was chosen to be 32 km thick and of an average density of 2.82 g/cc, overlying an upper mantle of constant density 3.27 g/cc. It is characterized by elevations close to sea level and zero Bouguer anomalies. Most of the positive and negative undulations in the Bouguer gravity can then be attributed to anomalous crustal masses with densities deviating from the 2.82 g/cc average.

Figure 13 shows a crustal section that offers a possible explanation of the Bouguer anomalies observed in profile 2. The location of the section is given in Fig. 9. The 95 km long profile runs in a northwest-southeast direction perpendicular to the regional tectonic trends from

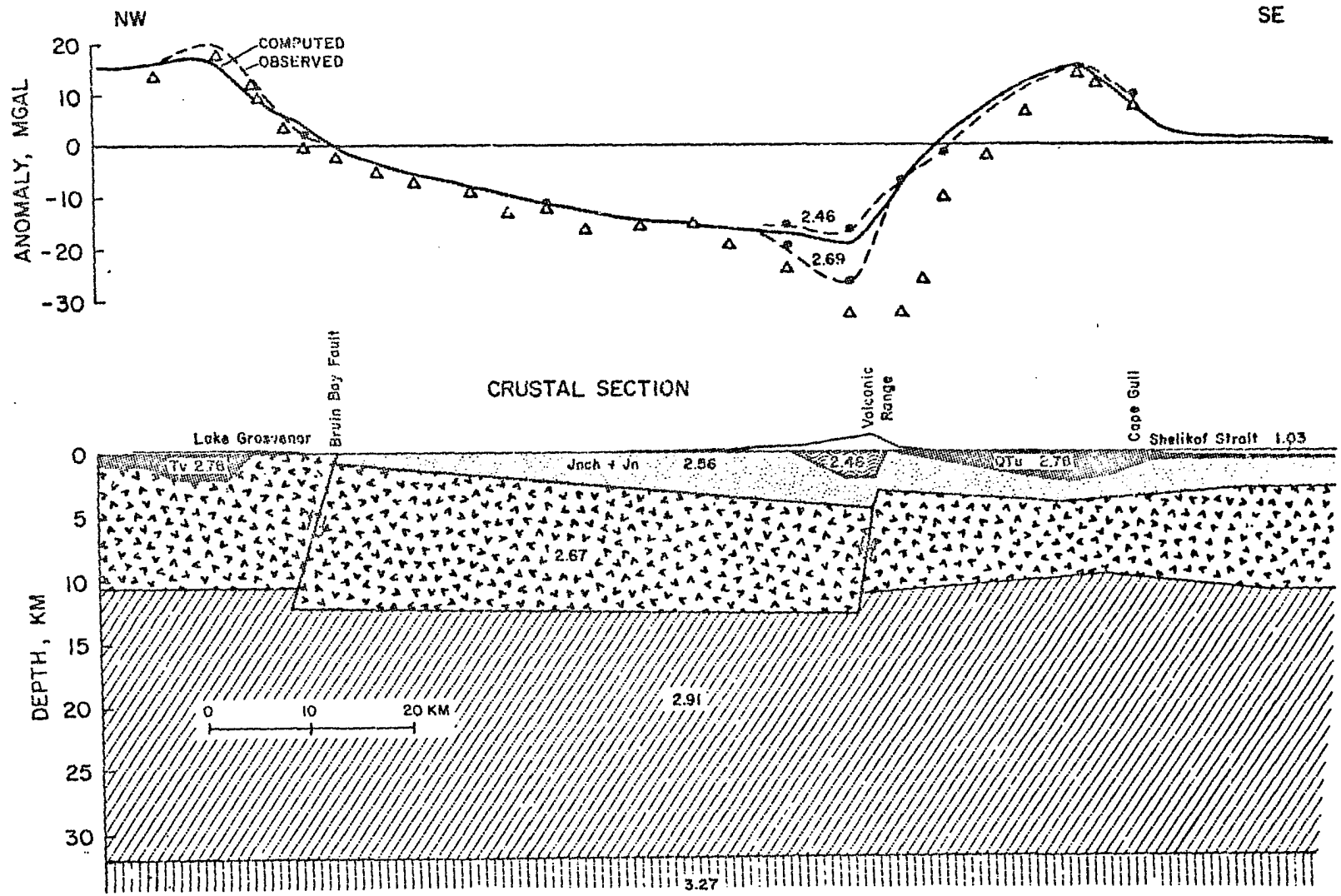

Figure 13. Lower: Computed crustal section across the volcanic range along gravity profile 2 (see Fig. 9). Upper: Observed simple Bouguer gravity (open triangles), observed complete Bouguer gravity (dashed line), both with geologic corrections, and computed attraction (solid line) of proposed structure.

Lake Grosvenor (Grosvenor Camp) across the volcanic range between Snowy Mountain and Mt. Denison to Cape Gull on the Shelikof Strait. According to Keller and Reiser's (1959) geologic map of Katmai it crosses from northwest to southeast, Eocene folded volcanic rocks (Tv, 2.78 g/cc). Lower and Middle Jurassic silicic and mafic intrusive rocks brought into contact with the Naknek Formation by the Bruin Bay Fault (Ji, 2.67 g/cc), gently folded shallow water deposits of the Naknek Formation (Inch + Jn, 2.75 g/cc to 2.44 g/cc) and undifferentiated igneous rocks (QTu), mainly consisting of two volcanic units: folded volcanic rocks of probably Eocene age (Tv, 2.78 g/cc) and predominantly Quarternary undeformed volcanics (QTv, 2.46 g/cc), that overlie uncomformably the older volcanic sequences. The open triangles in Fig. 13 denote simple, geologically corrected Bouguer anomalies calculated by assigning the various densities shown to the different geologic units. Complete Bouguer anomalies (also geologically corrected) were interpolated (dashed line) between stations, where the terrain effects had been calculated (solid points). This "observed curve" is matched with the "computed curve" calculated from the proposed structure section (Fig. 13).

The difference between geologically or density corrected and standard (2.67 g/cc) Bouguer anomalies over the profile was only significant for the high elevation stations K02-9 and K02-11 (K02-10 was a glacier station; about 6 mgal of its negative gravity value can be attributed to the underlying ice, which using an infinite slab approximation and a density contrast of 1.77 g/cc corresponds to about 82 m of ice underneath station K02-10).

The theoretical gravity curve (solid line) in Fig. 13 was computed two-dimensionally using the density contrasts between the rocks of the various geologic units and the average value of 2.82 g/cc for the crust that would produce a zero Bouguer anomaly as discussed above. The computations were done on the IBM 360/40 at the U/A using a program written by M. Talwani (1959) to compute the gravity effects of two-dimensional bodies.

The gravity profile clearly reflects the subdivision of the Katmai area into 3 major geologic units, the dividing lines being the Bruin Bay fault and the volcanic axis. The area northwest of the Bruin Bay fault is characterized by positive Bouguer gravity values which probably connect to the Bristol Bay high (Wollard et al. 1960). Adjacent to the fault, dense folded volcanic rocks overlie the hornblende granites of granitic basement complex that forms a 5 to 20 km wide belt paralleling the fault. The sedimentary units of the Naknek Formation, as exposed between the Bruin Bay fault and the volcanic axis cause negative gravity anomalies achieving minimum values along the volcanic axis. Southeast of the volcanic range, the gravity values rise rapidly to a + 15 mgal high associated with the dense and highly altered and folded volcanics that are exposed along the Shelikof Strait.

The northeasterly alignment of the Katmai volcanoes suggests structural control, such as a fault. Surface evidence for this fault, however, is not seen in outcrop, only two gentle anticlines trending toward each other are mapped between Kejulik Pass and Kaguyak Crater (Keller and Reiser, 1959).

There is, however, seismic and gravimetric evidence for the existence of such a fault. In order to obtain epicenter locations for Katmai earthquakes with minimal location errors, it was necessary to modify the Jeffreys-Bullen crustal model to a composite model with significantly different structures on either side of the volcanic range (Berg, Kubota and Kienle, 1967). The southeastern block appears to be uplifted with respect to the northwestern block along the volcanic axis. The depth distribution of earthquakes occurring during the summer of 1965 in a section perpendicular to the range hints at a grouping of foci along a zone that dips steeply from the volcanoes to the northwest (op. cit., p. 1372, Fig. 4). Another cross section prepared by Matumoto and Ward (1967, p. 2505, Fig. 10) shows a more or less vertical grouping of 1965 Katmai earthquake foci underneath the volcanoes. The greatest concentration occurs at shallow depths. If the earthquake foci delineate a faulted zone of crustal weakness below the volcanoes it must be vertical or nearly so.

Gravimetrically, the negative middle section of gravity profile 2 between the Bruin Bay thrust and the volcanoes could be explained by the combined effects of the low density sedimentary units that are thickening toward the volcanoes and a relatively downdropped 53 km wide section of 2.67 g/cc upper crust (Fig. 13). The offsets along the Bruin Bay fault and the hypothetical fault below the volcanoes deduced from the observed gravity effects are about 1.6 km.

About 40 km to the southeast in profile D,1, a similar offset of about 3 km causing a 30 to 35 mgal gravity offset was postulated by Berg, Kubota and Kienle (1967, p. 1389). It was then associated with the 3 km

step (from 15 to 12 km depth) of the interface between seismic layer 1 and 2 across the volcanic range. This was calculated without taking into account the density variations in the uppermost crustal layers which in profile D,1 also cause positive anomalies southwest of the volcanic axis; i.e. only part of the 30 to 35 mgal anomaly could be attributed to the postulated fault, which reduces the magnitude of its displacement.

Rough estimates of the total thickness of the Naknek sediments in Katmai can be obtained from Keller and Reiser's work (1959, p. 270). They observed:

1,000 ft	marine, irregularly bedded Chisik basal conglomerate (as described by Mather, 1925, p. 169)
800 ft	fine to coarse grained arkose
2,000 ft	thin bedded siltstone, fine grained sandstone, and sandy shale
3,000-6,000 ft	locally massive conglomerate, interbedded with fine-to-coarse-grained arkose, siltstone, and shale

or in summary up to 1,000 ft of Chisik basal conglomerate overlain by 6,000 to 9,000 ft of Naknek sediments.

A well at Becharof Lake (Mobile Bercharof No. 2) reached granitic basement at about 14,000 ft depth, most of that distance was drilled in Mesozoic sediments.

The maximum thickness of about 4 km assumed for the low density sediments beneath the volcanic axis seems therefore not to be unreasonable. The Naknek Formation decreases in thickness as one travels from the Katmai volcanoes to Lake Grosvenor, where large exposures of Chisik basal conglomerate are found. The general dip of the strata is about 4 to 8

degrees to the southeast in the profile area; the assumed dip of the sediment-basement interface in the crustal model is about 5 degrees.

The positive gravity anomalies northeast and southwest of the relatively downdropped block can be attributed in part to the relatively upthrown blocks on either side of the "graben" structure, and in part to the high density folded and altered Eocene (?) volcanics that make up the surface rocks in both areas. Northwest of the Bruin Bay fault these overlie the early Jurassic batholith; southeast of the volcanoes they most probably overlie the Naknek Formation.

The relationship between near surface geology and gravity directly beneath the volcanic range is not too clear. Using a Bouguer reduction density of 2.67 g/cc, profiles D,1 (Fig. 19) and 2 (Fig. 13) show a local low associated with the volcanoes. It is superimposed on the more regional gravity low caused by the Naknek sediments. In Profile 2 it is possible to remove the local low by using a reduction density of 2.46 g/cc, the density found for the young vesicular volcanics (QTv) of Mts. Martin, Mageik, Trident, Katmai and Knife Peak. However, one rock sample taken at gravity station KO2-9, which was located on a Nunatak of Serpent Tongue Glacier, had a density of 2.69 g/cc. The 2.69 g/cc gravity curve is therefore also shown in Fig. 13. In order to explain the resulting local gravity low a low density body had to be assumed underneath the volcanoes. Geologically, this could imply a highly disturbed sedimentary zone that is impregnated with vesicular andesitic rocks, because it is here where one would expect the andesitic magmas to break to the surface through the sediments.

As we will see later in profile D,1, 40 km to the southwest (Fig. 19) a similar local gravity low seems to be related to the active volcano Mt. Trident and associated low density material at shallow depths. All the gravity anomalies of profile 2 could satisfactorily be explained with known shallow depth mass anomalies within the upper crust. It was not necessary to assume a root-like structure beneath the volcanoes and the crust-mantle interface was found to be constant at 32 km depth, which is in accord with the already discussed analysis of the regional crustal structure (Sections 4.3 and 4.4). It appears that the crust in Katmai is rigid enough to support the load of the volcanic range without local isostatic adjustment, a result that could be expected if one considers the relatively small width of the topographic features that form the volcanic range.

4.6 The Kulik Lake Intrusion

A major gravity low was detected on the northwestern end of gravity profile 4 (Figs. 10 and 16) in the Kulik Lake area and adjacent mountains to the southeast. This low was not found in profile 8, 16 km to the northeast and profile 7, 20 km to the southwest (Figs. 15 and 17). Both of these profiles, like profile 4, trend northwest-southeast. Unfortunately the sparcity of gravity stations in the Kulik Lake area permits only a schematic outline of the gravity low between the northwestern ends of profiles 7 and 8. Terrain corrections were very large, on the order of 7 to 15 mgal in the deep valley southeast of Kulik Lake and along the southwestern shore of the Lake, which itself lies in a deep depression (Table 4, Stations 4-1 to 4-8).

The terrain corrected anomaly has an amplitude of 19 mgal (Fig. 16) if one removes a regional gradient of 0.55 mgal/km in the northwest-southeast direction, the gradient ascribed to the sedimentary basin. A profile at right angles along the southwest-northeast trending zero isoanomaly gives a terrain corrected anomaly of about -20 mgal.

The Kulik Lake gravity low of roughly 20 mgal could be caused by the surficial geology or by an intrusive. No extensive low density alluvial deposits exist in this very mountainous area.

A rough idea as to the depth of the mass deficiency can be found by using the half width of the anomaly--the width of the profile at half the maximum amplitude $W_{1/2}$--which is 23 km in the NW-SE profile and 22 km in the NE-SW profile. If the mass deficiency is approximated by a simple geometric form such as a sphere, the depth to its center d is given by

$$d = 0.65\ W_{1/2}$$

(Nettleton, 1940, p. 123). This formula gives depths of 15 km and 14.3 km, i.e., the mass deficiency is to be sought well within the crust and is probably due to the intrisive body which crops out in the crest of the Kamishak Anticline 15 km west of the southeastern end of Kulik Lake.

The mass deficiency in tons is

$$M = 6.5\ \Delta g_{max} \cdot (W_{1/2})^2,$$

where Δg_{max} is measured in mgal and $W_{1/2}$ in feet (Grant and West, 1965, p. 29).

For a Δg_{max} of 20 mgal and a $W_{1/2}$ of 22.5 km or 73,800 feet the mass deficiency of the Kulik Lake intrusion is roughly 7×10^{12} tons.

The radius of the sphere R depends on the assumed density contrast $\Delta\rho$ between the quartz diorite stock and the intruded rock. For a depth of 14.7 km to the center of the sphere some possibilities are:

$\Delta\rho$ (g/cc)	R (km)
0.05	14.5
0.1	11.5
0.2	9.2
0.3	8.0

The 14.7 km depth to the center of the spherical mass deficiency represents a maximum figure; wider (i.e., more lens-shaped) mass anomalies at much shallower depth can produce exactly the same gravity effect at the surface as the one resulting from a spherical body at greater depth.

A more detailed analysis in the Kulik Lake area is not justified because neither the detailed gravity field nor the density contrast between the intruding and the intruded rocks are known. Nevertheless, the gravity data produces evidence for a much larger intrusive body than indicated by the relatively small outcrop of Tertiary quartz diorite within the anomaly in the crest of the Kamishak Anticline.

With additional helicopter time the intrusive could be traced rather easily by establishing gravity stations in the numerous valleys that dissect the mountains at the southeast end of Kulik Lake. Terrain effects, however, would be rather severe.

4.7 The Mt. Trident Low

A very local gravity low in the immediate vicinity of the new eruptive center of Mt. Trident, which has formed since 1953 (Ray, 1967, Eruptive

History of Mt. Trident, pp. 180-188) was first detected by Decker (1963) in a gravity profile from Naknek Lake through Katmai Pass to the Shelikof Strait. His data is included in this thesis. Decker had previously stated:

> "The gravity low centered on the volcanic axis has a local component caused by some shallow density contrasts about 4 miles wide, the low density materials being related to the presently active volcanic axis."

This local negative component, which is superimposed on the more regional low that can be attributed to the Naknek sediments, is centered about 2 km south-southeast of Katmai Pass at the foot of the new Mt. Trident flank cone, first formed in 1953. In addition to Decker's stations 17, 18 and 19, ten more gravity stations were established in the Mageik Creek flats, which define the anomaly in more detail (stations 1 and 7 to 15, Table 3). These observations correspond to Decker's data within the errors due to inaccurate elevations, which were good to only $\pm$ 20 to $\pm$ 50 feet for both sets of data. This corresponds to $\pm$ 1.2 to $\pm$ 3.0 mgal error in the simple Bouguer gravity for a reduction density of 2.67 g/cc.

A complete Bouguer 2.67 g/cc gravity map of Mt. Trident and vicinity is given in Fig. 10 together with the local geology. Terrain corrections in the Mageik Creek flats and on the lower slopes of Mt. Trident ranged from 4 to 7 mgal.

Kubota and Berg (1967) observed a screening effect which attenuated predominantly the vertical component of the elastic shear waves from earthquake wave trains that traveled across the volcanic range. An analysis of the wave paths in two crustal layers and the upper mantle led to the

location of possible magma reservoirs in these three layers in the Katmai area. The shallow reservoirs of the upper crustal layer are believed to be associated with the young volcanic vents in Katmai, all of which are presently active. The location of two magma chambers (1-C and 1-D) seems to coincide with the Trident gravity low. It is here in the vicinity of the new eruptive center of Mt. Trident that one would, indeed, expect the magma to rise to the surface from depth. Perhaps the earliest observed evidence of forthcoming volcanic activity in the Mageik Creek valley at a time where the new Trident flank cone was not yet in existence can be found in Father Hubbard's description of his ascent to the Valley of Ten Thousand Smokes from Katmai Bay (Shelikof Strait) in September 1934. Following the southwestern flank of the then "dormant" Mt. Trident, his expedition noticed strong H_2S odors (Hubbard, 1935, p. 212).

Father Hubbard states:

> "Though there was no perceptible odor or gases in the rapidly dying Valley of Ten Thousand Smokes, throughout the Mageik Bad Lands that constituted the basin between the mountains there were several spots where strong sulphur odors prevailed."

His ideas about the cause of volcanic eruptions are amusing:

> "Below the surface of the earth are deposits of sulphur, and nearby other deposits of iron ore. When these are shaken together by an earthquake, or in some other way combustion is set up, just as with the minerals in the test tube. The heat melts the nearby rocks, whose water content then expands into steam; and the pressure grows until a vent is forced upward. A volcanic eruption is the result."

Kubota and Berg (1967, p. 28) find that magma chambers 1-A, 1-B, 1-C and 1-E occur at depths of some 10 km and extend horizontally less than 5 km. The same authors also attempted a preliminary interpretation of the Trident gravity low observed in profile D,1 based on a reduction

density of 2.67 g/cc and tried to correlate it with their magma chamber 1-C (op. cit., pp. 33-36). Using a density contrast of 0.25 g/cc between the andesitic magma and the host rock, the magma being less dense, they found that cylinders of a common radius of 5 km and varying depths of burial and lengths could produce the observed 20 mgal negative anomaly. However, the geometry of the anomaly, which is characterized by its half width, i.e.,the width of the anomaly at half maximum amplitude, was neglected. The observed half width of the Trident low for a reduction density of 2.67 g/cc is about 7 km (Fig. 19, profile D,1). Condensing Kubota and Berg's postulated cylinders to vertical mass lines (cylindrical analogy to mass point) would produce anomalies that are characterized by the following approximate half widths $W_{1/2}$:

Cylinder No.	H	D_1	$W_{1/2}$
1	5.8 km	2 km	6 km
2	10	3	10
3	70	5	-
4	∞	5.6	19

where H = length of the cylinder and

D_1 = depth of burial.

The above half widths were calculated using the formula for the attraction of a buried vertical semi infinite mass line. If D_1 is the depth to the top end A of the line, the vertical component of its gravity effect at the surface point 0 above the line is

$$\Delta g = G \cdot \lambda \cdot \frac{1}{D_1} ,$$

where λ is the line density in g/cc. The depth to the line is linearly related to the half width $W_{1/2}$

$$D_1 = W_{1/2} \cdot \frac{1}{2\sqrt{3}} \cdot$$

The gravity effect of a finite length mass line extending from A to B at some depth greater than A is given by the difference between the gravity effects of mass line A - ∞ and B - ∞. The greater the depth of burial of semi infinite mass lines, the flatter is their gravity effect at the surface and the bigger is the half width $W_{1/2}$. From the four cylinders discussed above, all of which cause a maximum anomaly of 20 mgal, only the anomaly of cylinder No. 1 is sharp enough to fit the observed Trident anomaly; the other three models, cylinders No. 2 through 4 can be ruled out.

Kubota and Berg (1967) used a very unlikely density contrast of 0.25 g/cc between the andesitic magma chamber and the host rock, the magma being less dense than the surrounding rock. This figure was derived from two examples of density changes associated with the solid-liquid phase transition of two diabases, one from the Palisades, the other from Vinal Haven (E. B. Dane, Jr., Handbook of Physical Constants, Table 3-2, Birch et al. 1942). The transition took place with a 9.9% and 8.4% density decrease, respectively, the densities of the liquids being 2.60 and 2.64, respectively. Assuming a host rock density of 2.5 g/cc and a density decrease of about 10% for the liquid phase Kubota and Berg arrived at a host rock--magma density contrast of 0.25 g/cc.

The magma, however, is not derived from the host rock, but rises from great depth. If the magma chamber is located in the upper crustal

layer, host rock densities of about 2.67 g/cc could be expected. In the same Table 3.2 (Birch, 1942) densities of the liquid phase of a basalt and a diorite are given with 2.63 and 2.60 g/cc respectively. Since andesites are an eruptive equivalent of diorites, one could expect a density of about 2.6 g/cc for andesitic magma. If the 2.6 g/cc figure is correct, this could even cause positive contrast and positive anomaly if the chamber is embedded in 2.5 g/cc host rock. It is, in this context, interesting to note that Ryall and Bennett (1968) ascribe local gravity highs of + 33 and + 18 mgal to shallow depth basaltic magma reservoirs beneath the Kilauea summit area and below the southward extension of the Mauna Loa southwest rift zone. The Kilauea summit magma chamber was detected seismically and was also deduced from inflation and deflation measurements of the Kilauea summit region. Assuming a density of 2.63 g/cc for the basaltic magma (Table 3.2, Birch, 1942) and Strange's et al (1965) density of 2.3 g/cc for vesicular Hawaiian basalts above sea level, a density contrast of about 0.3 g/cc results and will indeed cause positive anomalies.

If there exists an andesitic magma chamber in the upper crustal layer in the vicinity of Mt. Trident, its density contrast with the 2.67 g/cc upper crustal material will be 2.67 - 2.60 = 0.07 g/cc. A small anomalous mass with such a density contrast at a depth of about 10 km, the depth range suggested by Kubota and Berg for the upper crustal magma chambers, cannot produce a gravity effect of the amplitude and shape of the Trident gravity low.

Kubota and Berg's interpretations were based on a 2.67 g/cc Bouguer reduction density. New laboratory hand specimen density determinations

of Keller and Reiser's (1959) Quarternary and recent undeformed volcanic rocks, generally consisting of vesicular andesites, indicate low densities of 2.46 g/cc. These are the volcanics that are exposed in the Trident low area and cap an upper Jurassic sediment platform that rises to an elevation of very roughly 2000 ft in the area in question. The average density for the Bouguer plate consisting of sediments, penetrated and overlain by low density andesites, was assumed to be 2.5 g/cc. Using 2.5 g/cc as reduction density for the Trident gravity stations diminishes the amplitude of the 2.67 g/cc Trident low from 20 to 13 mgal and the half width from 7 to 4.5 km as seen in profile D,1 (Fig. 19), where complete Bouguer anomalies for reduction densities of 2.67 g/cc, 2.5 g/cc and 2.2 g/cc are plotted.

The Trident anomaly is assumed to be circular in shape (Fig. 10) and about 10 km wide. It could, however, also be elongate in a southeast-northwest direction coinciding with the volcanic axis and the geologic unit of undeformed young volcanics. Unfortunately, the inaccessability of Mt. Trident and Mt. Katmai northeast of the Mageik Creek flats and Mt. Mageik and Mt. Martin southwest of the anomaly did not permit a closer gravimetric control of the anomaly in the southeast-northwest direction. Besides, terrain corrections would be enormous for such mountain stations.

Assuming that a spherical mass anomaly causes the Trident low, the observed half width of 4.5 km indicates a depth of

$$d = 0.65 \cdot W_{1/2} = 2.9 \text{ km}$$

to the center of the anomalous mass. This depth is a maximum figure, because,as mentioned above,wider and thinner masses at much shallower

depth can produce exactly the same surface gravity effect.

The mass deficiency is

$$M = 6.5 \cdot \Delta g_{max} \cdot (W_{1/2})^2$$

$$[\text{ton}] = [\text{mgal}]\,[\text{feet}]^2$$

$$M = 184 \cdot 10^8 \text{ tons} .$$

The radius of the sphere depends on the density contrast. Judging from the structure section (Fig. 13) one would expect lower stratigraphic units of the Naknek Formation or basement at a depth of 2.9 km beneath the volcanoes. If andesitic magma causes the anomaly a density contrast of only 2.67 - 2.60 = 0.07 g/cc between the basement and the magma could be assumed. If the host rock is composed of Naknek sediments the contrast is even less. A density contrast of 0.1 g/cc, which is a maximum possible contrast for andesitic magma in the upper crust in Katmai, results in a radius of 3.4 km for a spherical magma chamber. This solution has to be discarded because the depth to the center of the sphere is only 2.9 km. Higher density contrasts give much more reasonable dimensions for the mass anomalies; some possibilities are:

$\Delta\rho$ (g/cc)	R (km)
0.2	2.7
0.3	2.4
0.4	2.1

It is therefore unlikely that the mass deficiency causing the Trident low is an andesitic magma chamber. Geologically, higher density contrasts than 0.1 g/cc could be attributed to voids, vugs and cavities in the

strata or, as already discussed under 4.5, to a sedimentary zone that is penetrated and impregnated with vesicular low density andesitic rock. It is apparent that here, in the immediate vicinity of active Mt. Trident, the andesitic magmas must break through the Naknek sediments to the surface.

Maximum depth rules, derived by Bott and Smith (1958) also indicate very shallow depths for the Trident mass anomaly as derived above. Theorem 3 (op. cit., p. 3) gives h, the maximum depth to the top of a three-dimensional mass as:

$$h \leq \frac{48 \cdot \sqrt{5} \; A_{max}}{125 \cdot \left|\frac{dA}{dx}\right|_{max}}$$

where A_{max} is the maximum amplitude and $\frac{dA}{dx}_{max}$ is the maximum gradient of the anomaly. The corresponding parameters of the Trident low are 13 mgal and 6 $\frac{mgal}{km}$ and h is then : $h \leq 1.9$ km.

Conclusion

1. The mass anomaly causing the Trident low has to be sought at very shallow depth, the maximum depth to the top of the anomaly being 1.9 km. The maximum depth to its center is 2.9 km.
2. In order to study screening effects of earthquake S waves across the volcanic range, Kubota and Berg (1967, p. 24) restricted the analysis to seismic wave trains that arrive at Baked Mt. Hut with angles of emergence of 28 to 37 degrees. Mt. Trident is located 9 km southwest of BMH. Assuming a constant seismic velocity for the upper crustal layer places the seismic wave paths at depths from 12 to 17 km beneath Mt. Trident. This means that even if magms is present

in the shallow depth Trident mass anomaly it could not be "seen" by the seismic wave trains studied by Kubota and Berg. A direct correlation between magma chambers 1-C and 1-D (op. cit., pp. 33-36) and the Trident gravity low is therefore very unlikely.

3. Because andesitic magmas and upper crustal material in Katmai have very similar densities, such magma cannot cause an anomaly of the size and shape of the Trident low. The contrast to the vesicular Trident andesites could even be positive.

4. It is interesting to note that a Bouguer reduction density of 2.2 g/cc for Trident gravity stations would eliminate the entire local anomaly. Geologically, this could imply that the sediments beneath the Trident gravity low are heavily impregnated with low density vesicular andesites. An average bulk density of 2.2 g/cc for such andesites does not seem to be too unreasonable if one considers the average bulk density of 2.3 g/cc for the denser Hawaiian basalts above sea level as derived by Strange et al (1965, p. 384). Since the groundwater table in Hawaii is found around sea level, 2.3 g/cc is the average bulk dry density of Hawaiian rocks above sea level. No information is available about the water table in Katmai, i.e. whether dry or wet bulk densities should be used in the Bouguer reduction. The bulk dry density of one Trident andesite was 2.39 g/cc, the bulk wet density (ssd) for the same sample was 2.44 g/cc, its porisity was 2.3%. These, however, are the densities of one individual rock sample and there are likely to be other negative contributions to the overall bulk density of the Trident volcanics such as voids and vugs within the flows.

The negative correlation between station elevation and Bouguer anomaly for reduction densities greater than 2.2 g/cc for the Trident low is additional evidence that the assumed reduction densities for the Trident gravity stations are too high. For 2.2 g/cc no correlation with the local topography exists.

5. If a reduction density of 2.5 g/cc, which is the mean value between the wet bulk densities of the young undeformed Katmai andesites (QTv) and the upper Naknek sediments is correct, the resulting Trident gravity low can be satisfactorily explained by shallow depth (2.9 km) spherical mass deficiencies with density contrasts ranging from 0.2 to 0.4 g/cc and radii ranging from 2.1 to 2.7 km. A more detailed analysis of the Mt. Trident gravity field is not justified considering the limited accuracy and the sparsity of the gravity stations that define the Trident low, the poor density data and the lack of seismic control.

A tripartite seismic network in the Mageik Creek flats could prove extremely useful in monitoring volcanic earthquakes associated with eruptions of Mt. Trident. Such earthquakes have extensively been used in studying Hawaiian and Japanese volcanoes to trace the crustal paths of rising magma columns and to detect the storage chambers. Time correlations between photographed volcanic eruptions of Mt. Trident and volcanic explosion earthquakes recorded 9 km to the north-northwest at BMH were established for 5 events with correct S-P times and roughly the same direction of approach in the summers of 1966 and 1967. Volcanic earthquake

swarms (B-type) that may have originated in the Mt. Trident area were also recorded during the same time. Unfortunately, accurate location of these events was not possible with only one seismic station recording the events, i.e. Baked Mt. Hut.

6. As pointed out above, magma chambers 1-C and 1-D, located at a depth of about 10 km or deeper northwest and southwest of Mt. Trident below Mt. Katmai and Mt. Mageik, respectively (Kubota and Berg, 1967, p. 28), are not directly associated with the Trident gravity low because their size and density contrasts are too small to cause appreciable gravity effects at the earth's surface. They could, however, represent seismically detectable magma reservoirs which are connected by magma ducts to the active volcanoes Mt. Katmai, Mt. Mageik and Mt. Trident with its shallow depth mass deficiency causing the Trident gravity low.

4.8 Gravity Profiles

Most of the Katmai gravity data was taken along northwest-southeast striking profiles that cut across the regional tectonic trends and the volcanic range. The gravity traverses are about 100 km in length and end at the shores of the Shelikof Strait. The principal data, simple Bouguer anomalies, free-air anomalies and station elevations for seven gravity profiles are plotted in Figs. 14 to 20. The profiles are briefly discussed below, taken in order from northeast to southwest; i.e. in the order K9, K8, K4, K7, K2, KD,1 and K3. For location of the traverses see Fig. 9.

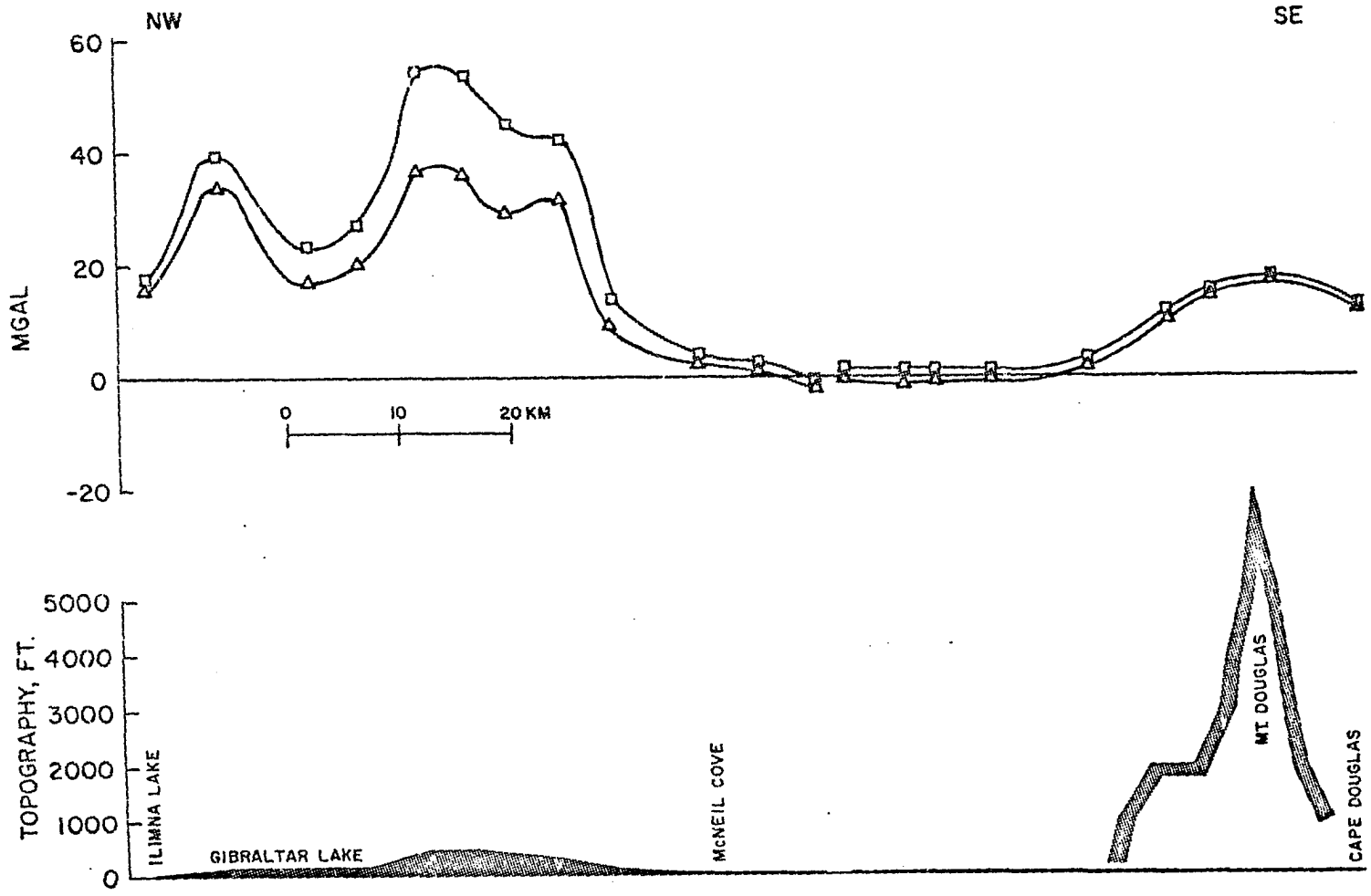

Figure 14. Gravity profile 9 (see Fig. 9) from Iliamna Lake to Cape Douglas, open triangles represent simple Bouguer (2.67) gravity anomalies, open squares represent free-air anomalies, profile topography is shaded, adjacent topography outlined.

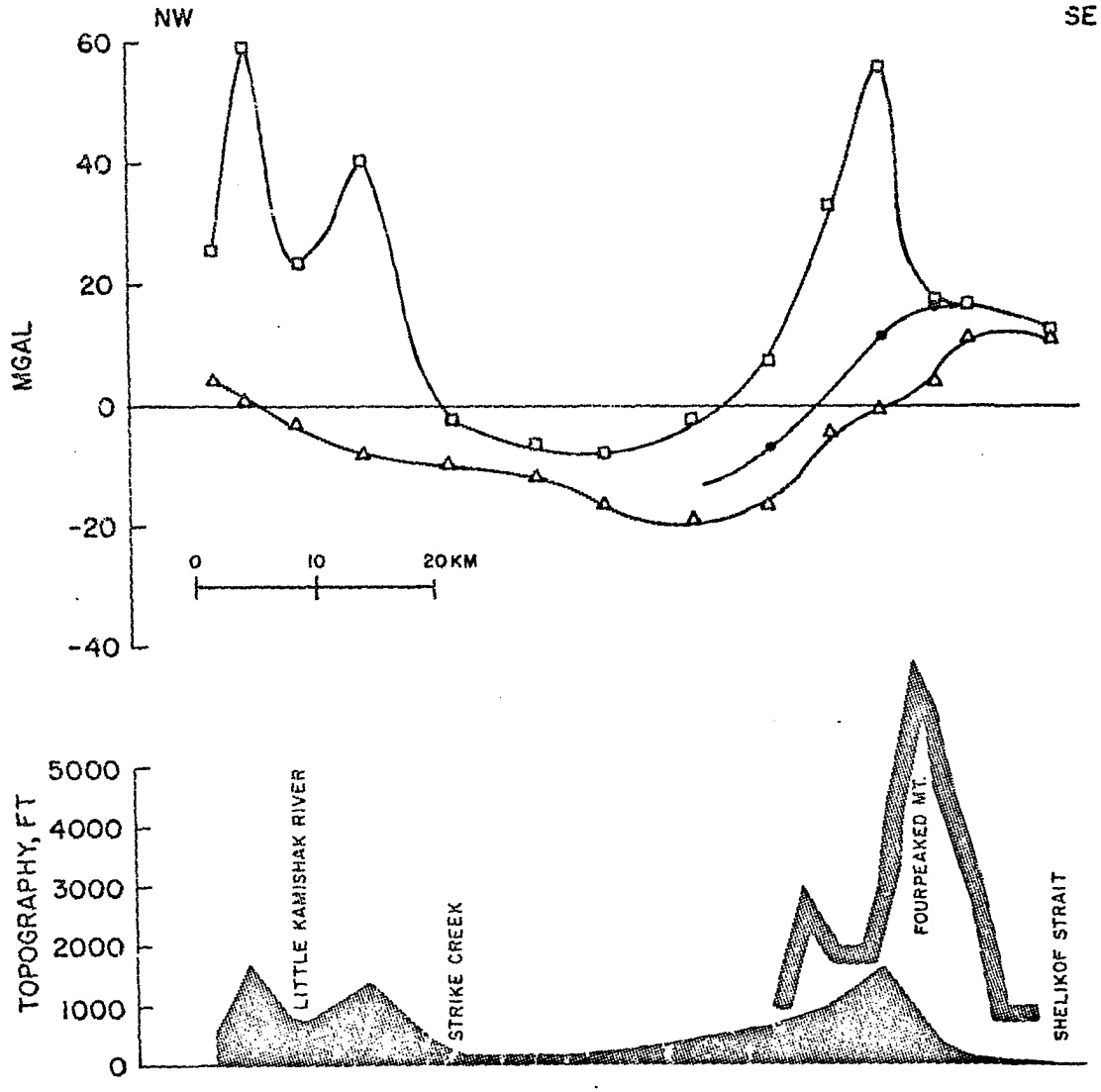

Figure 15. Gravity profile 8 (see Fig. 9) from Pirate Lake to Kaguyak Bay, open triangles represent simple Bouguer (2.67) gravity anomalies, open squares represent free-air anomalies, points represent complete Bouguer (2.67) gravity anomalies, profile topography is shaded, adjacent topography outlined.

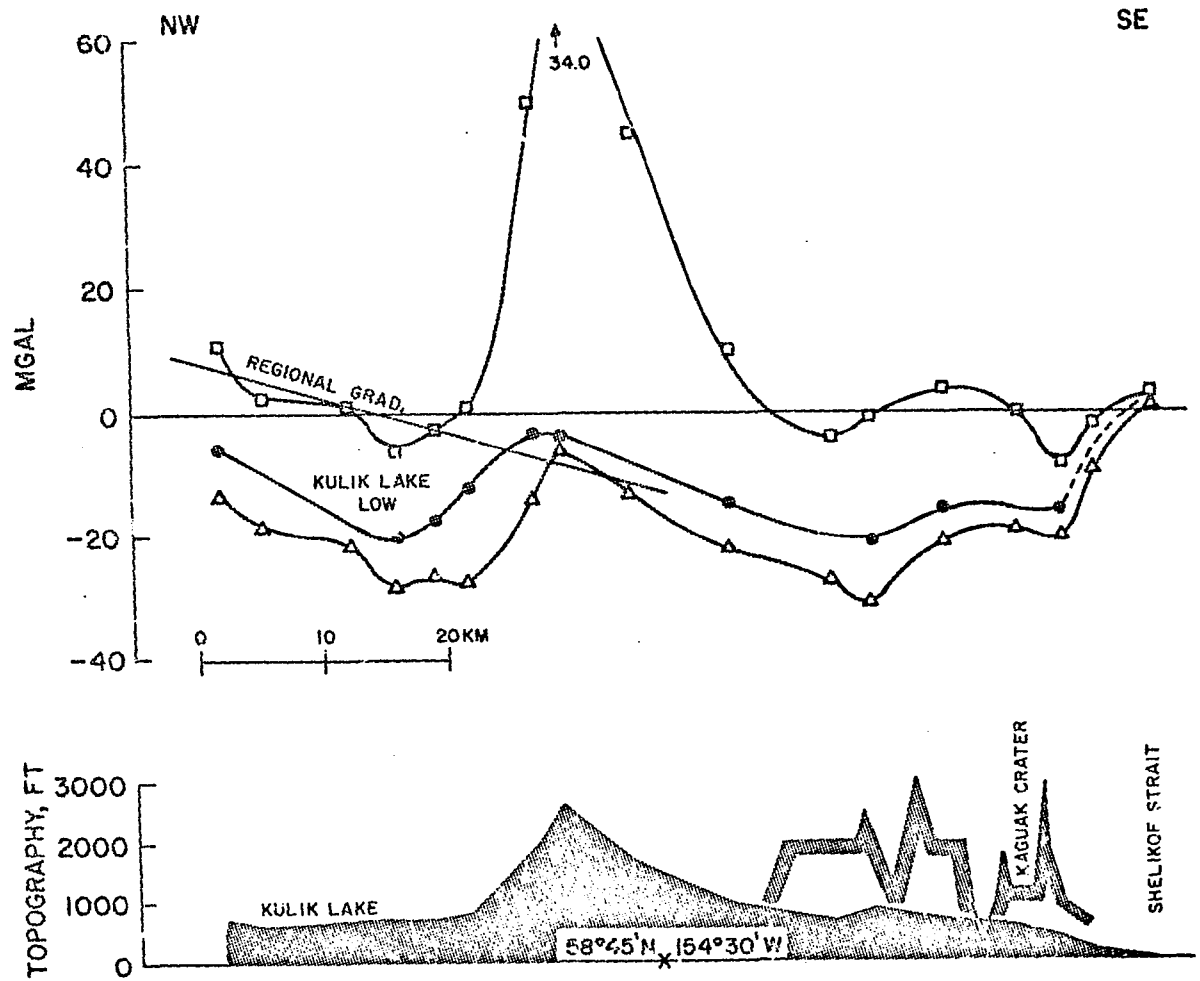

Figure 16. Gravity profile 4 (see Fig. 9) from Kulik Lake to Cape Chiniak, open triangles represent simple Bouguer (2.67) gravity anomalies, open squares represent free-air anomalies, points represent complete Bouguer (2.67) gravity anomalies, profile topography is shaded, adjacent topography outlined.

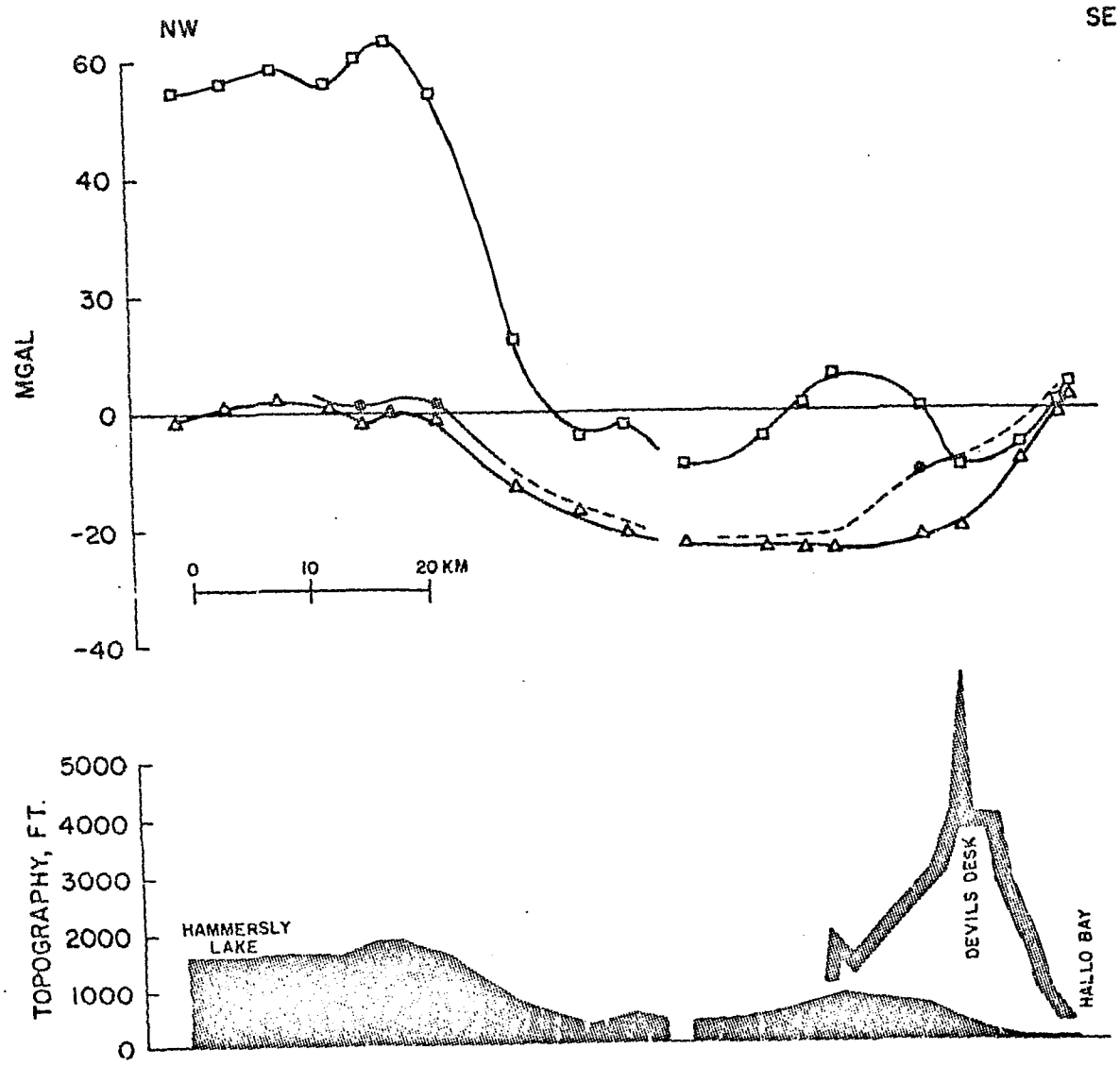

Figure 17. Gravity profile 7 (see Fig. 9) from Hammersly Lake to Hallo Bay, open triangles represent simple Bouguer (2.67) gravity anomalies, open squares represent free-air anomalies, points represent complete Bouguer (2.67) gravity anomalies, profile topography is shaded, adjacent topography outlined.

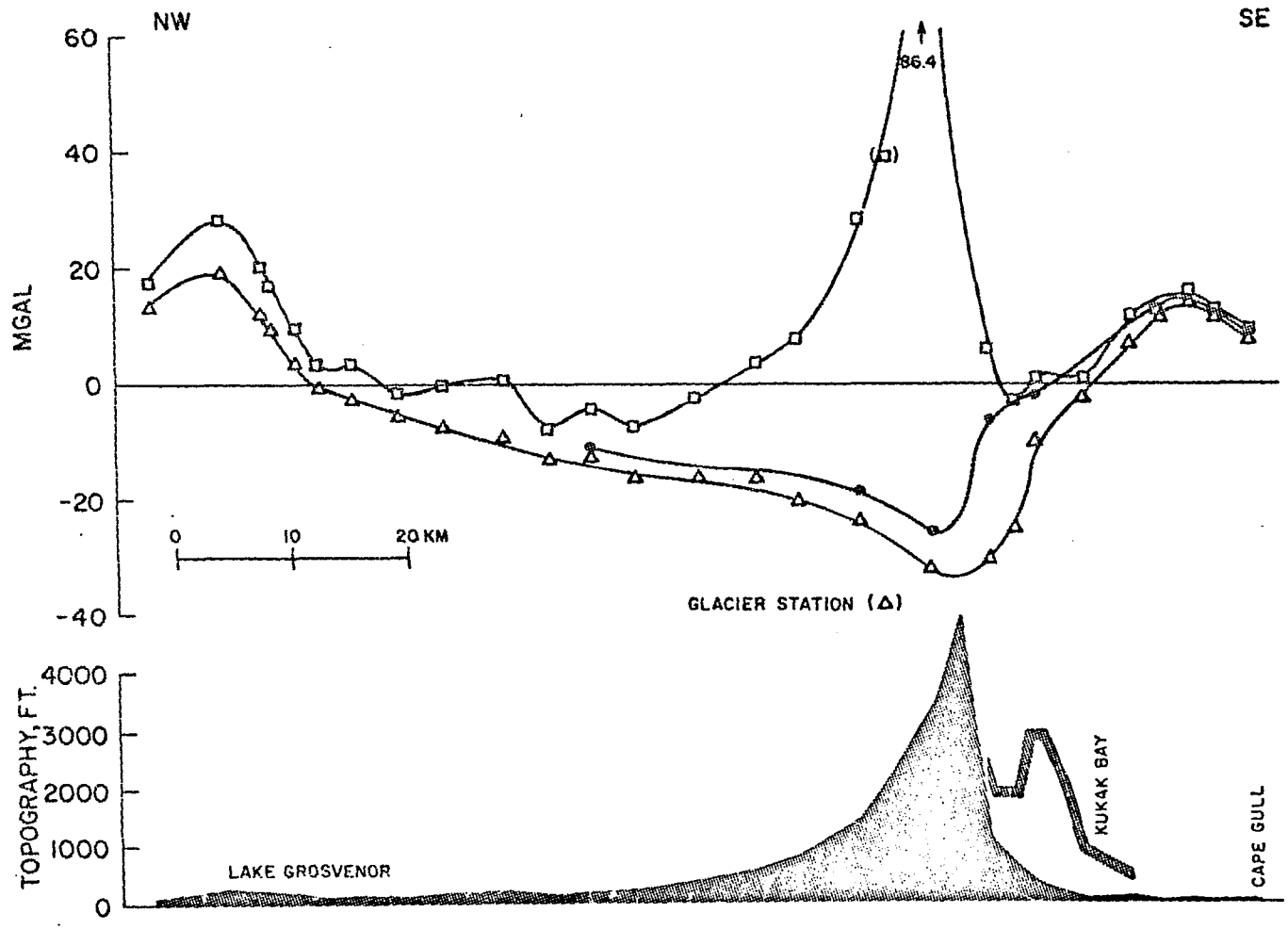

Figure 18. Gravity profile 2 (see Fig. 9) from Grosvenor Lake to Cape Gull, open triangles represent simple Bouguer (2.67) gravity anomalies, open squares represent free-air anomalies, points represent complete Bouguer (2.67) gravity anomalies, profile topography is shaded, adjacent topography outlined.

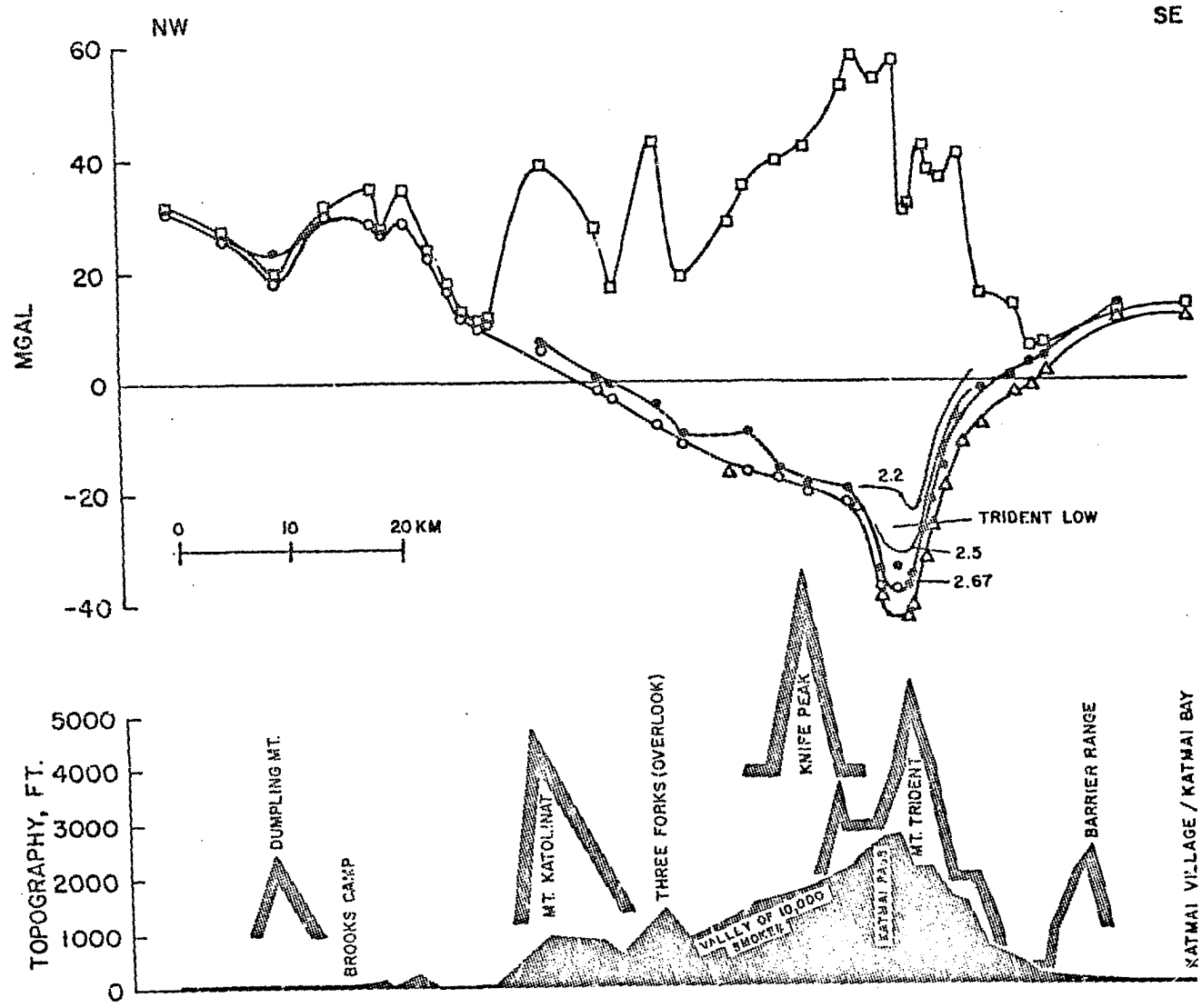

Figure 19. Gravity profile D,1 (see Fig. 9) from Naknek Lake to Katmai Bay, open triangles and circles represent simple Bouguer (2.67) gravity anomalies, open circles represent Decker's data of 1963, open squares represent free-air anomalies, points represent complete Bouguer (2.67) gravity anomalies, profile topography is shaded, adjacent topography outlined.

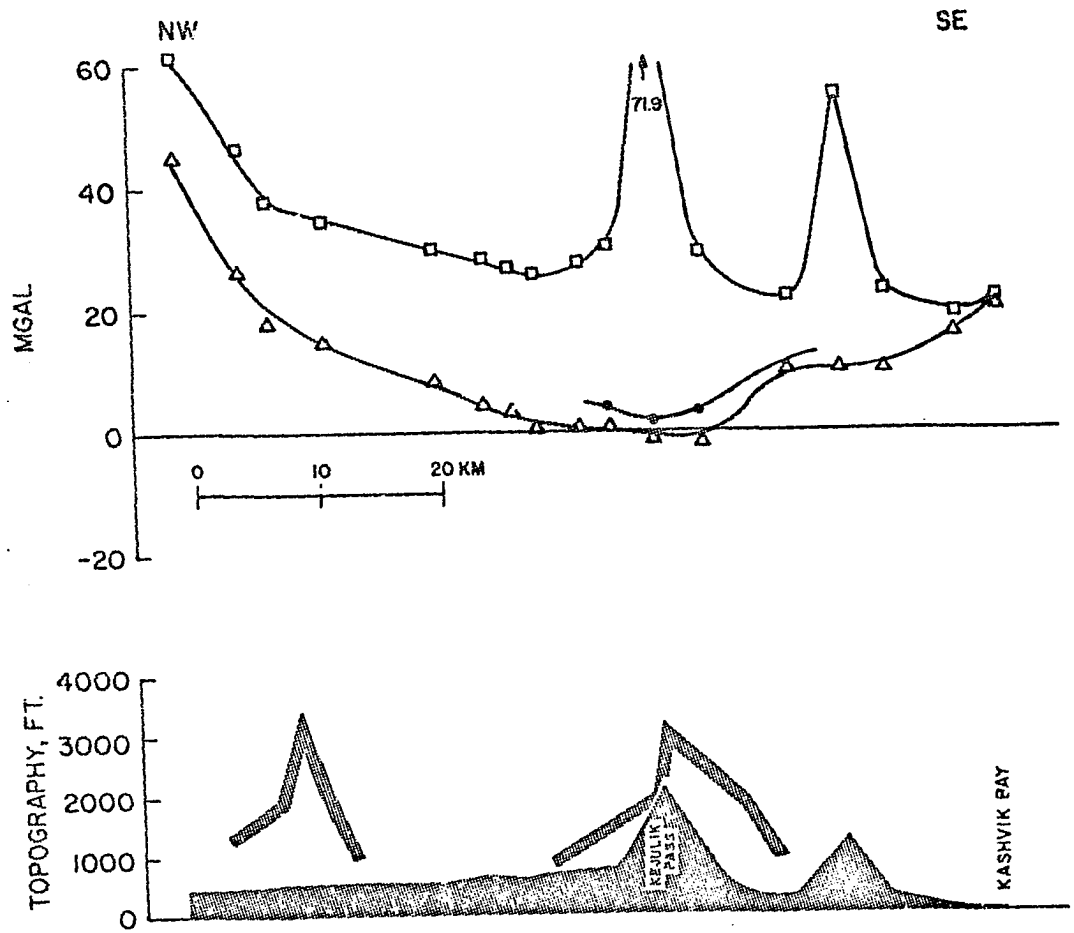

Figure 20. Gravity profile 3 (see Fig. 9) from Contact Creek to Kashvik Bay, open triangles represent simple Bouguer (2.67) gravity anomalies, open squares represent free-air anomalies, points represent complete Bouguer (2.67) gravity anomalies, profile topography is shaded, adjacent topography outlined.

Profile 9 (Fig. 14) is the longest of the profiles and extends over 115 km along the base of the Alaska Peninsula from the village of Kakhonak on Iliamna Lake to Cape Douglas on the northeastern end of the Shelikof Strait. The northwestern half of the traverse from Iliamna Lake to McNeil Cove (Kamishak Bay) is characterized by a positive mean gravity of about + 25 mgal, which seems to be associated with an uplifted northwestern block, raised along the Bruin Bay fault that places the Lower and Middle Jurassic granitic basement complex northwest of the fault in fault contact with the sediments to the southeast. Rapid variations in the simple Bouguer gravity with amplitudes of ± 10 mgal are locally superimposed on this larger scale gravity high and reflect the near surface geology of the area. Positive gravity values are associated with the folded and altered early Tertiary andesites and basalts that are exposed along the southern shore of Lake Iliamna, and correspond to the Shelikof Strait exposures of the same geologic unit. The relatively low values in the Gibraltar Lake region may correspond to Lower Jurassic volcanics (Jv, Fig. 2). Further to the southeast, relatively high gravity values can be correlated with a structural high that exposes metamorphosed Permian and Lower Mesozoic rocks within the Lower and Middle Jurassic igneous complex.

The gravity values decrease with a steep gradient toward the basin of Naknek sediments to the southeast and across the Bruin Bay fault. Southeast of the fault zero mgal anomalies are typical for the southern shores of Kamishak Bay. This is in general agreement with Barnes' simple Bouguer gravity map of southern Alaska (Barnes, 1967) which shows near zero mgal anomalies in the entire Kamishak Bay. These observations

change Woollard's et al (1960) Bouguer iso-anomaly map of Alaska considerably in that region. According to their map the Kamishak Bay and base of the Alaska Peninsula lie still well within the regime of the large Cook Inlet gravity low with gravity anomaly values of less than -50 mgal. Therefore, the Cook Inlet graben structure (op. cit., p. 1035) probably does not extend far beyond the entrance of the Inlet.

A local gravity high of about + 15 mgal seems to be related to the probable mid-Tertiary pluton of Cape Douglas, composed of unique magnetite rich quartz diorite and granodiorite (Burk, 1965, p. 122), similar to other coastal plutons of the Alaska Peninsula at Wide Bay, Kuiukta Bay and Belkofski Bay.

Profile 8 (Fig. 15) spans 75 km from Pirate Lake to Kaguyak Bay (Shelikof Strait). It exhibits, perhaps most clearly of all profiles, the gravimetric signature of the sedimentary Mesozoic basin occupied by the Naknek Formation and older sedimentary units. The minimum gravity value is observed about 15 km northwest of the volcanic axis. To the southeast the Bouguer gravity rises rapidly to about + 15 mgal, a high that seems, as in profile 9, to be related to the mid-Tertiary Cape Douglas pluton. The extension of a fault mapped by Keller and Reiser (1959) along the northwestern flank of the Cape Douglas pluton coincides with the steep rise in gravity following the gravity minimum which indicates uplift of the southeastern block.

Profile 4 (Fig. 16) roughly parallels Keller and Reiser's geologic structure section D-D' and extends over 80 km of very mountainous country from Kulik Lake to Cape Chiniak (Shelikof Strait). The

northwestern half of the traverse is dominated by the Kulik Lake low discussed previously. The southeastern half reflects the low density Mesozoic sediments. Steep gradients leading to positive gravity anomalies at the coastline are again observed at the volcanic axis, here marked by the currently inactive Kaguyak Crater.

Profie 7 (Fig. 17) stretches over 80 km from Hammersly Lake to Hallo Bay and corresponds roughly to the geologic structure section C-C' of Keller and Reiser. The northwestern third of the profile still shows the influence of the Kulik Lake low, which interrupts the generally positive gradients observed northwest of the Bruin Bay fault. The southeastern part of the traverse shows again the characteristic decrease in gravity toward the volcanic range followed by a very rapid gravity increase at and beyond the volcanic axis.

Profile 2 (Fig. 18) of about 100 km from Grosvenor Lake to Cape Gull on the Shelikof Strait has been already discussed in great detail. A crustal section that could explain the observed anomalies is presented in Fig. 13.

Profiles Decker and 1 (Fig. 19) extend from the Naknek Lake system over 95 km to Katmai Bay. Decker (1963) collected the first gravity data in Katmai along that traverse. He tentatively suggested that the Lower and Middle Jurassic intrusives of the Naknek Lake granitic basement complex represent a positive density contrast to the Upper Jurassic Naknek Formation. This has been confirmed in all our traverses. Invariably gravity increased northwest of the Bruin Bay fault which places the igneous rocks in fault contact with the Naknek sediments. Positive Bouguer anomalies of about 25 mgal are found northwest of that fault.

The gravity values decrease from the Bruin Bay fault to the volcanic range where they reach a minimum of approximately -20 mgal. The superimposed local Trident anomaly has been already discussed in detail.

The continuation of Decker's profile from the Katmai volcanoes to Shelikof Strait showed the typical rapid increase in gravity of about 30 mgal over a very short distance. This steep positive gradient is about 6 mgal/km in profile 1 and is highly suggestive of a fault which may control the position of the volcanic vents. Positive 15 mgal anomalies are typical of the Barrier Range, which rises between the volcanic axis and the Shelikof Strait.

Profile 3 (Fig. 20), the southernmost profile is 80 km long and reaches the Shelikof Strait at Kashvik Bay. Its gravity pattern reflects the very gentle synclinal setting of the Mesozoic sediments, which reaches a minimum at the synclinal axis in the Naknek sediments, as mapped by Keller and Reiser (1959). Very steep positive gradients of about 3.5 mgal/km are observed across the Bruin Bay fault--anomalies that are probably related to the Bristol Bay high (Woollard et al, 1960, p. 1036), a high that may be due to an intracrustal mafic pluton.

Profile 3 at the southwestern end of the Katmai gravity survey and profile 9 at its northwestern end are both characterized by zero or positive Bouguer anomalies. The zero mgal anomalies in the center of the two profiles indicate a closure of the major Katmai gravity low (see also Fig. 9).

Unlike the other profiles, profile 3 does not show an exceedingly steep rise in gravity southeast of the volcanic range, which is in accord

with the absence of the dense, folded, early Tertiary andesites and basalts that are exposed further northeast along Shelikof Strait. The smoothly increasing gravity values in profile 3 across the volcanic range seem also to indicate that somewhere between profiles 1 and 3 the fault that may be associated with the volcanic axis as suggested by the steep gravity gradients further northeast terminates. It is, in this context, interesting to note that profile 3 also represents the southwestern border of the active and narrowly spaced Katmai volcanoes. The closest evidence of recent volcanism is the volcanic neck, Mt. Peulik, 75 km further southwest. In the same general area of profile 3, the Bruin Bay thrust and the Naknek Lake granitic basement complex are either terminated or are masked by the thick Tertiary cover of the Bristol Bay lowlands.

Summarizing, it can be said that all gravity profiles between traverses 3 and 9 show very consistent gravity patterns,which are characteristic for the Katmai area::

1. The Mesozoic sediments of the Matanuska geosyncline (Fig. 7) are the cause of a major negative anomaly closure of 20 to 25 mgal, which covers an area of about 160 by 100 km. In the Katmai area the sediments are entirely composed of the Upper Jurassic Naknek Formation that is unconformably overlain by Upper Cretaceous rocks of the Kaguyak Formation in the Cape Douglas region. Even though no exposures of sediments older than Upper Jurassic have been found in Katmai they most likely underlie the Nakneks in considerable thicknesses as shown in exposures southwest and north of Katmai.

Southwest of Katmai from Puale Bay to Wide Bay the Naknek rocks are conformably underlain by upper Middle Jurassic (Callovian) shales and conglomerates of the Shelikof Formation. Stratigraphically lower sedimentary units include the Middle Jurassic Kialagvik Formation, Early Jurassic sandstones, shales and volcanic breccias, thin Late Triassic limestones and Middle and Early Triassic volcanic flows, breccias and tuffs.

In the Iliamna Lake - Kamishak Bay region north of Katmai the Callovian Chinitna Formation (Tuxedni Bay) underlies conformably the Naknek sediments and is conformably underlain by the Middle Jurassic Tuxedni group. Older sedimentary units include Early Jurassic porphyritic flows, breccias, tuffs and some graywacke, Late Triassic shales and cherts (Kamishak Formation), Middle and Early Triassic greenstones, volcanic flows, tuffs and breccias that overlie Paleozoic (?) slates (Burk, 1959 and Fig. 21).

The axis of the large elongate Katmai gravity anomaly coincides at least in its southwestern half with the volcanic axis and then gradually swings north along the western flank of Fourpeaked Mountain and Mt. Douglas, the last two Katmai volcanoes to the northwest. Even though the Naknek Formation extends much further beyond the Katmai area to the southeast, the anomaly associated with the Mesozoic sediments has a southern closure in profile 3 which may indicate a rise in the basement separating different sedimentary troughs.

The southeastern extension of the Naknek Formation below the Shelikof Trough (Fig. 7) lies outside the surveyed area, but is not found beyond

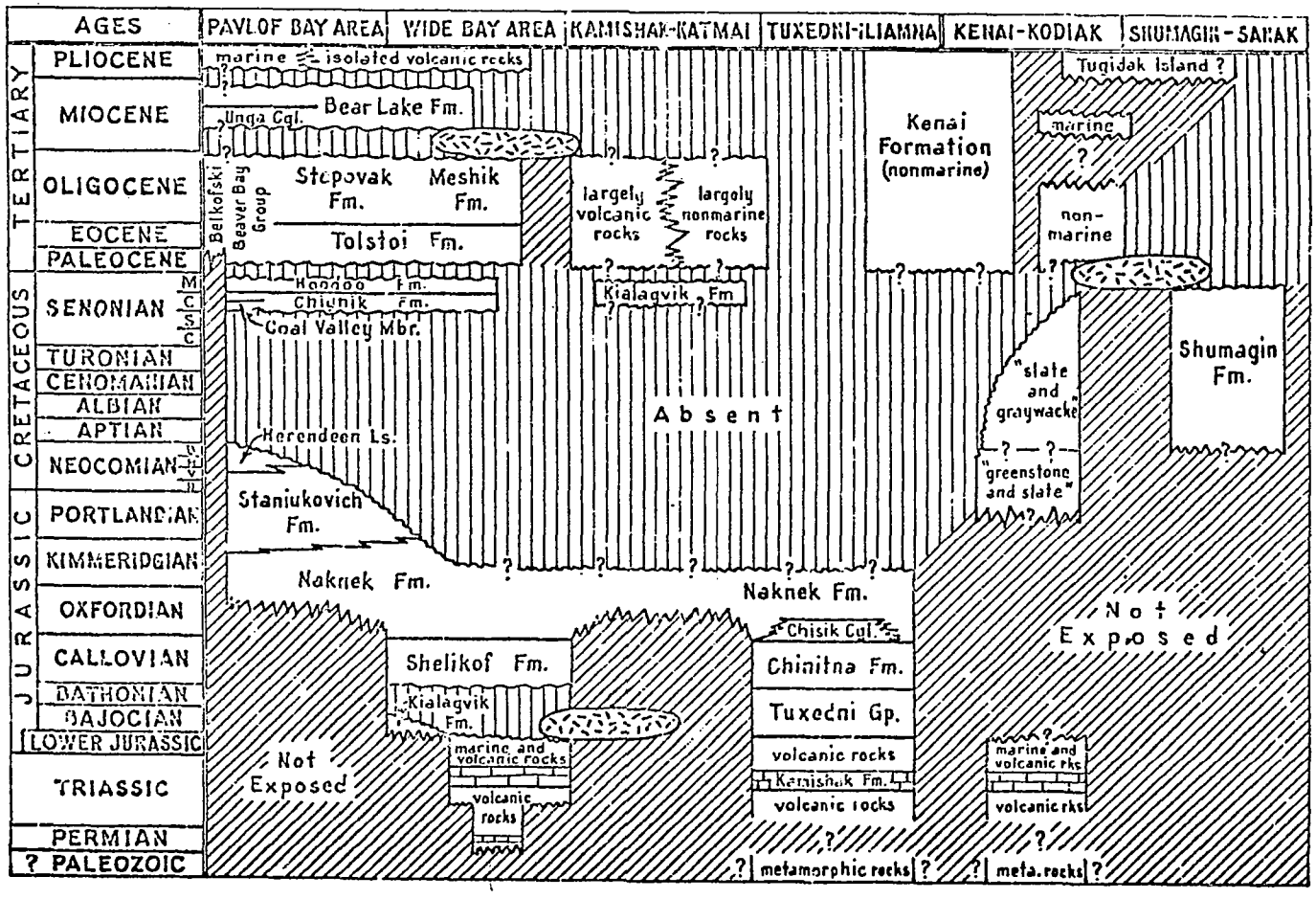

Figure 21. Stratigraphic relationships of the Alaska Peninsula (Burk, 1965, p. 138, Fig. 24).

the northern edge of the Cretaceous "slate - graywacke belt" (Burk, 1965, p. 109) which roughly coincides with the northwestern shore of Kodiak Island.

2. In the entire study area the Bruin Bay fault places the Naknek Formation in fault contact with a north block composed of granitic rocks which parallels the fault from the Naknek Lake system to the northwestern shore of Cook Inlet. These granitic rocks represent a positive density contrast against the Naknek sediments, which are largely composed of detritus from these same granitic rocks. This causes the gravity anomalies to rise rapidly across the fault--a pattern which was observed in all profiles.

3. Steep positive gravity gradients are found to be associated with the volcanic axis from Mt. Trident to Fourpeaked Mountain over a distance of about 100 km, and may indicate local and near vertical fault control of the volcanic trend along the relative upthrow of the southeastern block. This is in qualitative agreement with our findings from earthquake data (Berg, Kubota and Kienle, 1967), even though the amount of displacement (structure section, Fig. 13) is much less, and is limited to the upper crustal layers.

4. The igneous rocks of the Cape Douglas pluton in the Mt. Douglas-Fourpeaked Mt. area and the Lower Tertiary volcanic flows, sills and clastics that form the coastal mountains between the volcanic axis and the Shelikof Strait between Katmai and Hallo Bay, represent a positive density contrast against the Naknek sediments and the Quaternary and recent volcanics to the northwest. These sections can account for much

of the positive anomalies associated with the coastal mountains as shown in the structure section (Fig. 13). A combination of local uplift and the effect of the high density Tertiary rocks as described above can explain the consistent increase in gravity to positive values across the volcanic range which is observed in all gravity traverses between the axis of the sedimentary basin and Shelikof Strait.

CHAPTER V

GRAVITY TRAVERSES IN THE VALLEY OF TEN THOUSAND SMOKES

5.1 Introduction

In 1965, as part of the 1965-1967 Katmai expeditions of the Geophysical Institute of the University of Alaska, four gravity traverses were surveyed across the main branches of the Valley of Ten Thousand Smokes in order to determine the thickness of the Valley deposits. Several theories of the origin and mode of emplacement of the 1912 ash flow have been forwarded. Most of these contain estimates of total thicknesses and volume. The total area covered by the 1912 ash flow is about 38.5 square miles (Fig. 6) and comprises the Ukak Valley, the main Valley, the southeast branch and the south branch (Fig. 6) as subdivided by Fenner (1923).

Gravity methods similar to those applied by Thiel and others (1957) to determine the thickness of Lemon Creek Glacier in Alaska were used. A two dimensional computerized model analysis developed by Talwani (1959) greatly facilitated the computations.

In this Chapter four cross sections for the Valley deposits are presented. Each cross section consists of 2 models, one assuming that all material between the surface and bedrock (in this case Naknek sandstones, and shales) consists of pumice and the second assuming that all this material consists of alluvial fill. In reality the 1912 tuff and ash most generally overlies pre ash flow glacial valley fill, but there is no way of separating the two units by gravimetric methods alone. The two models give an upper and lower limit of the depth to bedrock.

5.2 Previous Work

In 1900 J. E. Spurr gave the only description available today of the valley floor before it was filled with the ash flow deposits in 1898, cited by Fenner (1923):

> "The main valley is filled with horizontally stratified sand in which are great angular boulders, which are also beautifully arranged in layers. This deposit has a generally level top, but there are many sharp hillocks formed of bunches of huge boulders. The streams have cut deep channels through this....
>
> The valleys of the streams which drain both sides of the pass (Katmai Pass)are deeply excavated, especially that on the northwestern side(Lethe River), which has cut down at least 100 feet through lava boulders....
>
> All along the valley leading to the pass are stratified gravels, which near the beginning of the trail across the pass begin to be filled with great angular boulders; these are, however, beautifully layered. Dotting the level are many sharp hillocks formed of huge striated boulders, evidently dumps of icebergs. This deposit runs quite up to the foot of the existing glaciers, there being no unmodified drift except recently abandoned moraines."

In 1912 this topography of the Valley was completely buried by pumice and ash of the great 1912 Katmai eruption. Subsequently the ash flow degased very rapidly, and when first seen in 1916 by R. F. Griggs, he named it the Valley of Ten Thousand Smokes.

At present the fumarolic activity in what would now be more appropriately called "Valley of Ten Smokes" has practically ceased and is reduced to two zones of active fumaroles. The first zone is located on the ridge leading from Novarupta to the southeast knoll of Broken Mountain. Here, the fumarolic activity is mostly concentrated along a series of NW-SE striking fissures flanking Broken Mountain on the south. Fenner (1950)

describes this area as "a succession of great faults, with downthrow to the southeast, and with total displacement estimated to be 300 feet." The fumarolic activity in this zone consists of quiet emission of mostly water vapor from large, very damp flat areas covered with vividly colored clays and moss. Novarupta itself still shows considerable fumarolic activity.

If one connects the Broken Mt. fumarole fields with Novarupta by a straight line, its southwestern extension passes through Falling Mountain, the southern slopes of Mt. Cerberus and the north peak of Mt. Mageik. This line was cited as a possible old fracture and source of the 1912 tuff and ash deposits by Bordet et al (1963).

The second zone, a line marked by some impressive active fumaroles, runs along the west side of Baked Mountain from its southern tip to the NW ridge of Broken Mountain. This line may well be controlled by a series of block faults that occur on the west flank of Baked Mountain and are downdropped on the Valley side, since it is aligned with the western edge of a high terrace on the same flank of Baked Mountain.

This same terrace was the site of the 1919 Baked Mountain Camp of the National Geographic Society expedition under R. F. Griggs, which was subsequently destroyed in a storm. In 1966 a group from the Fish and Wildlife experimental station at Brooks found some remains of this camp. A closer search produced remnants of the tent, chemical equipment, some poles, a plane table, a bead necklace and a rubber overboot. Griggs in his 1921 National Geographic Magazine article, "Our Greatest National Monument," shows photos of the Camp before and after the storm

(p. 250 and 251). A photo on p. 248 taken from Baked Mountain Camp and looking toward Mt. Martin shows a gigantic fumerole just below the camp. This fumerole on the southern tip of Baked Mountain was still active in 1967 and marks the southern end of the Baked Mountain fumerole line. It is the only large fumerole left in the Valley of Ten Thousand Smokes. It is about 6 m deep, emits mostly vapor and is related to the fumeroles further north through a clearly visible fissure. The line of fumaroles turns to the northeast at the north tip of Baked Mountain and is marked by extinct fumeroles and some minor hot spots between Baked and Broken Mountains.

An extension of the Baked Mountain fumerole line meets the Novarupta "fracture" at Mt. Cerberus, with the bearings of the two zones subtending an angle of 45 degrees. Hypotheses as to the nature and location of the vents for the ash flow have been postulated by various authors and are well summarized by Bordet et al (1963, pp. 17-20).

B. G. Escher (1921) thought that the 1912 Valley deposits were due to a hot lahar or mudflow coming from the crater of Mt. Katmai, which is now believed to have formed after the 1912 eruption as pointed out by Fenner (1923). Fenner's view is reinforced by the topography shown on the 1 inch to approximately 3 1/4 miles United States Coast and Geodetic Survey Chart No. 8555, surveyed from 1897 to 1908, that shows Katmai Volcano to consist of 3 distinct peaks of 7500, 7360 and 7260 feet elevation, without a crater.

R. F. Griggs (1922) assumed that a granitic batholith rising from great depth reached the earth's surface underneath the Valley of Ten Thousand Smokes and split the Valley floor into numerous fissures, that subsequently extruded hot mud. Our gravity data shows no evidence of

such a batholith.

C. N. Fenner (1923), observing the rapidly decreasing fumarole activity and analying the 1912 products geochemically and petrologically, opposes both ideas. He finds the deposits to be a hot sandflow rather than a mudflow and postulates the following hypothesis for its origin. A sill of magma was wedged into old fissures in the strata of shale and sandstone of the Valley, and these deviated the magma that was rising directly to Katmai Crater. The incandescent magma responsible for the Valley deposits emerged from longitudinal fissures in the Valley floor undergoing rapid expansion due to degasing.

H. Williams and others (1956) assume that the 1912 material came from NE-SW striking, deep, vertical fissures at the head of the Valley in the Novarupta-Broken Mountain area, and that Novarupta itself emerged from one fissure at a later stage of the eruptive history.

G. S. Gorshkov (1959), observing the great eruption of Bezymianny Volcano in Kamchatka, assume that the Katmai "nuée ardente" descended from Mt. Katmai itself in a way similar to that in which the deposits of the Valley of Sukhaya Khapitsa--the "Valley of Ten Thousand Smokes of Kamchatka"--came from Mt. Bezymianny. However, there are some major obstacles to this theory, since Broken, Baked and Falling Mountains would be in the way of such a flow from Mt. Katmai. In addition, Fenner (1923) could not find any channels that would have been carved into the Knife Creek Glaciers on the north slopes of Mt. Katmai by such a nuée ardente.

Bordet and others (1963) believed the 1912 Valley deposits to be true Ignimbrites, which were emitted as a nuée ardente from fissures at the

head of the Valley in the Novarupta area. Ejection of tuff from Mt. Katmai and of pyroclastics from Novarupta followed this phase. It may, at this point be appropriate to state that the feature seen on their Plate II, Figure 2 and claimed to be a huge mudflow (lahar) coming from Mt. Katmai is in reality an ash covered glacier as already recognized by Fenner (1923). On July 2, 1967, N. Sperlich of the Geophysical Institute of the University of Alaska and the author chose the next glacier to the south as ascent route to the rim of Katmai Crater. It had a normal crevasse pattern and was thickly covered with coarse pumice. The terminus of the glacier shown by Bordet and others as "coulee boueuse" was vertical ice with interbedded ash layers.

5.3 Field Procedure

Four gravity traverses across the Valley of Ten Thousand Smokes comprising a total of 85 stations were surveyed on foot, using the Baked Mountain Hut (BMH) as a secondary gravity base, A Worden Geodesist No. 607, Model 121, gravimeter was used, as described in Chapter II. All data are drift corrected. The stations in each traverse were aligned by eye on straight profiles across the Valley; the distances between stations were chained off and plotted on 1 inch to the mile Geological Survey quadrangles. Station elevations were determined by altimetry as discussed above (see Chapter II). All elevations are tied to the BMH elevation of 2,550 $\pm$ 20 feet absolute and therefore inherit the same error in absolute elevation.

For the problem of determing the thickness of the Valley deposits, however, only good relative station elevations are necessary.

Temperature and barometric pressure changes during the altimeter survey severely affect the elevation quality. In order to detect such changes our survey was always closed on check points and the base station BMH. In some cases monitoring of barometric pressure with the Taylor altimeter was maintained at BMH during the survey. All elevations are temperature and barometric pressure corrected. Elevations of profiles KV-1, KV-2 and KV-3 were resurveyed in 1906. It is interesting to note that the amount of erosion from summer 1966 to summer 1967 was practically zero, especially in KV-2, where in 1967 we still saw the foot prints and imprints of the board that was used to stabilize the gravimeter in the 1966 survey.

The relative station elevations are of varying accuracy in the different profiles, depending on the barometric pressure conditions of the survey day.

Profile KV-1 was surveyed in 1966 with the Pauling altimeter. A Taylor altimeter was read continuously at BMH to record the barometric pressure. The profile that was staked out for the Lamont hammer seismic project in 1967 unfortunately does not exactly coincide with the old 1966 gravity profile KV-1. Station 0 of the 1967 line lies 1,000 feet SSE of Station 1 of the 1966 gravity profile. The western end of the 1967 profile meets the 1966 profile at the Lethe River. The relative elevation accuracy of the gravity stations is

$\pm$ 3 ft for stations 1 - 11, no barometric correction was necessary

$\pm$ 5 ft for stations 11 - 17

$\pm$ 15 ft for stations 18 - 23 west of the Lethe River, where a very large correction had to be applied.

Profiles KV-2A and B were resurveyed in 1967 under excellent barometric conditions, and many of the old marks of the 1966 survey were relocated. The closure was accurate to within a foot and no barometric correction was necessary. Relative station elevations are probably accurate to at least ± 2 feet.

Profile KV-3 was surveyed in 1966 with the Pauling altimeter. It was necessary to apply large barometric corrections to the data. The profile was resurveyed in 1967 under reasonable barometric pressure conditions but with the Taylor altimeter since the Pauling altimeter had suffered some damage. Temperatures and barometric pressure corrected relative gravity station elevations are therefore only good to ± 8 feet.

Profile KV-4 was surveyed in 1966 with the Pauling altimeter. The barometric pressure variation was again rather large. The relative station elevations are accurate to ± 8 feet.

5.4 Data Reduction

A simple Bouguer reduction was applied to the observed drift corrected gravity values using a Bouguer density of 2.67 g/cc. The resulting simple Bouguer anomalies contain terrain effects, regional anomalies and the local geological effect of the low density Valley deposits, which we want to evaluate.

Terrain effects were calculated directly using Hammer's zone chart. They are, of course, greatest at the end points of the gravity traverses, which were usually on bedrock, and smallest in the middle of the valleys. For all profiles at least these three extreme points were terrain corrected. The terrain corrections were calculated for 5 stations

of profile KV-1, 4 of profile KV-2A, 5 of profile KV-2B, 3 of profile KV-3 and 3 of profile KV-4. These are identified by their station number in Fig. 24 to 27. If the contribution of a certain Hammer zone around the gravity station was constant for all gravity stations in a given profile, i.e. if it was the same for the end points as well as for the mid valley station, no zones further out of the gravity station were calculated, because their contribution would be constant over the entire profile. For profile KV-1 the contribution of zones M, N, etc., were constant. For the other profiles zones L, M, etc. were constant. Table 6 lists the terrain corrections for the calculated valley stations out to the constant zone (exclusive) and also through zone M for 2 different densities: 2.0 g/cc and 2.67 g/cc. It also gives the complete Bouguer anomaly (through zone M) for a density of 2.67 g/cc for the 19 terrain corrected valley stations. The terrain corrections for the other 66 stations were interpolated, assuming that the terrain effects due to the surrounding mountains vary smoothly across the very flat laying Valley floor.

Regional gravity gradients, representing larger scale geological effects, have to be removed from the data in order to expose the very local effect of the low density Valley deposits. This step is a very critical one and involves subjective judgement. Where possible the regional gradient was interpolated linearly between terrain corrected bedrock gravity stations. This gradient was then checked against the gradient estimated from the complete Bouguer anomaly map (Fig. 10) that includes the Valley of Ten Thousand Smokes.

TABLE 6

Terrain corrections and complete Bouguer (2.67) anomalies for selected gravity stations in the Valley of Ten Thousand Smokes

Station	No.	Ele. (ft)	Q	2.0 B - L	2.67 B - L	2.0 B - M	2.67 B - M	Complete Bouguer 2.67
KV1-01	204	2063	y	2.0	2.7	2.1	2.8	-14.9
KV1-10	213	1806	y	1.5	2.0	1.6	2.1	-17.0
KV1-15	218	1763	y	1.3	1.8	1.4	1.9	-18.0
KV1-20	223	1810	z	1.7	2.3	1.8	2.4	-15.0
KV1-23	226	2010	z	2.4	3.3	2.5	3.3	-13.5
				B - K				
KV2-01	227	2548	y	2.4	3.2	2.7	3.6	-16.3
KV2-04	230	2185	y	1.6	2.1	1.9	2.5	-16.2
KV2-07	233	2141	y	1.2	1.5	1.5	1.9	-16.5
KV2-13	239	2232	y	2.1	2.8	2.4	3.2	-15.5
KV2-14	240	2014	y	1.9	2.5	2.2	2.9	-15.4
KV2-21	247	1847	y	2.0	2.7	2.3	3.1	-18.4
KV2-24	250	1855	y	2.6	3.5	2.9	3.9	-15.7
KV2-28	254	1887	y	4.4	5.9	4.7	6.3	-13.2
				B - K				
KV3-01	255	2400	y	2.1	2.8	2.4	3.2	-16.9
KV3-07	261	2332	y	1.6	2.2	1.9	2.6	-20.6
KV3-13	267	2400	y	2.8	3.7	3.1	4.1	-23.6
				B - K				
KV4-01	268	1274	y	3.3	4.4	3.8	5.1	-9.9
KV4-11	278	1310	y	1.7	2.2	2.2	2.9	-13.4
KV4-17	284	1411	y	3.9	5.2	4.4	5.9	-10.6

In Figs. 22 and 23 the complete Bouguer anomalies (2.67 g/cc) are plotted for each profile. The applied terrain corrections have been calculated through zone M and the assumed regional gradients are also shown.

For profile KV-1 the regional gravity was assumed to be constant and given by the value of bedrock end station 23 with -13.5 mgal (Fig. 22). This value is somewhat higher than one would estimate from the gravity map (Fig. 10) which in this area is based on Decker's Valley stations. Their gravity values are influenced by the ash flow and correspond well to the values observed at the mid-Valley stations of this profile.

In profile KV-2 the regional gradient was assumed to be linear with 0.7 mgal/km increase between the two bedrock stations 3 and 28, (Fig. 22) which were also used to construct the Bouguer map (Fig. 10) in the profile area.

The gradient for profile KV-3 was estimated from the Bouguer map (Fig. 10) since no bedrock stations were available (Fig.23). It is very steep and the assumption that it is linear with a 4.8 mgal/km decrease from station 1 to 11 may not be good. South of station 11 the gradient steepens even more and the effects of strong regional trends and the Valley deposits could not be separated. A regional value of -16 mgal was assumed for station KV 3-1. This is again a somewhat higher value than one would estimate from the gravity map, which in the profile area is based on 2 Valley stations.

In profile KV-4 the regional gradient was considered to be linear with 0.2 mgal/km increase between bedrock station 18 and station 1 (Fig. 23), where the thickness of the ash flow down to bedrock was

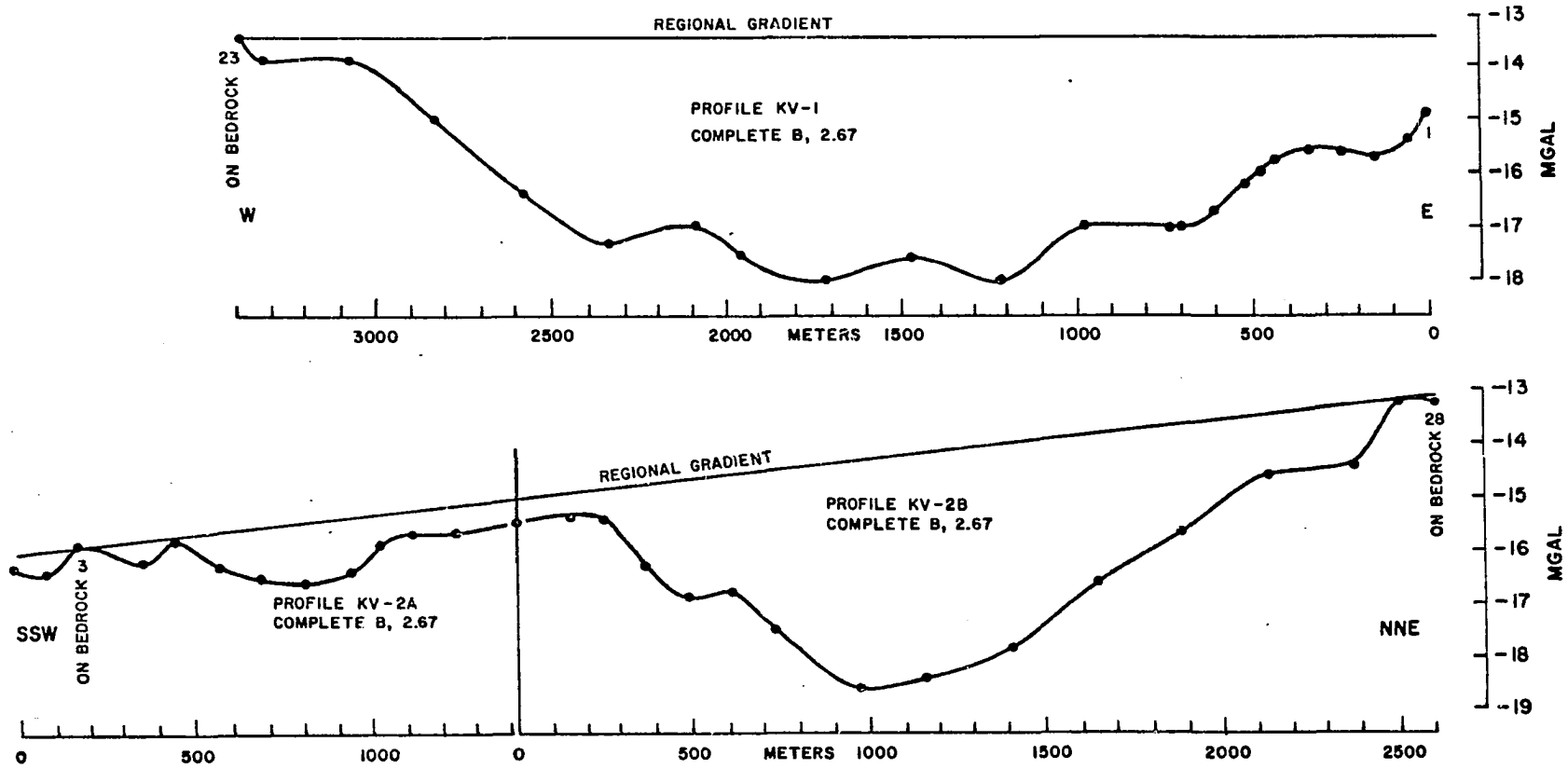

Figure 22. Complete Bouguer (2.67) gravity anomalies of Valley of Ten Thousand Smokes gravity profiles KV-1 and KV-2 (see Fig. 6) and assumed regional gradients.

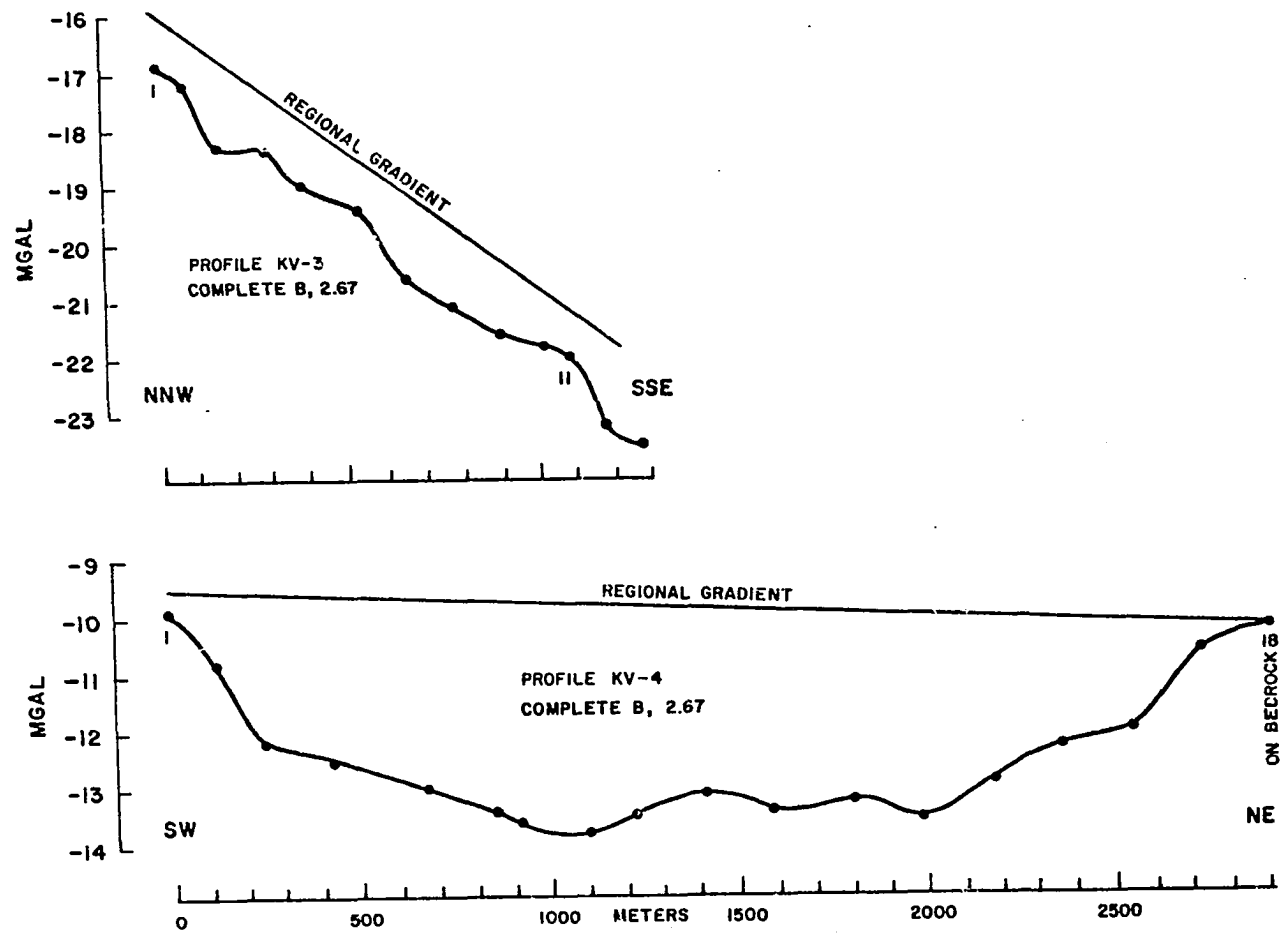

Figure 23. Complete Bouguer (2.67) gravity anomalies of the Valley of Ten Thousand Smokes gravity profiles KV-3 and KV-4 (see Fig. 6) and assumed regional gradients.

known and where the undisturbed regional value could therefore be estimated. According to the gravity map (Fig. 10) in the profile area constant regional values of about -10 mgal would be expected, which agrees well with the assumed gradient.

The observed curves in Fig. 24 to 27 represent the complete Bouguer anomalies for a density of 2.67 g/cc with the regional gradients removed. These are now the reduced data, which can be interpreted in terms of thicknesses of the Valley deposits.

5.5 Density of the Valley Deposits

However, before we can analyze the processed data, we have to make some assumptions about the density of the Valley deposits. These are generally composed both of pre ash flow glacial valley fill and of the 1912 ash flow overlying the Naknek shales and sandstones.

Five ash flow samples were collected in 1966 and their wet bulk density determined within 24 hours to avoid pore water loss. Two samples were taken at point A from the middle section of the flow, one at point B below Overlook from the base of the flow, and two at point C from the upper part of the flow (Fig. 6). All densities fell within a range of 1.00 g/cc to 1.09 g/cc, the average was 1.03 g/cc. Welded tuff was not found by the author. In 1967 M. Sbar (personal communication) from Lamont Geological Observatory, Palisades, New York, found a mean seismic P-wave velocity of 0.54 km/sec for the tuff and ash layer in profile KV-2A, which correlates well with its very low density observed by the author.

Underlying the ash flow, Sbar observed a layer with a mean P-wave velocity of 1.89 km/sec in the same profile KV-2A, which he interprets

as bedrock. Using Drake's curve (in Grant and West, 1965, p. 200) which relates P-wave velocity to bulk density, 1.89 km/sec correspond to 1.87 g/cc. At 1.90 the histogram of small-specimen bulk densities of soil and alluvia prepared by Birch (1942) shows the major peak. The density of 1.87 g/cc was therefore assigned to the pre ash flow Valley fill rather than to the bedrock. The wet bulk bedrock density of the underlying Naknek Formation averaged to 2.62 g/cc, as determined in the laboratory. This should give P-wave velocities in the 5 km/sec range.

5.6 Two Dimensional Analysis, Results

M. Talwani (1959) developed a method for rapid gravity computations for two-dimensional bodies, which can readily be computerized. A program written for an IBM 1410 computer was made available to us by P. Dehlinger, Oregon State University, Corvallis, and was converted for use in the IBM 360/40 at the University of Alaska. The low density deposits in the Valley of Ten Thousand Smokes are very well suited for such a two dimensional analysis. The problem of obtaining cross sections down to bedrock (in this case down to the Naknek sediments) is however complicated by the fact that, at least in the main branches of the Valley, the deposits consist of a minimum of two layers: pre ash flow glacial valley fill as described by Spurr (1898) and the 1912 ash flow. If seismic control were available the gravity anomalies could be explained by a 2 layer model, but unfortunately this control is not available at present. Two limiting models for each profile were therefore derived from the gravity data. One assumes that all material between the surface and bedrock consists of glacial Valley fill (Model F) with a density of 1.87 g/cc

giving a minimum depth to bedrock and the second assumes that all material between the surface and bedrock consists of ash flow material (Model P) with an average density of 1.03 g/cc., giving a maximum depth to bedrock. The real two layer case reaches bedrock somewhere in between these two limits.

In Figs. 24 and 27 the two models P (pumice) and F (fill), the corresponding computed gravity curves and the observed gravity curve are plotted for each profile. Profiles KV-2A and KV-3 may contain a negligible amount of glacial fill and model P could therefore come rather close to reality. The deposits of the other profiles KV-1, KV-2B and KV-4 are very likely composed of both glacial fill and 1912 ash flow material.

In the summer of 1967 a team from Lamont Geological Observatory under T. Matumoto ran a hammer seismic traverses on profiles KV-1, KV-2A and KV-3. At present only preliminary results for KV-2A on velocities and thicknesses of the ash flow layer are available to the author.

Profile KV-1 (Figure 24) cuts across the south branch of the Valley from Baked Mt. to the Buttress Range. The wavy appearance of the observed gravity curve in the middle part of the profile is most likely due to poor elevation control. An error of $\pm$ 5 feet in altitude corresponds to $\pm$ 0.3 mgal in the simple Bouguer anomaly for a density of 2.67 g/cc, which is about the amplitude of the undulations. If they are real, an undulating bedrock surface or sharp inhomogeneities in the Valley deposits could be the explanation. The bedrock topography in general is U-shaped as one would expect for an old glacial valley, like the Valley of Ten Thousand Smokes. The terrace on the west side of Baked Mt. is thickly covered with ash flow material. The maximum depth to bedrock was found to be

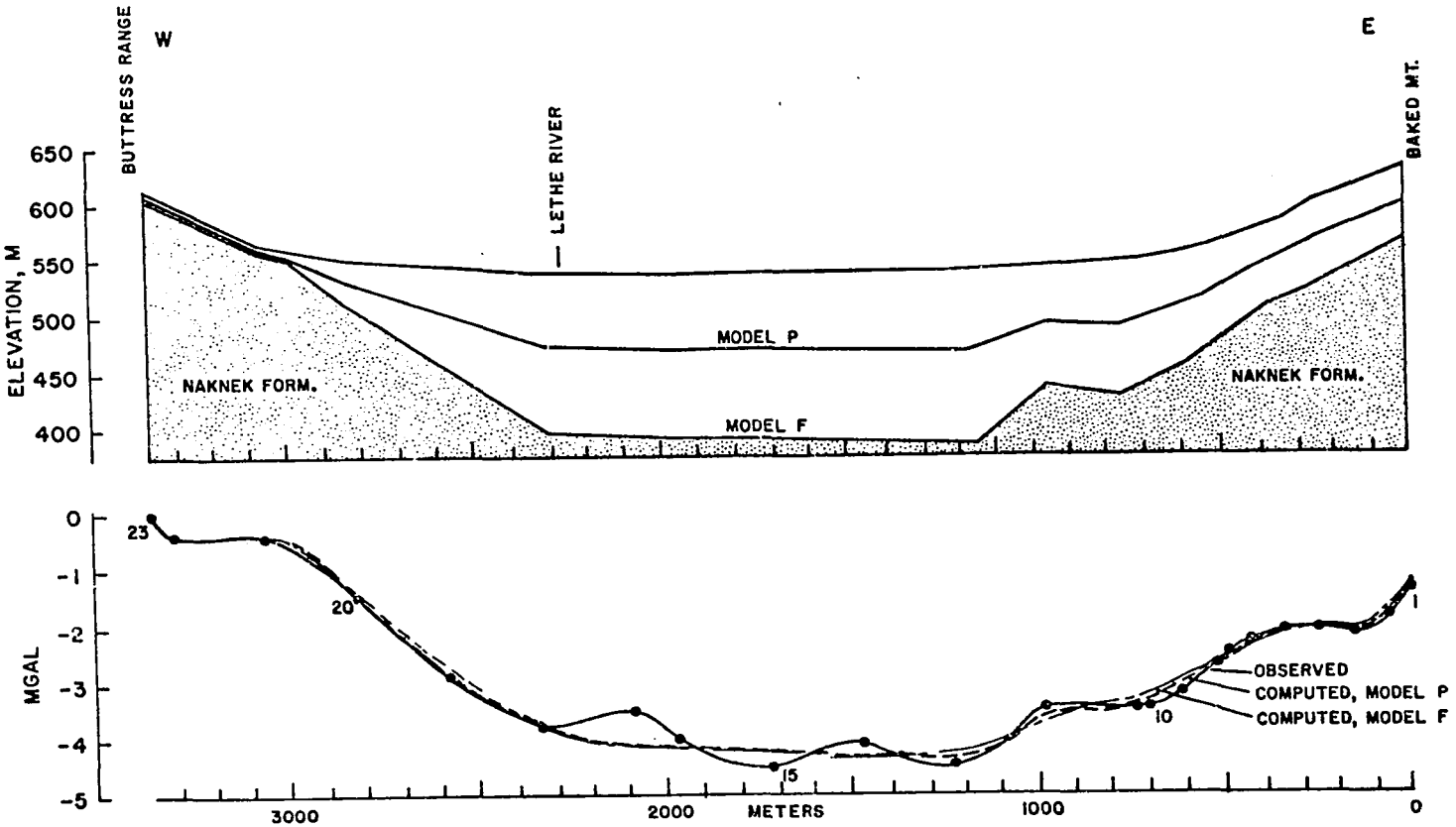

Figure 24. Profile KV-1 (see Fig. 6). Upper: Proposed Valley cross sections computed by assuming that all Valley deposits consist of pumice and ash (model P) and that all Valley deposits consist of fill (model F). Lower: Observed complete Bouguer (2.67) gravity anomalies with regional gradient removed and computed attraction of the two models.

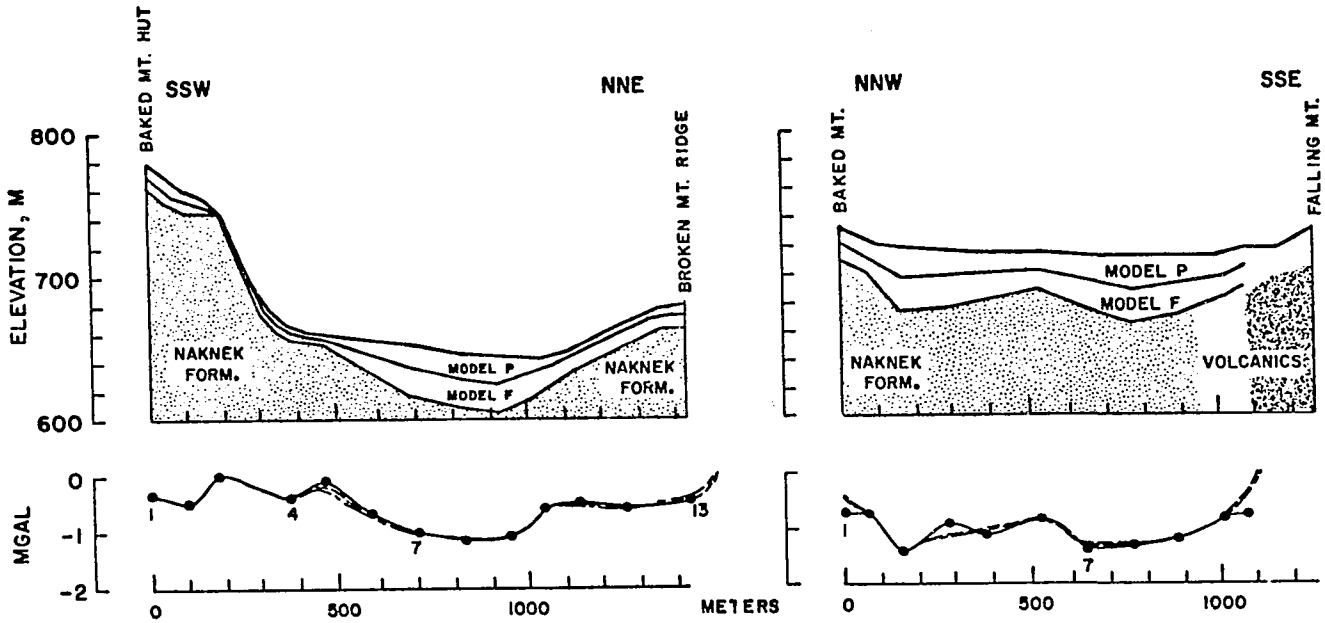

Figure 25. Profiles KV-2A (see Fig. 6) (left) and KV-3 (see Fig. 6) (right). Upper: Proposed Valley cross sections computed by assuming that all Valley deposits consist of pumice and ash (model P) and that all Valley deposits consist of fill (model F). Lower: Observed complete Bouguer (2.67) gravity anomalies with regional gradient removed and computed attraction of the two models.

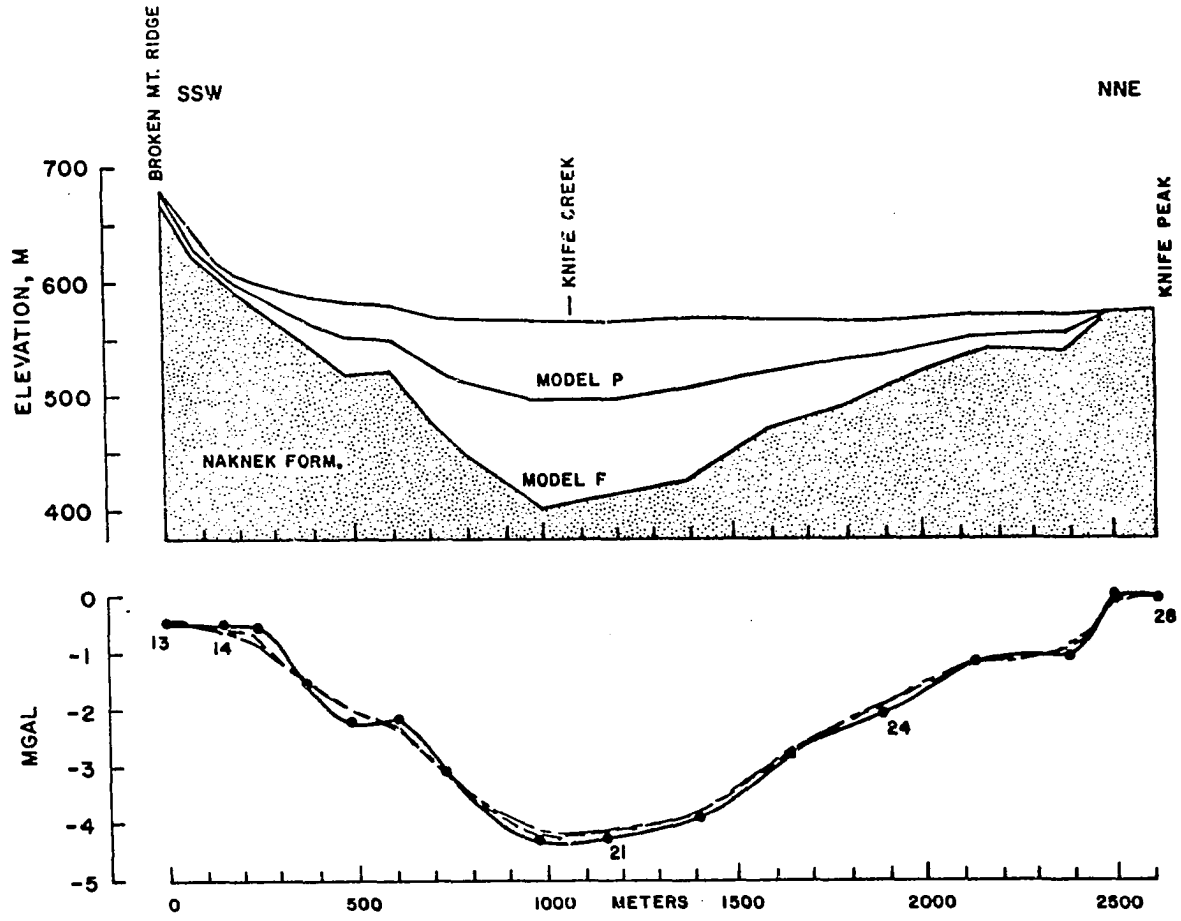

Figure 26. Profile KV-2B (see Fig. 6). Upper: Proposed Valley cross sections computed by assuming that all Valley deposits consist of pumice and ash (model P) and that all Valley deposits consist of fill (model F). Lower: Observed complete Bouguer (2.67) gravity anomalies with regional gradient removed and computed attraction of the two models.

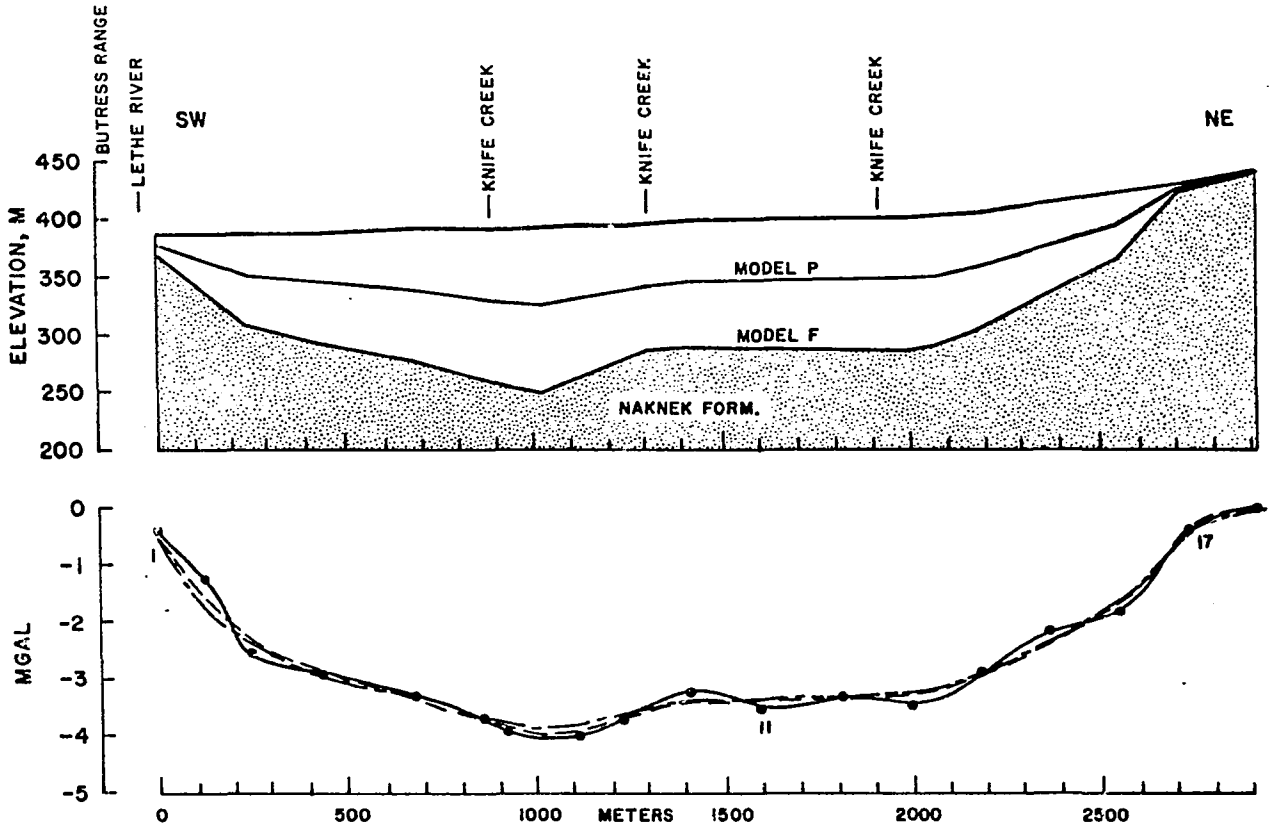

Figure 27. Profile KV-4 (see Fig. 6). Upper: Proposed Valley cross sections computed by assuming that all Valley deposits consist of pumice and ash (model P) and that all Valley deposits consist of fill (model F). Lower: Observed complete Bouguer (2.67) gravity anomalies with regional gradient removed and computed attraction of the two models.

148 m (model F); the minimum depth is 70 m (model P). The ash flow layer can be measured directly in the canyon of Lethe River to a thickness of at least 8.5 m.

Profile KV-2A (Figure 25, left) traverses the small valley between Baked Mt. and Broken Mt. The elevation control was very good for this profile with maximum errors of ± 2 feet in relative elevation, (± 0.1 mgal for 2.67 g/cc). Not much alluvial fill would be expected here and model P is therefore more likely than model F. The minimum depth to bedrock (model P) is found to be 18 m. The thickness of the tuff and ash layer on Broken Mt. Ridge, where a fill layer is quite unlikely is calculated to be 8 m.

Williams et al (1956) and Bordet et al (1963) consider a system of fissues which cuts the sediments of Baked Mt. northwest of Novarupta and continues through the Valley between Baked Mt. and Broken Mt. as a possible source of the 1912 ash flow. No unusual gravity patterns were found in profile KV-2A but it is indeed doubtful if filled fissures could produce a density contrast with the Naknek that could be detected gravimetrically.

The pumice under BMH is about 6 m thick assuming that the alluvial layer is negligible on the high platform where BMH is located.

Profile KV-2B (Figure 26) leads across the southeast branch of the Valley from Broken Mt. Ridge to the foot of Knife Peak. The elevation control was again very good and errors are ± 3 feet in relative altitude. The gravimetrically derived bedrock topography is U-shaped; glaciers occupy the head of this branch of the Valley. The old riverbed of

Knife Creek is clearly expressed in the bedrock topography. It is here, where the maximum bedrock depth of 164 m (model F) is found. The bed of present Knife Creek lies on top of the ash flow at the same location. It is a very shallow meandering creek in this part of the Valley and has not cut into the ash flow. No direct measurement of the 1912 deposits was therefore obtained in this section.

Profile KV-3 (Figure 2.5 right) crosses the Novarupta branch of the Valley from Baked to Falling Mt's. If the Novrupta area was the source for the 1912 deposits, this should be reflected in thicknesses of the ash flow in this branch of the Valley, However, steep regional gradients and poor elevation control (± 8 feet) make the calculated models less reliable than those for the other profiles. Seismic control would be very desirable for this profile, but even if the absolute elevations of the bedrock are not correct, the shape of the bedrock topography can still be approximated. If this is done a double valley with a medial ridge is seen. Interestingly enough, the present drainage of the Novarupta branch of the Valley consists of two creeks too.

The maximum and minimum depths to bedrock in the northern valley were computed to be 45 m and 21 m, respectively, and 48 m and 22 m in the southern valley. In the southern rivercut, which was still entirely in tuff and ash, the tuff and ash were found to be at least 10 m thick.

Profile KV-4 (Figure 27) spans the main branch of the Valley from the Buttress Range to the mountains NW of Knife Peak. Relative elevations are only accurate to ± 8 ft- which corresponds to ± 0.5 mgal in the Bouguer anomaly for 2.67 g/cc. An uncertainty of 0.5 mgal would correspond to

variations in thickness of 7.5 m of tuff and ash (density contrast to the Naknek Formation: 1.59 g/cc)and 15.9 m of glacial fill (density contrast to the Naknek Formation: 0.75 g/cc) if infinite horizontal slabs are assumed as a first approximation. The Valley is very wide here and of typical U-shape. Station 1 at the Buttress Range end of the profile is located on top of the 1912 flow. Here the Lethe River has cut the deposits, exposing 12 m of pumice and ash directly overlying bedrock. Three branches of Knife Creek including two deeply incised canyons are cut by the profile. An ash flow thickness of 25.3 m was directly measured in the canyon at station 6 and 10.7 m of tuff and ash are exposed in the canyon between station 12 and 13.

The bedrock topography clearly shows the old stream bed of Knife Creek between stations 7 and 8, where the Valley deposits were also thickest. Maximum bedrock depth was found to be 142 m (model F); minimum bedrock depth was derived to be 65 m.

At location A which is located in the main Valley 1.7 km south-southeast of Overlook (Three Forks), a section of the 1912 deposits is exposed down to bedrock on the southwest wall in a canyon of Knife Creek. The 1912 coal layer was found at a depth of 50 feet, directly overlying the Naknek Formation. The Naknek Formation - ash flow contact dips steeply northeast at this location, exposing 25 m of the 1912 flow on the northeast wall of the canyon.

5.7 Volume of the Valley's Tuff and Ash

Fenner (1923, p. 67) gives the following estimates for volume and weight of the Valley of Ten Thousand Smokes deposits from 1912:

"At any rate, the volume of material is enormous. I have made an attempt to arrive at an approximate figure, but it must be understood that the result represents only a rough approximation at best, because of the uncertainty regarding thickness. Those assumed are believed not to be excessive. Figures are as follows:

In Ukak Valley 3 mi. x 3/4 mi. x 10 ft. = 627,264,000 cu.ft.
In main Valley 7 1/2 mi. x 2 1/2 mi. x 100 ft. = 52,272,000,000 cu.ft.
In southeast branch 5 mi. x 1 1/2 mi. x 200 ft. = 41,817,600,000 cu.ft.
In south branch 5 mi. x 2 mi. x 200 ft. = 55,756,800,000 cu.ft.

Total = 150,473,664,000 cu.ft. or a little more than one cubic mile. Assuming a weight of 90 lb. per cu. ft. for the material in place, we arrive at a weight of about 6,750,000,000 tons. This calculation takes no account of the deposit in Katmai Pass or in the valley of Megeik Creek, which would considerably increase the total, nor of the large amount that much have floated off in the atmosphere."

Converted to the metric system, his total volume of the deposits is 4.27 km^3, his density is 1.44 g/cc and his weight is 6.15 x 10^{12} kg.

If we now take the derived all-pumice models (model P) for the four profiles, i.e. if we assume that the entire gravity anomaly is produced by the low density (1.03 g/cc) tuff and ash layers in the Valley, we obtain a maximum thickness cross section of the 1912 deposits for each profile. Taking the mean thickness over the entire width of the profile and assuming that it is representative for the branch of the Valley where it is located we can estimate the maximum volume of the tuff and ash.

The following figures were obtained using Keller and Reiser's (1959) geological map:

Ukak Valley	7 800 000 m^2	. 4 m =	31 200 000 m^3
Main Valley	37 500 000 m^2	. 40 m =	1500 000 000 m^3
Southeast Branch	22 500 000 m^2	. 30 m =	675 000 000 m^3
South branch	33 100 000 m^2	. 45 m =	1489 500 000 m^3
Baked Mt. - Broken Mt. branch	3 100 000 m^2	. 10 m =	31 000 000 m^3
Novarupta branch	6 200 000 m^2	. 17 m =	107 100 000 m^3
	Total		3833 800 000 m^3

This figure of roughly 3.8 km^3 ash flow material corresponds well to Fenners figure of 4.27 km^3, which he derived without making any assumptions about the density of the deposits. It is important to keep in mind that the 3.8 km^3 were derived assuming that all material overlying the Naknek Formation consists of tuff and ash with an average density of 1.03 g/cc. Using Fenner's density of 1.44 g/cc the volume increases to about 5.36 km^3. Fenner believed that his estimate was a conservative one. From our data 3.8 km^3 is the maximum volume expected for the Valley deposits.

3.8 km^3 of tuff and ash correspond to a total weight of about $3.9 \cdot 10^{12}$ kg assuming a density of 1.03 g/cc.

The observed volume of the ash flow deposits exceeds all known nuée ardente deposits from historic volcanic eruptions. However evidence of much larger scale nuée ardente deposits does exist. Cook (1963) describes enormous Miocene Ignimbrites deposits in the Great Basin of the U.S.A. with an estimated total volume of 35,000 cubic miles. Some individual units cover an area of more than 50,000 square miles and have an average thickness of 200 feet. Cook applies the term Ignimbrite to "tuff or tuffbreccia; it may be welded, partially welded or entirely unwelded." According to him these huge deposits are very likely to be of nuée arente origin.

The eruption of the 1912 ash flow as a nuée ardente from fractures in the bedrock at the head of the Valley of Ten Thousand Smokes in the Novarupta-Broken Mt. - Baked Mt. area seems to be the most probable origin, based on gravity data and the pattern of present day surviving fumarolic activity.

CHAPTER VI

CONCLUSIONS AND FUTURE WORK

6.1 Conclusions

1. The absence of a well developed crustal root under the Katmai segment of the Aleutian Range as suggested by the absence of large negative Bouguer anomalies, seems to indicate regional rather than local isostatic compensation of the topography in Katmai. However, seismic depth control, velocity and density information for the crust in the Katmai area is very poor. Discrepancies between a composite crustal model in Katmai derived from earthquake data (Berg, Kubota and Kienle, 1967) and gravity derived depths to the Moho do exist. Both the seismic and gravimetric models could be in considerable error. The seismic model is of necessity oversimplified and consists of average two layered crustal structures with horizontal interfaces. The gravimetric depth to the Moho was estimated using Woollard's empirical relation (1960) between Bouguer anomalies and depth to the Moho. Abnormal crustal compositions and large departures from isostatic equilibrium could introduce large errors. The depth to the Moho is therefore only approximate.

2. Because of the near-zero free-air and Bouguer anomalies in the section from Katmai across the Shelikof Strait to Kodiak Island, it appears that the crustal thickness is typical of continental margins with an average depth to the Moho of about 32 km. The crust northwest of the Bruin Bay fault, characterized by significant positive free-air anomalies and complicated magnetic patterns, seems to be abnormal in composition and or thickness. This is based on the observations of Woollard and Strange (1962) that regional positive free-air anomalies indicate a thicker and more dense crust than that derived from observed Bouguer anomalies in areas of isostatic equilibrium.

3. The gravity anomalies in Katmai are clearly associated with the Mesozoic and Cenozoic structural trends of that area. Most of the variations in Bouguer gravity values can be explained by density contrasts located in the upper crust and the near surface rocks. Almost all gravity profiles across the geologic structures in Katmai show consistent regional gravity gradients. The central Mesozoic sedimentary basin is characterized by moderate negative Bouguer anomalies. Typically, the Bouguer gravity values become positive across the two major linear tectonic elements on either side of the basin including the Bruin Bay fault in the northwest and the volcanic axis to the southeast. This relationship indicates that both the Naknek Lake basement complex and the Tertiary volcanics exposed along the Shelikof Strait, provide a positive density contrast against the Mesozoic sediments. This characteristic gravity pattern in the Katmai area is shown in the crustal section presented in Fig. 13. Local fault control of the alignment of the Katmai volcanic eruptive centers is suggested by the steep gravity gradients across the volcanic axis which also indicates that the southeastern block has been relatively upthrown.

4. Two local negative gravity anomalies were mapped in Katmai

   (1) the Kulik Lake low, which suggests the presence of a Tertiary intrusive of much larger dimensions than that indicated by a relatively small outcrop of quartz diorite located in the crest of the Kamishak Anticline, and

   (2) the Mt. Trident low. A preliminary interpretation of this low was presented by Kubota and Berg (1967). A reinterpretation of the low, using additional gravity data and new density information presented in this study makes the direct correlation of the Trident

low and a hypothetical magma chamber as postulated by Kubota and Berg (1967) somewhat unlikely. The mass deficiency causing the gravity low, appears to be located at much shallower depth than the seismically detected magma chambers of Kubota and Berg.

5. A smaller scale local gravity survey across the Valley of Ten Thousand Smokes resulted in the first estimate of the volume of the 1912 ash flow by geophysical means. A maximum ash flow volume of 3.8 km^3 was derived. This compares favorably with Fenner's (1923) estimate of 4.3 km^3 based on geologic evidence.

6.2 Future Work

1. The major part of the Alaska Peninsula has not been investigated geophysically. The gravity data discussed in this thesis, including Decker's measurements of 1963 and the data of Berg and Kienle (1966) constitutes the only detailed gravity net on the Alaskan Peninsula known to the author. A few scattered gravity stations throughout the Peninsula were established by Thiel et al (1959) and Barnes (1967) but these are inadequate to delineate significant gravity patterns. The Katmai survey represents a northern extension of Barnes' (1967) simple Bouguer (2.67) gravity map, covering the coastal waters to the northeast and southeast of Katmai. It would be highly desirable to extend the Katmai gravity survey to the southwest along the Alaska Peninsula, to trace the continuation of the Mesozoic structures, particularly the sedimentary basin and the adjacent granitic basement complex. If the basement complex is present in the subsurface of the Alaska Peninsula southwest of Katmai, it is covered by a thick Tertiary and Quarternary sedimentary section. A continuation of the Katmai gravity

survey to the northwest into the Naknek Quadrangle,i.e., the Bristol Bay lowlands west of Katmai, could be even more useful. It is here, in an area of very low relief, where anomalous crustal conditions are indicated by positive regional free-air and Bouguer anomalies (Woollard et al, 1960). Intrusive masses, covered by thick Tertiary and Quarternary sediments are indicated by a very complex pattern of magnetic anomalies with variations of up to 2000γ (Andreasen et al, 1963a and b).

Unfortunately all these areas are only accessible by relatively expensive aircraft. A shipborn gravity survey of Bristol Bay, however, could be very important in delineating the Bristol Bay gravity high, which is a major positive anomaly in southwestern Alaska (Woollard et al, 1960), in more detail.

2. Aeromagnetic surveys are relatively easy to accomplish, and provide important geophysical data. Since three aeromagnetic maps are already available west of Katmai for parts of the Dillingham-, Naknek-, Karluk- and Ugashik Quadrangles (Andreasen et al, 1963a,b and Henderson et al, 1963) an extension of these surveys to the east over the Katmai area would be especially valuable. Large magnetic anomalies could be expected to be associated with the Katmai volcanoes. The maps mentioned above indicate that the Bruin Bay fault also has its own characteristic magnetic signature. From magnetic data it may be possible to get additional information about the depth to the basement below the Mesozoic sediments in Katmai. Other major magnetic anomalies might be expected to be associated with the Tertiary intrusions at Cape Douglas and Kulik Lake.

3. The lack of uniqueness of structural solutions derived from given gravity patterns makes additional structural control by other geophysical

or geological means a necessity. The above interpretation of the Katmai gravity data is supported by geologic and earthquake seismic data, both of which lack significant detail. It would therefore be very useful to establish at least one refraction profile across the ill-defined structure. A reversed refraction profile across a line of seismic stations extending from Naknek, King Salmon, Brooks, Overlook, Baked Mt. Hut to Katmai Bay could be obtained using shot points in Kvichak Bay and Shelikof Strait. Only with such additional control can the crustal structure and state of isostasy in Katmai be delineated with more confidence. Such a refraction profile could probably also prove or disprove the presence of the mafic intrusive at the head of Bristol Bay as proposed by Woollard et al (1960).

4. The Kulik Lake low (Section 4.6) is inadequately defined by gravity stations occupied to date. This low was only observed at the northwestern end of gravity profile 4, and as discussed earlier, it was not detected in adjacent profiles 7 and 8 (Fig. 9). The southwest-northeast extension of the suspected large intrusive could perhaps be traced by surveying the valleys that disect the mountains at the southeastern end of Kulik Lake.

5. Additional gravity stations close to the volcanic axis would help to delineate the shallow depth, low density crustal material that seems to be associated with the Katmai volcanoes as seen in profiles D, 1 and 2. In addition the southwest-northeast extension of the Trident low (Fig. 10) should be traced in more detail.

Since Mt. Trident is presently the most active of the Katmai volcanoes, with continuing lava production, it may be very interesting to observe possible gravity changes associated with forthcoming eruptions using stationary gravimeters.

A small seismic network of the type operated by the Geophysical Institute in the Savonoski Valley and at Cape Douglas during 1965 to 1967 Katmai expeditions could prove very useful in monitoring volcanic earthquakes and possible harmonic tremors associated with rising magma columns, if operated in the Mageik Creek flats at the foot of Mt. Trident. As discussed above (Section 4.7), volcanic explosions and B-type earthquakes from the Mt. Trident area were recorded at Baked Mt. Hut from 1965 to 1967.

6. Airborne infrared photography over the active Katmai volcanoes, particularly over Mt. Trident, could prove valuable in locating centers of high heat flow and in the detection of impending volcanic activity.

A detailed infrared survey over the Valley of Ten Thousand Smokes could contribute greatly to the controversy concerning the source of the ash flow deposits. If the ash flow was extruded from fissures in the Valley floor, as suggested by the alignment of many early fumaroles, corresponding heat flow patterns may still be detectable. The two zones of presently active fumaroles at the head of the Valley are very likely to produce marked heat flow anomalies and should be detectable on infrared photos. Continuations of these zones might also be found.

7. Drilling in the upper Valley of Ten Thousand Smokes would contribute greatly to many unsolved problems concerning the geochemistry and petrology (e.g. welded vs. unwelded), thicknesses and origin of the 1912 ash flow. In particular, density determinations throughout the ash flow could be used to reinterpret the Valley gravity anomalies discussed in Chapter 5 in terms of ash flow thicknesses measured by drilling. More accurate volume determinations of the 1912 ash flow could result.

BIBLIOGRAPHY

Andreasen, G. E., W. J. Dempsey, J. L. Vargo, and others, Aeromagnetic Map of Part of the Naknek Quadrangle, Alaska, U. S. Geol. Survey Map GP-353, 1963a.

Andreasen, G. E., W. J. Dempsey, J. L. Vargo, and others, Aeromagnetic Map of Part of the Ugashik and Karluk Quadrangles, Alaska, U. S. Geol. Survey Map GP-354, 1963b.

Balakina, L. M., General Regularities in the Direction of the Principal Stresses effective in the Earthquake Foci of the Seismic Belt in the Pacific Ocean, English Edition Bulletin (Izvestiya), Acad. of Sci. USSR, Geophysics Series,No. 11, 918-926, 1962.

Barnes, D.F., Four Preliminary Gravity Maps of Parts of Alaska, USGS, Open file report, copies available: Alaska Branch USGS, 345 Middlefield Road, Menlo Park, California, June 23, 1967.

Berg, E. and J. Kienle, Gravity Measurements in the Katmai Volcano Area, Alaska, Geophys. Res. Rep. UAG R-176, Geophys. Inst. University of Alaska, April 1966.

Berg E., S. Kubota and J. Kienle, Preliminary Determination of Crustal Structure in the Katmai National Monument, Alaska, Bull. Seism. Soc. Am., Vol. 57, No. 6, 1367-1392, 1967.

Birch, F., J. F. Schairer and H. C. Spicer, Handbook of Physical Constants, Geol. Soc. Am. Spec. Paper No. 36, 325 pp. 1942.

Bordet, P., G. Marinelli, M. Mittempergher, and H. Tazieff, Contributions à l'Etude Volcanologique du Katmai et de la Vallée des Dix Mille Fumées (Alaska), Mémoires de la Société Belge de Géologie, de Paléontologie et d'Hydrologie (Bruxelles), Série IN-8°-No. 7, 70 pp., 1963.

Bott, M. H. P., and R. A. Smith, The Estimation of the Limiting Depth of Gravitating Bodies, Geophys. Prospecting, Vol. 6, 1-10, 1958.

Burk, C. A., Geology of the Alaska Peninsula - Island Arc and Continental Margin (Part 1 - Text, Part 2 - Geologic Map in Two Sections, Part 3 - Tectonic Map), Geol. Soc. Am., Memoir 99, 250 pp. 1965.

Carey, S. W., Continental Drift, A Symposium, Convener S. W. Carey, Pub. by Geol. Dept., University of Tasmania, 177-355, 1956.

Coats, R. R.,Magma Type and Crustal Structure in the Aleutian Arc, AGU Geophysical Monograph 6, 92-109, 1962.

Cook, E. F., Ignimbrites of the Great Basin, U.S.A., Bull. Volcanologique, Tome 25, 89-96, 1963.

Davis, T. N. and C. Echols, A Table of Alaska Earthquakes, 1788-1961, Geophys. Res. Rep. UAG R-131, Geophys. Inst., Univ. of Alaska, Aug. 1962.

Decker, R. W., Proposed Volcano Observatory at Katmai National Monument: A Preliminary Study, Dartmouth College, Unpublished Report, 54 pp., Nov. 1963.

Decker, R. W., Geophysical Investigations in Katmai National Monument, Alaska (Abstr.), Trans. Am. Geophys. Union, Vol. 45, No. 1, 124, 1964.

Elvers, D. J.,Ch. C. Mathewson, R. E. Kohler and R. L. Moses, Systematic Ocean Surveys by the USC6GS Pioneer 1961-1963, Coast and Geodetic Survey Operational Data Report, C6GSDR-1, 18 pp. 1967.

Escher, B. G., On the Hot Lahar (Mudflow) of the Valley of Ten Thousand Smokes (Alaska), Proceed. Royal Academy of Amsterdam, Vol. 24, 282-293, 1921.

Fenner, C. N., The Katmai Region, Alaska, and the Great Eruption of 1912, J. of Geol.,Vol. 28, No. 7, 569-606, 1920.

Fenner, C. N., The Origin and Mode of Emplacement of the Great Tuff Deposit of the Valley of Ten Thousand Smokes, Nat. Geograph. Soc. Contributed Tech. Papers, Katmai Series, No. 1, 74 pp. 1923.

Fenner, C. N., The Chemical Kinetics of the Katmai Eruption, Part II, Am. J. of Science, Vol. 248, 697-725, 1950.

Garland, G. D., The Earth's Shape and Gravity, Pergamon Press, New York, 183 pp. 1965.

Gorshkov, G. S., Gigantic Eruption of the Volcano Bezimianny, Bull. Volcanologique, Tome 20, 77-109, 1959.

Grant, F. S. and G. F. West, Interpretation Theory in Applied Geophysics, McGraw-Hill, New York, 583 pp. 1965.

Griggs, R. F., Our Greatest National Monument, Natl. Geograph. Soc., Vol. 40, No. 3, 219-292, 1921.

Griggs, R. F., The Valley of Ten Thousand Smokes, Natl. Geograph. Soc., Vol. 31, 340, 1922.

Hammer, S., Terrain Corrections for Gravimeter Stations, Geophysics, Vol. 4, 184-194, 1939.

Hazzard, J. C., J. J. Bryan and E. Borax, Geology of Kamishak Bay Area, Cook Inlet, Alaska, Am. Assoc. Petroleum Geologists Bull.,Vol. 34, 2377, 1950.

Henderson, J. R., J. L. Vargo and others, Aeromagnetic Map of Part of the Dillingham Quadrangle, Alaska, U. S. Geol. Survey Map, GP-352, 1963.

Hubbard, B. R., S. J.,Cradle of the Storms, Dodd, Mead, New York, 285 pp. 1935.

Jacobs, J. A., R. D. Russell and J. T. Wilson, Physics and Geology, McGraw-Hill, New York, 424 pp. 1959.

Jeffreys, H. and K. E. Bullen, Seismological Tables, British Assoc. for the Advancement of Science, London, 1958.

Keller, A. S. and H. N. Reiser, Geology of the Mt. Katmai Area, Alaska, U. S. Geological Survey Bulletin, 1058-G, 261-298, 1959.

Keller, F. Jr., J. L. Meuschke and L. R. Alldredge, Aeromagnetic Surveys in the Aleutian, Marhsll and Bermuda Islands, Trans. Am. Geophys. Union, Vol. 35, No. 4, 558-572, 1954.

Kubota,S. and E. Berg, Evidence for Magma in the Katmai Volcanic Range, Bull. Volcanologique, Tome 31, 175-214, 1967.

Lensen, G. J., Principal Horizontal Stress Directions as an Aid to the Study of Crustal Deformation, Publ. Dom. Obs. Ottawa, Vol. 24, No. 10, 389-397, 1960.

Matumoto, T. and P. L. Ward, A Microearthquake Study of Mount Katmai and Vicinity, Alaska, J. Geophys. Res.,Vol. 72, No. 10, 2557-2568, 1967.

Menard, H. W., Marine Geology of the Pacific, McGraw-Hill, New York, 271 pp. 1964.

Nafe, J. E. and C. L. Drake, Physical Properties of Marine Sediments, in "The Sea", Vol. 3, John Wiley & Sons, New York, pp. 794 - 815, 1963.

Nettleton, L. L., Geophysical Prospecting for Oil, McGraw-Hill, New York, 444 pp. 1940.

Payne, T. G., Mesozoic and Cenozoic Tectonic Elements of Alaska, Misc. Geol. Inv. Map 1-84, U.S. Geol. Surv., 1955.

Peter, G., Geological Structure of the Aleutian Trench Southwest of Kodiak Island, J. Geophys. Res., Vol. 70, No. 2, 353-366, 1965.

Press, F. and D. Jackson, Alaska Earthquake, 27 March 1964: Vertical Extent of Faulting and Elastic Strain Energy Release, Science, Vol. 147, No. 3660, 867-868, 1965.

Ray, D. K., Geochemistry and Petrology of the Mt. Trident Andesites, Katmai National Monument, Alaska, Unpublished Dissertation, Geophysical Institute, University of Alaska, 1967.

Ray, D. K., R. B. Forbes, T. Katsura, H. Matsumoto and H. Haramura, The Petrology and Geochemistry of the Mt. Trident Andesites (Abstr.) Proc. 11th Pacific Science Congress, Tokyo, Japan, in press.

Ryall, A. and D. L. Bennett, Crustal Structure of Southern Hawaii Related to Volcanic Processes in the Upper Mantle, J. Geophys. Res.,Vol. 73, No. 14, 4561-4582, 1968.

Scheidegger, A. E., Principles of Geodynamics, Springer Verlag, Berlin, 280 pp. 1958.

Schwiderski, E. W., The Deep Structure of the Earth Inferred from a Satellite's Orbit, Part I: The Density Anomaly, U. S. Naval Weapons Laboratory, Dahlgreen, Virginia, Technical Report No. 2077, 68 pp. 1967.

Shimozuru, D., Geophysical Evidences for suggesting the Existence of Molten Pockets in the Earth's Upper Mantle, Bull. Volcanologique, Tome 26, 181-195, 1963a.

Shimozuru, D., Poisson's Ratio of Rocks at High Temperatures - Seismological Application, Geophys. Papers dedicated to Kenzo Sassa, 517-522, 1963b.

Shor, G. G. Jr., Seismic Refraction Studies off the Coast of Alaska: 1956-1957, Bull. Seism. Soc. of Am.,Vol. 52, No. 1, 37-57, 1962.

Spurr, J. E., A Reconnaissance in Southwestern Alaska in 1898, U. S. Geol. Survey, 20th Ann. Rep. (7), 43-263, 1900.

Stauder, W. and G. A. Bollinger, The Focal Mechanism of the Alaska Earthquake of March 28, 1964, and of its Aftershock Sequence, J. Geophys. Res.,Vol. 71, No. 22, 5283-5296, 1966.

Stone, D.,Paleomagnetic Research in Alaska, Annual Report, Geophysical Institute, University of Alaska, 98-110, 1966-67.

Stoneley, R., The Structural Development of the Gulf of Alaska Sedimentary Province in Southern Alaska, Quarterly Journal of the Geol. Soc. of London, Vol. 123, 25-57, 1967.

Strange, W. E., L. F. Machesky and G. P. Woollard, A Gravity Survey of the Island of Oahu, Hawaii, Pacific Science, Vol. 19, No. 3, 350-353, 1965a.

Strange, W. E., G. P. Woollard and J. C. Rose, An Analysis of the Gravity Field over the Hawaiian Islands in Terms of Crustal Structure, Pacific Science, Vol. 19, No. 3, 381-389, 1965b.

Talwani, M.,J. L. Worzel and M. Landisman, Rapid Gravity Computations for two-dimensional Bodies with Application to the Mendocino Submarine Fracture Zone, J. Geophys. Res.,Vol. 64, No. 1, 49-59, 1959a.

Talwani, M., G. H. Sutton and J. L Worzel, A Crustal Section Across the Puerto Rico Trench, J. Geophys. Res.,Vol. 64, No. 10, 1545-1555, 1959b.

Thiel, E., E. La Chapelle and J. Behrendt, The Thickness of Lemon Creek Glacier, Alaska, as determined by Gravity Measurements, Trans. Am. Geophys. Union, Vol. 38, No. 5, 745-749, 1957.

Thiel, E., N. A. Ostenso, W. E. Bonini and G. P. Woollard, Gravity Measurements in Alaska, Arctic, Vol. 12, No. 2, 67-76, 1959.

Tide Tables, West Coast North and South America including the Hawaiian Islands, U. S. Department of Commerce, Coast and Geodetic Survey, 1965 and 1966.

Tobin, D. G., and L. R. Sykes, Relationship of Hypocenters of Earthquakes to the Geology of Alaska, J. Geophys. Res.,Vol. 71, No. 3, 1659-1667, 1966.

Tsuboi, Chuji, Thickness of the Isostatic Earth's Crust in Various Parts of the United States of America, Geophys. Notes, Geophys. Inst., Tokyo Univ.,No. 3, 1-37, 1950.

Tsuya, H. and R. Morimotu, Types of Volcanic Eruptions in Japan, Bull. Volcanologique, Tome 26, 209-222, 1963.

Ward, P. L. and T. Matumoto, A Summary of Volcanic and Seismic Activity in Katmai National Monument, Alaska, Bull. Volcanologique, Tome 31, 107-129, 1967.

Williams, H., G. H. Curtis and W. Juhle, Mt. Katmai and the Valley of Ten Thousand Smokes, Alaska(a New Interpretation of the Great Eruption of 1912), Proc. 8th Pacific Science Congress, Univ. of Phillippines, Vol. 2, 129, 1956.

Woollard, G. P., Crustal Structure from Gravity and Seismic Measurements, J. Geophys. Res., Vol. 64, No. 10, 1521-1544, 1959.

Woollard, G. P., N. A. Ostenso and E. Thiel, Gravity Anomalies, Crustal Structure, and Geology in Alaska, J. Geophys. Res., Vol. 65, No. 3, 1021-1037, 1960.

Woollard, G. P., and W. E. Strange, Gravity Anomalies and the Crust of the Earth in the Pacific Basin, AGU Geophysical Monograph 6, 60-80, 1962.

Worzel, J. L., Pendulum Gravity Measurements at Sea 1936-1959, John Wiley and Sons, New York, 422 pp., 1965.

Wyckoff, R. D., Study of Earth Tides by Gravitational Measurements, Trans. Am. Geophys. Union, Vol. 17, 46-52, 1936.

Zeitz, I., G. E. Andreasen and Arthur Grantz, An Aeromagnetic Study of the Cook Inlet Area, Alaska, (Abstr.), Geophysics, Vol. 23, No. 5, 1059, 1958.